Department of Electrical & Electronic Engineering

Reduced Complexity Asynchronous Multi-User Receivers for Spread Spectrum Multiple Access

by

Benjamin C Skelton, B.E. (Elec.) Hons. I

A dissertation submitted in partial fulfillment
of the requirements for the degree of

Doctor of Philosophy

2000

University of Canterbury

A dissertation submitted in partial fulfillment
of the requirements for the degree of Doctor of Philosophy

ABSTRACT

Benjamin C Skelton, *Reduced Complexity Asynchronous Multi-User Receivers for Spread Spectrum Multiple Access*, 2000

One of the major problems facing the implementation of multi-user detectors in a mobile radio multiple access environment is the complexity of the receiver structure. This thesis addresses this problem and develops three related receiver structures based on the maximum likelihood multi-user detector. They allow a degradation in performance to be traded for a reduction in the complexity of the receiver. The first family of reduced complexity receivers is derived considering a serial partitioning of the maximum likelihood trellis. A receiver with two degrees of freedom is developed by the application of reduced state sequence estimation (RSSE) techniques to the first receiver. A maximum-ratio combining-like detector with self-noise cancellation is derived for the multi-path fading channel. All three receiver structures allow for significant reductions in complexity with respect to the maximum likelihood detector with only modest performance reductions.

Keywords: Spread spectrum multiple access, multi-user detectors, maximum likelihood sequence estimation, reduced sequence estimation, mobile radio, fading channel

Ben Skelton, Communications Research Centre, Department of Electrical & Electronic Engineering, University of Canterbury, Private Bag, Christchurch, New Zealand

ACKNOWLEDGEMENTS

I am deeply indebted to my supervisor Des Taylor for his guidance and encouragement both over the time this thesis was produced and during my undergraduate years. I can safely say that without his tutorage this thesis would not exist.

This thesis has been produced entirely with free software under the Linux operating system. My thanks go to developers of Linux and LaTeX, The Free Software Foundation, the KDE and Octave projects and other developers within the free software community.

PREFACE

The mobile information society is definitely upon us. Each year the number of users "going mobile" increases. New Zealand has mirrored the world-wide trend in the growth in mobile subscriber numbers. Today few users are tolerant of large, bulky equipment, poor quality voice or slow data rates whether they are in the office, in the car down-town or at a rugby match. Consumer demand is not only for improvements in the quality of existing services but also for the expansion of services—emerging technologies include mobile internet browsing, video conferencing and other wide-band and multimedia services.

In order to meet these demands a lot of research effort has been spent developing solutions that are robust to the requirements of the mobile user—(a) small and light hand-held terminal, (b) quality service for diverse applications and (c) long battery life. A forerunner among contenders for the multiple access technology to be employed by Third Generation mobile communication systems is spread spectrum multiple access (SSMA) which has advantages over other techniques including soft capacity, soft hand-over, and the ability to resolve multi-path fading components to achieve a diversity gain. Capacity improvements in SSMA systems can be achieved in two main ways—(a) the application of powerful forward error correcting coding to the conventional spread spectrum detector and (b) the use of multi-user detection. In this thesis we consider the latter.

The outline of this thesis is a follows. In chapter 1 a review of multiple access techniques is presented. The fading channel phenomenom is presented and described. Spread spectrum multiple access fundamentals are summarised and reviewed in chapter 2. In this chapter we present a model for synchronous spread spectrum multiple access and describe spread spectrum basics such as pseudo-random spreading sequences, timing recovery and sequence acquisition

before presenting a summary of the different families of multi-user detectors.

The work considered original in this thesis follows in section 2.4.2 and in chapters 3, 4 and 5. The chapters follow a progression of three related receiver structures, with each chapter building on the previous to arrive at a reduced complexity multi-user receiver for the multi-path fading channel in chapter 5. Original contributions in these chapters appear in the following submitted papers—

- SKELTON, B. C., AND TAYLOR, D. P., "A Family of Reduced Complexity Multi-User Detectors for Asynchronous Spread Spectrum Multiple Access," submitted to *IEEE Trans. Commun.* 18 October 1999.

- SKELTON, B. C., AND TAYLOR, D. P., "RSSE Based Multi-User Detectors for Asynchronous Spread Spectrum Multiple Access," submitted to *IEEE Trans. Commun.* 29 November 1999.

- SKELTON, B. C., AND TAYLOR, D. P., "Multi-User Detectors with Decision Feedback for Asynchronous Spread Spectrum Multiple Access in Multi-path Fading Channels," submitted to *IEEE Trans. Commun.* 30 January 2000.

Ben Skelton

TABLE OF CONTENTS

Chapter 1

MOBILE MULTIPLE ACCESS COMMUNICATION

1.1 Multiple Access Communications

First generation mobile communication systems are characterised by the use of a single high-powered transmitting base station that transmits as much power as required in order to reach the mobile terminals within the required coverage area. In these analogue systems, multiple access is achieved through a frequency allocation for each user, to be discussed later. First Generation devices suffer from a large power requirement which in their time helped to leave mobile terminals mostly in cars. The services offered by First Generation systems are largely limited to voice and facsimile communications. In New Zealand and North America the most wide-spread First generation system is AMPS; NTT in Japan and NMT in Scandinavia.

Second Generation systems or *Cellular systems* [26, 61] divide the service area up into many smaller geographic regions or *cells* each utilising a lower powered transmitter whose power is enough to cover only the cell, the advantage being that cells far away enough away from a cell operating at a given frequency can re-use that frequency.

Cells are grouped into *clusters* in which different frequencies are allocated to different base-stations as shown in Fig. 1.1. In this case a cluster of size of three is illustrated but other common cluster sizes are four, seven and twelve [61]. Each cell in the system is connected to a Mobile Switching Centre (MSC) which provides the interface between the cell system and the Public Switched Telephone Network (PSTN). The MSC has further functions including determining if the mobile user is available to take an incoming call, determining

which cell the mobile is in, service quality monitoring and handover functions. Handover is the procedure to transfer a call in progress from one base-station to another as the mobile user moves from one cell to another. Second Generation systems allow multiple users to communicate by offering each user a separate time to talk. This time allocation, which will be discussed shortly, is used in most Second Generation systems including GSM in New Zealand and Europe, and IS-54 in America. Both systems, being fully digital, allow the user to send and receive data as well as voice communications.

The move from First to Second Generation systems and the trend in consumer and office computer use suggests that Third Generation systems will need to offer users faster data transfer for mobile Internet access as well as providing good quality voice communications. "Bursty" communications such as voice and Internet traffic are ideally suited to a third method of multiple access which is not limited in frequency or time allocation, but in instantaneous received power. This technique called Spread Spectrum Multiple Access (SSMA) is a leading contender for Third Generation mobile communication system and the area of research of this thesis.

Multiple access techniques allow mobile users within each cell to communicate using the same band of frequencies. The main three methods for multiple access are frequency division (FDMA), time division (TDMA) and spread spectrum (SSMA) multiple access, also called code division multiple access (CDMA). These three techniques are illustrated in Fig. 1.2. FDMA users transmit simultaneously and are separated by limiting their transmission to smaller frequency bands within the cell's greater frequency allocation. In a TDMA system all users share the same overall frequency band, but are allocated different time slots. Users share time and frequency domains in SSMA systems which rely on spreading sequences or codes to distinguish users. Other multiple access techniques based on two or more of these techniques are called hybrid multiples access schemes such as the hybrid TDMA/SSMA systems in [35, 58]. The transmission technique known as frequency-hopped spread spec-

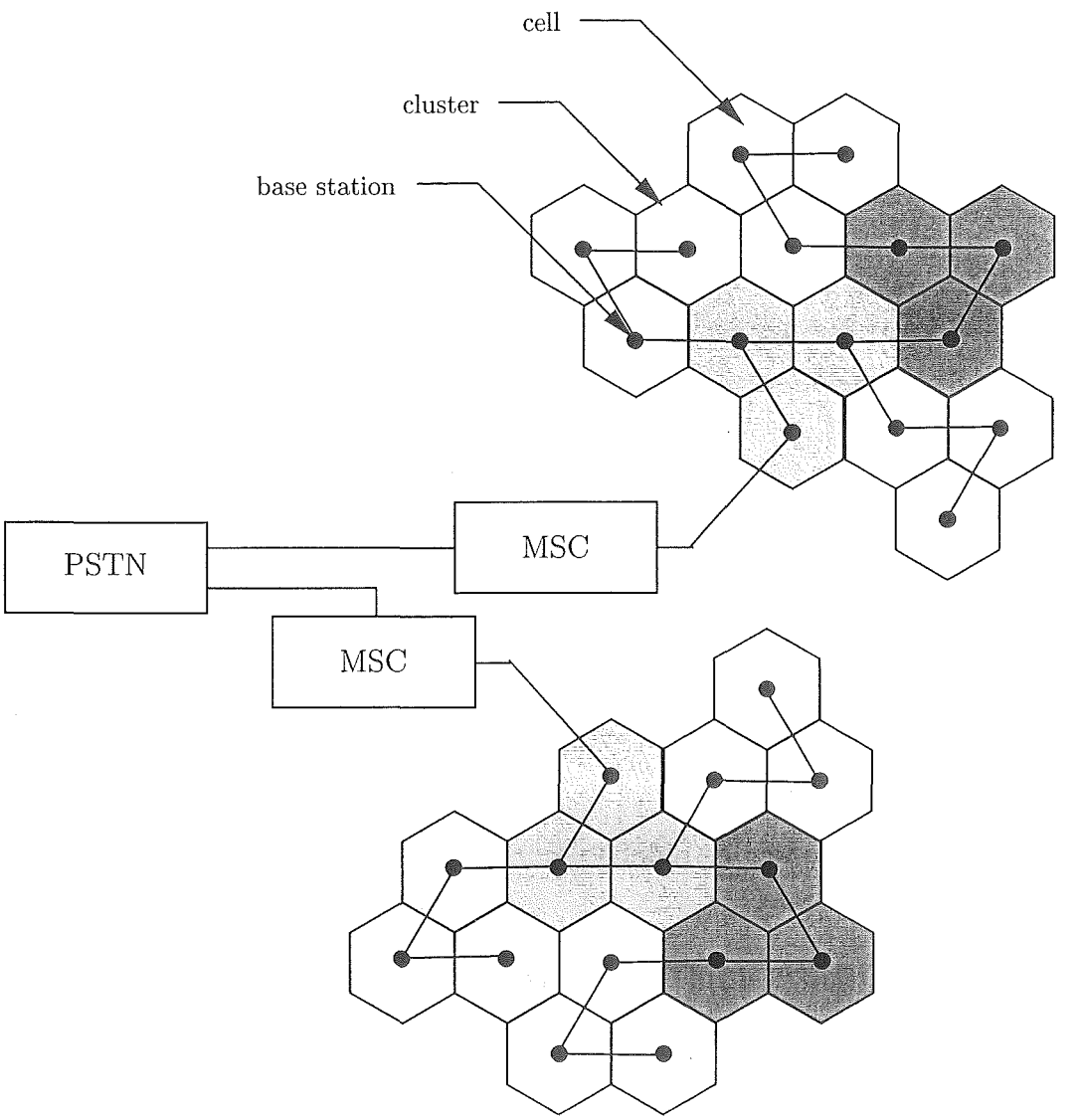

Figure 1.1: A cellular communication system with a cluster size of three. The base stations are connected to the Mobile Switching Centre (MSC) which connects to the Public Switched Telephone Network (PSTN).

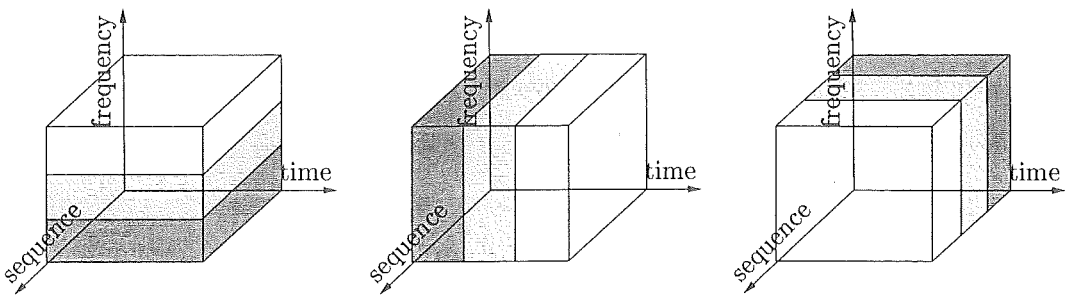

(a) FDMA (b) TDMA (c) SSMA

Figure 1.2: Fundamental multiple access techniques.

trum multiple access is a hybrid TDMA/FDMA system where different users transmit over different sequences of pseudo-randomly determined frequencies.

In a *frequency division multiple access* scheme [61, 83], users in the cell transmit in their own frequency channel within the greater band of frequency allocated to that particular cell. In this system each user is orthogonal in frequency. In a *time division multiple access* system [61, 83] the same frequency resources are shared by allocating each user a time slot in which to transmit. In this case users are orthogonal in the time domain. TDMA is the choice of multiple access system for modern Second Generation digital communication systems such as GSM and IS-54 [61, 83].

With the third multiple access technique, *spread spectrum multiple access* [61, 83], all users may transmit at the same time using the same carrier frequency. The separation of users is performed by the use of spreading sequences or codes [22, 43, 64]. For years the domain of the military, spread spectrum systems received their first in-depth public treatment in [70] and in the tutorial of [55]. Since then the application to multiple access systems has seen the bulk of attention in the publicly available literature [7, 54]. Note that in Fig. 1.2 we have shown SSMA utilising orthogonal spreading sequences. While orthogonal sequences provide maximum capacity they suffer from the requirement of strict signal timing in that bit and chip synchronism need to be maintained. A

further hurdle is that they require synchronous and inter-symbol interference free (or only single path) channels. These requirements are a consequence of the cross-correlation properties of the orthogonal sequences which exhibit poor non-zero lag cross correlations. Typically, the orthogonality requirement is relaxed and semi-orthogonal sequences are used. This allows for asynchronous systems and results in multiple access interference (MAI) which may be the limiting factor in the performance of a SSMA system. We will have more to say about this in the next chapter.

The question of which multiple access technique provides maximum capacity is difficult to determine and many papers appear in this area [21, 23, 94]. However, SSMA systems have many advantages over other schemes such as—

- *soft capacity*: unlike FDMA and TDMA which have fixed slots for the transmission of each user, SSMA is interference limited. Performance degrades gracefully as the number of users increases.

- *soft hand-over*: a mobile user near a cell boundary may be in contact with two or more base stations, as the mobile leaves one cell and enters the next the conversation is maintained by both base stations until the received signal from the new base station is strong enough for reliable communication, that communication with the previous base station is stopped.

- *timing*: there is no strict signal framing requirement as with TDMA systems.

- *less power*: since the energy in the signal is spread over a wider bandwidth the mobile can transmit with less power—the transmitted signal has a lower power spectral density.

- *narrow-band interference rejection*: SSMA system can actually overlay existing narrow band services [66] in some situations—(a) the power spec-

tral density in the band of the narrow-band service is not too great (ie the number of users in the SSMA system is small) to cause a too-severe drop in performance of the narrow-band service and (b) the bandwidth of the narrow-band service is small compared to the SSMA service so that the post-filtered and de-spread narrow-band service at the SSMA receiver has an acceptably small effect on SSMA performance. In both cases it is a problem of power spectral density.

- *multi-path resolution*: SSMA systems can resolve multi-path interference and take advantage of diversity combining.

The two main disadvantages of SSMA systems are *multiple access interference* and the *near-far problem* [83]. MAI occurs when users use spreading sequences which are not orthogonal. A lot of research effort has been spent finding sequences with good correlation properties (see section 2.2). The near-far problem occurs when one user transmits with a greater signal power than the other users. This has the effect of worsening the MAI problem. Solutions to this problem include stringent power control algorithms [73, 84, 85, 96] using a protocol channel and multiple user detectors [14, 50]. We will have more to say about these in the next chapter.

1.2 The Mobile Radio Channel

Mitigating the effects of the channel is fundamental to the design of modern communications systems which must operate reliably in channels which offer obstacles to efficient communications. The physical mobile radio environment is illustrated in Fig. 1.3. Natural obstacles such as trees and hills, and man-made obstacles such as buildings and cars influence the transmission between the base station and the mobile terminal. Channel sounding of the wide-band spread spectrum mobile radio channel has been performed [66, 67]. From these studies the time-dispersive nature of the channel is evident. It is caused by reflections, scattering and diffraction of the transmitted signal resulting in

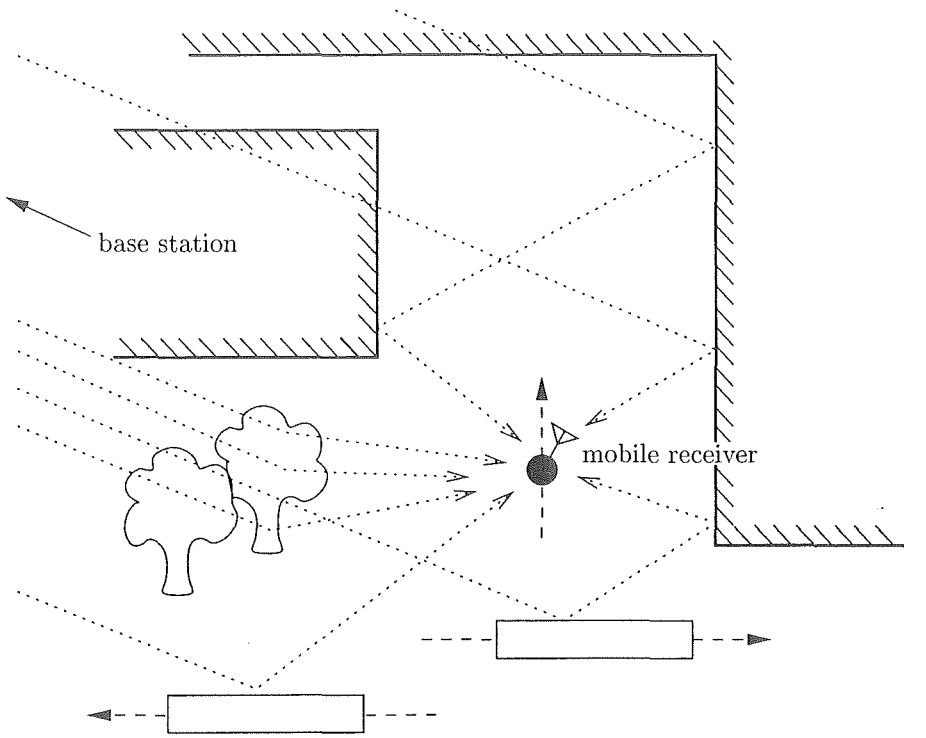

Figure 1.3: The mobile radio environment.

replicas of the transmitted signal arriving at the receiver with different delays. Frequency dispersion occurs when there is a relative movement between transmitter and receiver resulting in distortion due to the Doppler effect. The rays arriving at the receiver exhibit a time varying amplitude and phase distortion due to localised scattering and shadowing.

The rate of distortion is characterised by the relative velocity of the transmitter and receiver. If the velocity of the mobile is $v(t)$ and the angle of the received ray with respect to the direction of the mobile is $\theta(t)$, then the Doppler shift is given by,

$$f_d(t) = \frac{1}{c} f_c v(t) \cos\theta(t), \tag{1.1}$$

where f_c is the carrier frequency, and c is the velocity of light. If the maximum velocity of the mobile terminal is v_m then the maximum Doppler shift

experienced is written as,

$$f_D = \pm \frac{1}{c} f v_m. \tag{1.2}$$

In the literature, the quantity $f_D T$ is often reported. This quantity is the *normalised Doppler frequency* and is a measure of the ratio of the maximum Doppler shift experienced by the mobile's carrier frequency to the bit rate. For a carrier frequency of 1 GHz and a bit rate of 32 kb/s, a mobile moving at 200 km/h directly toward or away from the base station experiences a normalised Doppler shift of approximately $f_D T = 0.005$. For lower carrier frequencies, slower moving mobiles and other arrival angles the normalised fade rate is slower.

The phenomenon is shown in Fig. 1.4 where we have plotted the amplitude and phase of a simulated fading signal for normalised Doppler frequencies of $f_D T = 0.05$ and 0.005. In Fig. 1.5 the fading envelope is shown with the unfaded transmitted bits. Note that the fading envelope is quasi-periodic and that 180° phase swings are common within deep envelope fades.

Due to the complex nature of the mobile radio channel, statistical channel models are employed. The key work on time-varying channel characterisation is that of Bello [2, 3] who describes the channel in terms of four inter-related functions of time and delay in the time and frequency domains. These are inter-related through the Fourier transform. In the present work we make use of only a sub-set of the generalised theory. Bello describes the channel in terms of a time varying impulse response (called the *input delay spread function*) $c(\xi; t)$ where ξ is the delay variable. The channel output is then given by the convolution,

$$r(t) = \int_{-\infty}^{\infty} x(t - \xi)\, c(\xi; t)\, d\xi, \tag{1.3}$$

where $x(t)$ is the transmitted signal. The delay spread function is often modelled as a zero-mean complex Gaussian process [26], resulting in an envelope which is Rayleigh distributed. In situations where the channel includes a line-

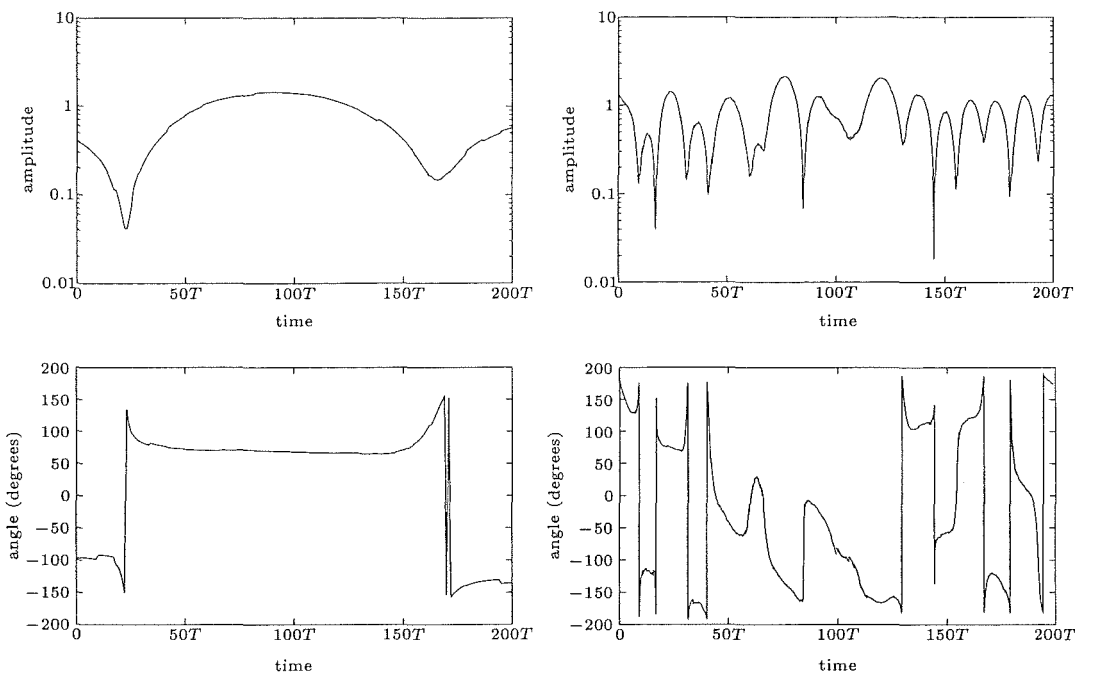

(a) $f_D T = 0.005$ (b) $f_D T = 0.05$

Figure 1.4: Amplitude and phase of a simulated fading process for normalised Doppler frequencies of $f_D T = 0.005$ and 0.05.

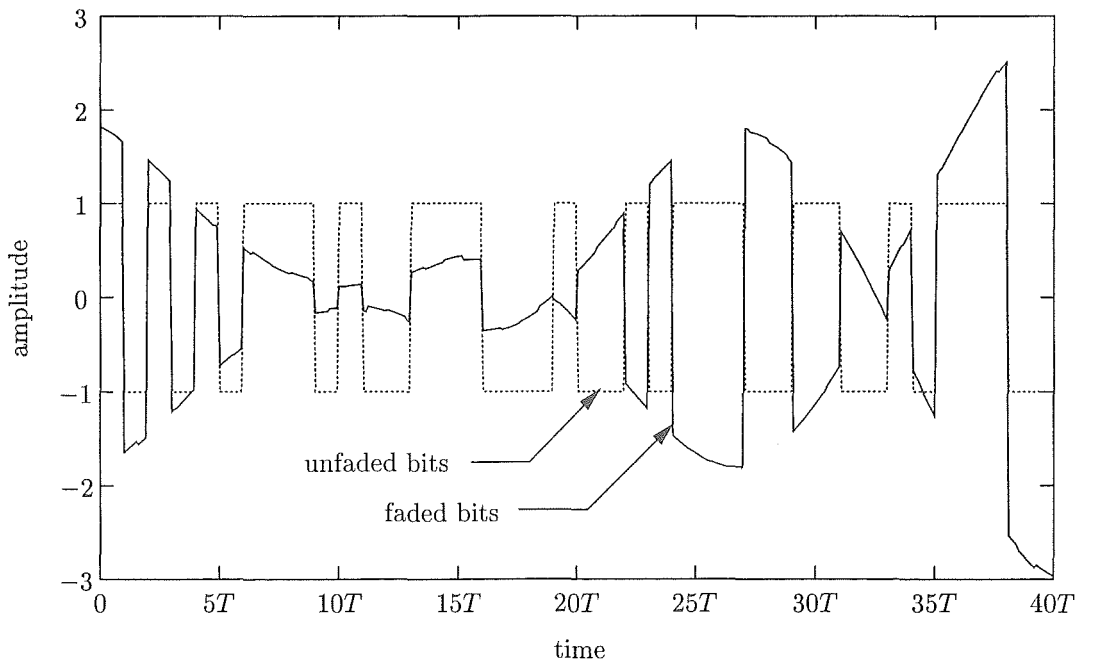

Figure 1.5: The envelope of a faded signal for normalised Doppler frequency of $f_D T = 0.05$.

of-sight component or a scatterer in the channel is time-invariant, the zero-mean model is no longer relevant and the envelope has a Rice distribution [59]. Another distribution that is sometimes used to characterise faded signals is the Nakagami-m distribution [48]. This distribution is of interest because it also provides a good approximation to the Rice distribution and has the Rayleigh distribution as a special case.

In this thesis we will be concerned with the Wide-Sense Stationary Uncorrelated Scattering (WSSUS) class of channel models commonly occurring in the literature [29, 59, 102, 103]. This class of models makes the assumptions that the input delay spread function is modelled as a zero-mean complex Gaussian process with stationary statistics (at least over the observation interval), and that the contributions from scatters of different path delays are uncorrelated. They provide an approximation that has been found in many cases, to adequately model real channel behaviour. With these assumptions the auto-correlation of the input delay spread function can be written as,

$$R_c(\xi_1, \xi_2\,; \Delta t) = \mathrm{E}[c(\xi_1; t)\, c^*(\xi_2; t + \Delta t)] \tag{1.4}$$

$$= r_c(\xi_1\,; \Delta t)\, \delta(\xi_1 - \xi_2), \tag{1.5}$$

where $r_c(\xi_1\,; \Delta t)$ is called the *auto-correlation profile* of the channel for the ξ_1-delayed path and whose Fourier transform gives the *scattering function* defined as,

$$S(\xi\,; f_d) = \int_{-\infty}^{\infty} r_c(\xi_1\,; \Delta t) \exp(-j2\pi f_d \Delta t)\, d(\Delta t). \tag{1.6}$$

It is well known that the fading auto-correlation profile for the mobile radio channel assuming isotropic scattering in the vicinity of the receiver can be modelled by [8],

$$r_c(\xi_1\,; \Delta t) = \mathrm{J}_0(2\pi f_D \Delta t), \tag{1.7}$$

where $\mathrm{J}_0(\cdot)$ is the zero-order Bessel function.

Averaging the scattering function over all Doppler shifts gives the *delay power spectrum* which in turn gives the average power distribution over the

various paths in the channel,

$$P_c^{\xi}(\xi) = \int_{-\infty}^{\infty} S(\xi\,;f_D)\,df_D. \tag{1.8}$$

The Doppler power spectrum gives the power profile as a function of Doppler shift,

$$P_c^{f_D}(f_D) = \int_{-\infty}^{\infty} S(\xi\,;f_D)\,d\xi. \tag{1.9}$$

The delay power spectrum and Doppler power spectrum have "bandwidth" parameters often measured at the 3 dB points on the spectra [83]. The bandwidth of the Doppler power spectrum gives the Doppler spread of the channel whose inverse gives the coherence time. Slowly changing channels exhibit small Doppler spread. The bandwidth of the delay power spectrum gives the coherence bandwidth of the channel. Frequency components of the signal separated by more that the coherence bandwidth experience different and independent channel effects and if the coherence bandwidth of the channel is smaller than the bandwidth of the transmitted signal the channel is said to be frequency-selective.

In this thesis we assume localised scattering and a discrete delay power spectrum with arriving paths separated by the bit period T. The multi-path fading models used later in simulation studies have delay power spectra

$$P_c^{\xi} = 0.5, 0.33, 0.17, \quad P_c^{\xi} = 0.75, 0.25, \quad P_c^{\xi} = 1.0$$

and normalised Doppler frequencies,

$$f_D T = 0.005, \quad f_D T = 0.05, \quad f_D T = 0.5.$$

The delay power spectra parameters are chosen to model a range of fading channels with decreasing power spectra. The decreasing power spectra profile is characteristic of the fading channel since paths of greater arrival time are usually associated with scatters further away from the receiver. We have shown that the normalised Doppler frequency usually expected in practise lies at the slower end of the range given here.

In this chapter the topic of multiple access communication in a mobile radio environment has been introduced. We have presented a description of the First and Second Generation mobile communication systems. The requirement for Internet and other data services as well as good quality voice communications has been suggested for Third Generation systems. These types of "bursty" communications are particularly suited toward SSMA systems in which all users transmit over the same frequency band at the same time. The result is that SSMA systems are interference limited. It was also shown that SSMA systems exhibit properties that make SSMA particularly attractive in a cellular mobile radio environment. These properties include: soft capacity, soft hand-over, narrow-band interference rejection, multi-path resolution, and reduced timing and power requirements.

In the following chapter we present spread spectrum fundamentals and existing spread spectrum techniques through a literature search. A sequence of three chapters follows developing three families of reduced complexity spread spectrum receivers leading toward a reduced complexity multi-user detector for the multi-path fading channel. Finally, a list of open problems and conclusions are given.

Chapter 2

SPREAD SPECTRUM MULTIPLE ACCESS FUNDAMENTALS

In this chapter basic concepts which will be extended in the remainder of the thesis are introduced. The synchronous spread spectrum multiple access model is described and we present a summary of the properties of pseudo-random sequences pertinent to the understanding of spread spectrum systems. A brief summary of spread spectrum signal acquisition is given. We show that the conventional spread spectrum receiver with forward error correction convolutional coding in a multiple access and slow fading environment requires computationally complex (high constraint length) codes to obtain a similar error-rate performance to the single user detector in the same fading environment. As a result we turn our attention to multiple user detectors and present a summary of existing receiver structures through a literature summary.

2.1 Spread Spectrum Multiple Access

2.1.1 The Synchronous Signal Model

In a SSMA system several users transmit data at the *same* time using the *same* frequency band. The transmitted data of different users are distinguished from each other by the application of distinct spreading sequences. Consider a user employing an N_s-length binary spreading sequence. The spreading process is illustrated in Fig. 2.1. The user's data signal is multiplied by the spreading sequence signal which is unique to each user to give the spread signal which in turn modulates the carrier signal, which is a frequency that is common to all users in the system, to produce the transmitted signal.

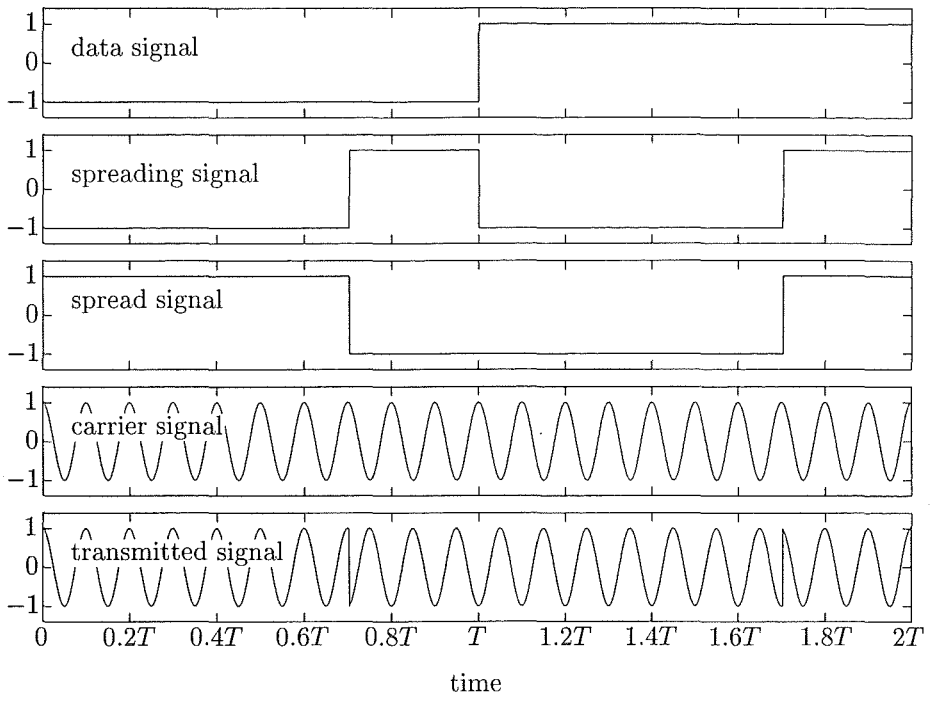

Figure 2.1: The direct sequence spread spectrum concept. The data signal is multiplied with the spreading signal to give the spread signal which modulates the carrier signal to give the transmitted signal.

The received signal in a synchronous multiple access environment consists of the transmitted signals of all K users and the additive white Gaussian noise (AWGN) written as,

$$r(t) = \sum_{i=0}^{N-1} \sum_{k=0}^{K-1} b_k(i) s_k(t - iT) + n(t), \tag{2.1}$$

where N is the number of transmitted bits, $b_k(i)$ is the k-th user's bit during the i-th signalling interval, $s_k(t)$ is the k-th user's spreading sequence (see section 2.2) defined over the bit period and $n(t)$ is the AWGN with power spectral density $N_o/2$.

The sampled output of the sequence-matched filter for the k-th user at the

end of i-th signalling interval can be written as,

$$\begin{aligned} y_k &= \int_{(i-1)T}^{iT} r(t)s_k(t-iT)\,dt \\ &= \sum_{k'=0}^{K-1} b_k(i)g_{k,k'} + n_k(i) \end{aligned} \tag{2.2}$$

where $g_{k,k'}$ is the cross-correlation between the k-th and k'-th user's spreading sequences written as,

$$g_{k,k'} = \int_{-\infty}^{\infty} s_k(t)s_{k'}(t)\,dt, \tag{2.3}$$

and n_k is the noise sample from the output of the correlator with variance given as

$$\mathrm{E}[n_k n_k'] = \frac{N_o}{2} g_{k,k'}. \tag{2.4}$$

For the case where orthogonal spreading sequences are used and chip and bit synchronism is maintained the cross-correlation $g_{k,k'} = 0$ for all $k \neq k'$. Therefore it is clear from (2.4) that in this special case no MAI is present and the receiver performance is identical to the single user case.

We can write the K matched filter outputs during the i-th signalling interval from (2.2) in a vector encompassing all K matched filter outputs as

$$\mathbf{y}_i = [\, y_0(i)\, y_1(i)\, \cdots\, y_{K-1}(i)\,]^{\mathrm{T}},.$$

Similarly vectors of transmitted bits and noise samples from all K matched filter outputs during the i-th signalling interval can be formed as

$$\mathbf{b}_i = [\, b_0(i)\, b_1(i)\, \cdots\, b_{K-1}(i)\,]^{\mathrm{T}},$$

and

$$\mathbf{n}_i = [\, n_0(i)\, n_1(i)\, \cdots\, n_{K-1}(i)\,]^{\mathrm{T}},$$

respectively. Writing a matrix of cross-correlations from (2.3) formed as $\mathbf{G}$: $G_{n,m} = g_{n,m}$ equation (2.2) may be rewritten in matrix form giving,

$$\mathbf{y}_i = \mathbf{G}\mathbf{b}_i + \mathbf{n}_i. \tag{2.5}$$

It should be noted that the AWGN has been transformed into a vector of correlated noise samples by the correlation process as shown in (2.4).

2.2 Pseudo-random Noise (PN) Sequences

A key element in SSMA systems lies in the generation and properties of the pseudo-random noise (PN) sequences used to distinguish one user in the system from another. The development of optimum sets of PN sequences has received much attention in an attempt to reduce the effect of MAI in conventional, correlator-type spread spectrum systems [6, 16, 36, 71].

In [65] the goals of good sequence design and selection are described as

- each sequence in the set being easy to distinguish from a time-shifted version of itself; the *auto-correlation property*,
- each sequence in the set being easily distinguishable from every other sequence in the set (including time-shifted versions of the sequences); the *cross-correlation property*.

For the most part non-military uses of spread spectrum systems have used linear, shift register feedback generators for sequence reproduction. While there has been some effort spent on non-linear sequence design, often with the goal of producing sequences of very long period in order to minimise eavesdropping, non-linear sequences [36, 54] are not considered in this thesis.

2.2.1 Maximal-length Sequences and their Derivatives

Maximal-length sequences, also known as m-sequences, form the basis for most of the other classes of linear spreading sequences [65]. The central work in this area is given in [22, 45, 65]. Maximal length sequences are so called, because they represent the set of linear feedback shift register generated sequences which have the longest period $N_s = 2^\nu - 1$, where ν is the sequence order corresponding to the length of the shift register in the sequence generator.

The generic linear feedback shift register generator is shown in Fig. 2.2. The state of the shift register is determined by the binary value of each shift register element and is written as $\mathrm{s} = [\,\underline{s}^1\,\underline{s}^2\,\cdots\,\underline{s}^\nu\,]^{\mathrm{T}}$.

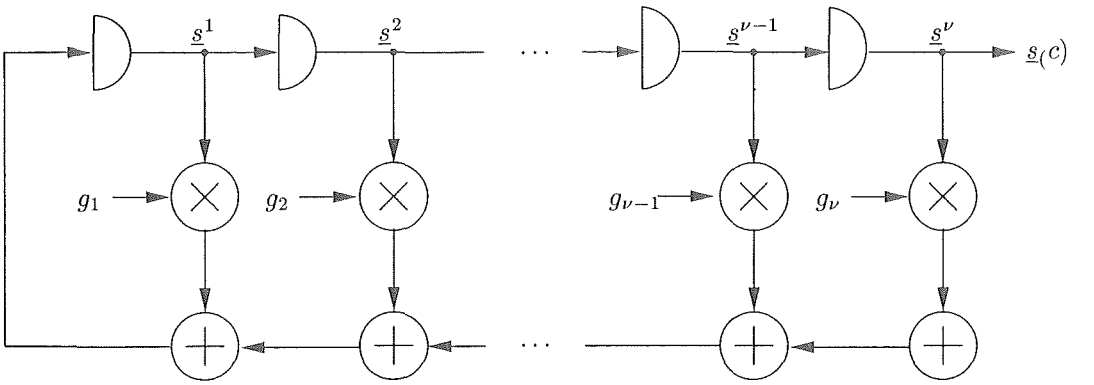

Figure 2.2: A linear feedback shift register PN-sequence generator.

TABLE 2.1
PRIMITIVE POLYNOMIALS FOR m-SEQUENCE GENERATION OF LENGTH 127, 255, AND 511 SPREADING SEQUENCES

degree, ν	generator polynomial (octal)
7	[211], [217], [235], [367], [277], [325], [203], [313], [345]
8	[435], [551], [747], [453], [545], [537], [703], [543]
9	[1021], [1131], [1461], [1423], [1055], [1167], [1541], [1333], [1605], [1751], [1743], [1617], [1553], [1157]

The gains g_ν at the inputs to the modulo-2 adders are binary elements and are the coefficients of the sequence generator polynomial [54]. Equivalently we may write the generator polynomial as a vector $\mathbf{g} = [\, g_1\, g_2\, \cdots\, g_\nu\,]^{\mathrm{T}}$. Maximal length sequences of period $N_s = 2^\nu - 1$ are generated by primitive polynomials of degree ν. Frequently in the literature generator feedback polynomials are represented in octal notation. In this thesis we use spreading sequences from the sets of sequences of length $N_s = 127, 255$, and 511 whose polynomial coefficients are provided in Table 2.1.

The sequence generator may be described in terms of a state transition matrix $\mathbf{F}$ which performs the transition from one state to the next. The j-th

state of the encoder is given by,

$$\mathbf{s}_j = \mathbf{F}^j \mathbf{s}_0 \qquad (\text{mod } 2). \tag{2.6}$$

where

$$\mathbf{F} = \begin{bmatrix} g_1 & g_2 & \cdots & g_{\nu-1} & g_\nu \\ 1 & 0 & \cdots & 0 & 0 \\ 0 & 1 & \cdots & 0 & 0 \\ \vdots & \vdots & \ddots & 0 & \vdots \\ 0 & 0 & 0 & 1 & 0 \end{bmatrix}. \tag{2.7}$$

In [45] the authors describe four properties which are said to belong to m-sequences, these properties are—

- *The Balance Property.* An m-sequence contains $2^{\nu-1}$ 1's and $2^{\nu-1}-1$ 0's.
- *The Window Property.* When a window of length ν is slid along the sequence each of the ν-tuples appear only once.
- *The "Runs" Property.* In an m-sequence 1/2 of all consecutive 1's or 0's (a run) are of length 1, 1/4 of all runs are of length 2, 1/8 are of length 3, and so on.
- *The Correlation Property.* An m-sequence has a two-valued periodic auto-correlation function given by

$$\hat{C}_{k,k}(m) = \sum_{i=0}^{N_s-1} \underline{s}_k(i)\underline{s}_k(i+m) = \begin{cases} N_s & m = 0 \\ -1 & \text{otherwise} \end{cases}. \tag{2.8}$$

The auto-correlation property is of particular importance in spread spectrum systems. From (2.8) is can be seen that an m-sequence can easily be distinguished from a time shifted version of itself.

There exist sets of maximal length sequences that minimise the discrete cross-correlation. These are known as *preferred pairs* and have a three valued

cross-correlation which can be bounded by [45]

$$\|\hat{C}_{k,k'}(m)\| \leq -1 + 2 \cdot 2^{(\nu+2)/2}. \tag{2.9}$$

In asynchronous spread spectrum systems the discrete aperiodic cross-correlation function is important because the timing boundaries between signalling intervals of different users are not (necessarily) the same—each user transmits without a common signal timing reference. The discrete aperiodic cross-correlation function is defined as

$$C_{k,k'}(m) = \begin{cases} \sum_{i=0}^{N_s-1-m} \underline{s}_k(i)\underline{s}_{k'}(i+m) & \text{for } 0 \leq m \leq N_s - 1 \\ \sum_{i=0}^{N_s-1+m} \underline{s}_k(i-m)\underline{s}_{k'}(i) & \text{for } 1 - N_s \leq m < 0 \\ 0 & \text{otherwise} \end{cases} \cdot \tag{2.10}$$

A relationship exists between the periodic and aperiodic functions. To illustrate consider the case in a two user system where one user transmits the all 1's sequence and where two consecutive bits of the second user are the same. If the two users are delayed by m chips then the periodic cross-correlation (also called the *even cross-correlation function*) between them is the sum of the two aperiodic cross-correlations:

$$\hat{C}_{k,k'}(m) = C_{k,k'}(m) + C_{k,k'}(m - N_s) \qquad \text{for } 0 \leq m < N_s.$$

If the two consecutive information symbols are different then the *odd cross-correlation function* is the difference of two aperiodic cross-correlation functions:

$$\hat{C}'_{k,k'}(m) = C_{k,k'}(m) - C_{k,k'}(m - N_s) \qquad \text{for } 0 \leq m < N_s.$$

Numbers of other sequence sets exist including Gold Sequences, Kasami Sequences and McEliece Sequences [65]. Gold sequences provide larger sets of sequences than m-sequences of the same length, while providing good correlation properties [64]. Gold sequences are formed by the chip-wise multiplication of two preferred pairs of m-sequences. Other sets include Kasami and McEliece sequences [65].

2.3 *Timing Recovery and Spreading Sequence Acquisition*

Synchronisation of a receiver to the spreading sequences is fundamental to the operation of spread spectrum systems. The aim of acquisition algorithms is to align the spreading sequences used in a system to within a fraction of a chip period. More precise chip alignment is performed by tracking algorithms.

A number of schemes exist to achieve synchronisation including brute force correlation and sliding-correlation methods [55], both of which are variations of *serial search techniques.* These involve the de-spreading of the signal by a hypothesised spreading sequence. If the hypothesised spreading sequence is correct then the output of the correlator or matched filter is greater than a pre-determined threshold, otherwise the received signal is de-spread with the next hypothesised spreading sequence. The set of hypothesised spreading sequences not only contains the set of all basic spreading sequences, but also all of their time shifted versions. The process continues until all spreading sequences have been found. Consequently, the acquisition system is an energy detection problem at the output of the correlator bank. These types of acquisition schemes are also known as low-rate-decision detectors since a large number of chips are required to be received in order to minimise the false alarm probability which is a function of the number of chips over which the correlation occurs and the signal-to-noise and interference ratio [56, 57, 75]. Multi-user detectors (to be discussed in the next section) must recover the spreading sequences of all K users. This goal can be achieved by a bank of K sequence detectors or a smaller number of detectors performing sequence detection for multiple users, one user at a time. The number of users that can be supported by one sequence detector is a function of the maximum tolerable acquisition time and the rate at which users require sequence acquisition. In some scenarios pilot sequences are used reducing the complexity of, or eliminating, the aquisition phase.

Other techniques exist such as the *rapid acquisition by sequential estimation*

(RASE) where the received chips are loaded directly into a shift register [97]. Clearly this technique is not suitable in a multiple access environment.

Spreading sequence tracking is performed by using phase-locked techniques some-what analogous to those used in coherent detection [55]. The main difference between tracking algorithms for sequence tracking and carrier phase tracking is in the discriminator [54]. The early work by Spilker and Magill [82] showed that the proper error signal could be derived from the received signal correlated with a generated first derivative of the spreading signal. The techniques of [82] have been refined in later work [25, 74, 98]. Summaries of code tracking algorithms and techniques are provided in [54, 78].

In the analogue domain the Phase-Locked Loop (PLL) is often employed to perform phase tracking of received signals. The digital equivalent is the Delay-Locked Loop (DLL) which performs delay tracking. The two systems are fundamentally similar. The major difference between the two is that the PLL has a periodic phase characteristic whereas the DLL does not. The DLL consists of a multiplier, a loop filter and the locally generated spreading sequence voltage-controlled source which takes the output from the loop filter as the control input to adjust the delay of the local sequence. The product of the local sequence and the received signal is filtered by the loop filter to obtain a term which is proportional to the difference in delay, this term becomes the control from which the local sequence source retards or advances the delay of the local sequence.

2.4 Multi-User Detection

The first paper published on multi-user detection for SSMA was by Schneider [69] who studied the zero-forcing decorrelating receiver. His receiver structure consisted of the forward-backward processing Viterbi receiver. The seminal paper in the field of multi-user detection was Verdú's treatment of optimum maximum-likelihood (ML) sequence detection of [91]. This detector performs an exhaustive search of all the possible transmitted sequences, choosing the

most likely through a maximisation of the joint *a posteriori* probability. A huge performance improvement was shown by the Verdú optimum receiver compared to the conventional correlator detector.

The conventional correlator receiver is optimal for the case of a single user in an additive Gaussian white noise channel. When non-orthogonal spreading sequences are utilised, multiple access interference results. In a multi-user system with multiple access interference the performance of this system is degraded. As stated earlier, there has been a lot of research effort aimed at reducing the MAI by the synthesis and exploitation of spreading sequences with low cross-correlation properties. In a bit synchronous system the use of Hadamard sequences, which are orthogonal when bit synchronism is maintained and no inter-symbol interference is present, reduces the MAI to zero and the correlator receiver performance is optimal [83, 96]. This was shown earlier in (2.4). Another way to improve the performance of multi-user systems is to exploit the knowledge about the structure and statistical properties of the MAI and to jointly detect all users in the system, thereby reducing the system's sensitivity to MAI.

The main impediment to the widespread application of the optimum detector is that it is exponentially complex in the number of users in the system. A research goal of recent times has been to reduce the complexity of the receiver without losing too much in performance. Suggestions for suboptimum multi-user receivers based on the ML algorithm are found in [62, 68, 99, 100].

The general multi-user receiver is shown in Fig. 2.3. It consists of a sequence-matched filter bank filtering the received signal at the i-th signalling interval $\mathbf{r}_i$ with the spreading sequences of each user. The corresponding sampled matched filter outputs $\mathbf{y}_i$ are given to the multi-user detector.

In the following we discuss some of the more common multi-user detectors. A hierarchy of various sub-optimal MUD techniques is given in Fig. 2.4. Sub-optimal receivers fall mostly into two categories—linear and non-linear receivers. In linear multi-user detection a linear transformation is applied to

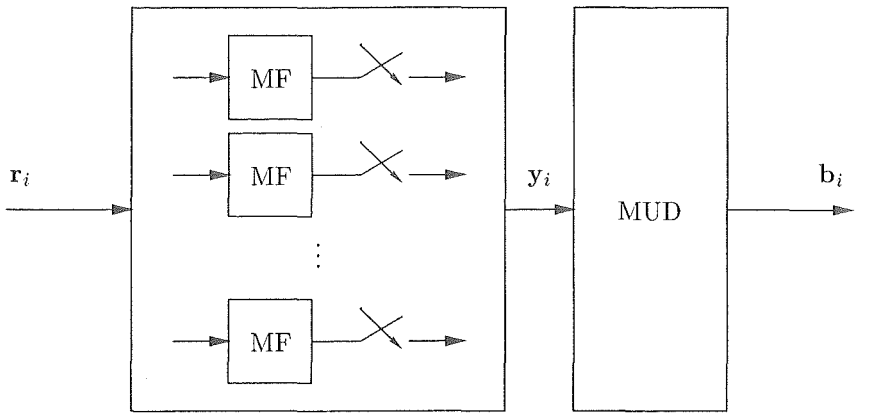

Figure 2.3: The generalised multi-user receiver: a bank of matched filters (correlators) and the Multi-User Detector (MUD).

the soft outputs of the conventional detector to produce decision variables in which the multiple access interference is greatly decoupled. Two of the most frequently cited linear multi-user schemes are the decorrelating detector [44] and the MMSE detector [101].

In non-linear multi-user detection systems (also called subtractive detection, or interference cancelling detection), interference estimates are removed from the received signal before detection. The novel detection techniques presented in this thesis are types of intereference cancellers whose interference estimates are deduced (in a maximum-likelihood sense) from the observation of other users' signals.

In the following discussion of some of the most important receiver types we will assume synchronous transmission for the sake of simplicity. This provides simple models for the study of these techniques. In most cases generalisations to asynchronism, and fading and multi-path channels are possible.

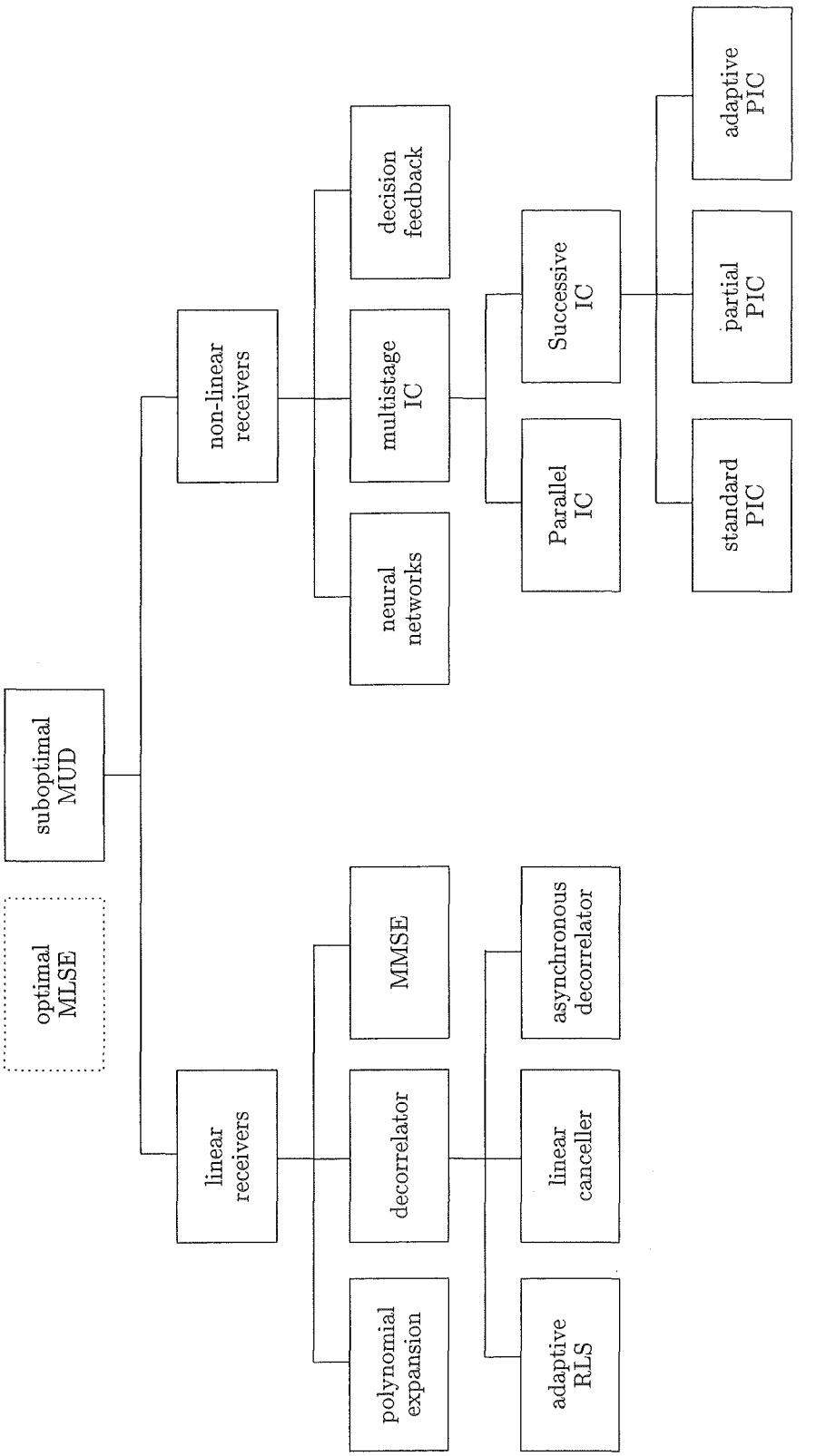

Figure 2.4: Hierarchy of various sub-optimal multi-user spread sprectrum systems.

2.4.1 Conventional Multi-User Detector

The conventional multi-user detector is merely a bank of decision devices, following the matched filter bank, estimating the transmitted bit vector as[1],

$$\begin{aligned}\hat{\mathbf{b}}_i &= \operatorname{sgn}(\mathbf{y}_i) \\ &= \operatorname{sgn}(\mathbf{G}_i\mathbf{b}_i + \mathbf{n}_i)\,. \end{aligned} \tag{2.11}$$

Note that in this case the receiver treats the MAI as noise. For non-orthogonal sequences or bit asynchronism among users, a large number of users in the system results in a greater combined noise and interference term and hence a greater probability of error for a given bit energy to noise power spectral density ratio. Techniques to accurately determine the performance of conventional spread spectrum systems employing Gaussian assumptions and models can be found in [49, 54, 60] and others.

2.4.2 Coded Conventional Multi-User Detectors

In this section we introduce the fading channel. We will show that forward error correction convolutional coding multi-user detectors in the slowly fading channel require computationally complex codes to obtain a similar error-rate performance to the single user detector in the same environment. This result is used to focus attention towards joint-detection multi-user detectors.

In a single-user SSMA system proposed by Viterbi [94] all spreading is performed by a low-rate convolutional code. A multi-user detector based on this single-user receiver consists of a bank of single-user receivers similar to the uncoded structure of the previous section. A sequence unique to each user, which we now call a masking sequence since it does not spread the encoded data, is added modulo-2 to the encoder output randomising the encoded data with respect to the other users in the system. At the receiver the desired user's

[1] the vector form of the Signum function is defined as $\operatorname{sgn}(\mathbf{y}_i) \triangleq [\operatorname{sgn}(y_0)\ \operatorname{sgn}(y_1)\ \cdots\ \operatorname{sgn}(y_{K-1})]$.

masking sequence is applied to the received multiple access signal before it is decoded to detect the user's data sequence.

The system consists of a rate-$1/N_s$ encoder for each user emitting a code sequence $\mathbf{c}_k(i)k = 0, 1, \cdots, K-1$ in the i-th bit interval. A pseudo-random noise (PN) signal is modulo-2 added to the code sequence. Note that the code sequence and the PN-sequence are of equal rates, so no spreading is performed by the PN-sequence which we now call the masking sequence. The masking sequence 'randomises' each user's signal, thus providing addressing information. Furthermore, the masking sequence tends to break up long runs of 1's and 0's in the encoder output.

Note that the combination of the encoder and the non-spreading masking sequence may describe:

- a fully coded spread spectrum system where all spreading is performed by the code—the encoder is a rate-$1/N_s$ convolutional encoder of constraint length κ with free distance d_f and code-weight spectrum $\beta(d)$;

- a conventional spread spectrum system—the encoder is a rate-$1/N_s$ repetition code ($\kappa = 1$, $d_f = N_s$, and $\beta(d_f) = 1$);

- a partially coded and sequence spread system—the encoder is a concatenation of a rate-$1/N_s'$ convolutional encoder (of constraint length κ, minimum distance d_f' and code-weight spectrum $\beta'(d)$) and a rate-$1/N_s''$ repetition encoder ($d_f'' = N_s''$). The concatenated code has rate $1/N_s = 1/N_s'N_s''$, constraint length κ, free distance $d_f = d_f'd_f''$, and code-weight spectrum $\beta(d) = \beta'(d_f''d)$.

The coherent receiver with K users receives the baseband signal written as,

$$r(t) = \sum_{i=0}^{N-1} \sum_{k=0}^{K-1} c_k(t - iT - \tau_k) h_0(t) \cos\phi_k s_k(t - iT - \tau_k) + n(t), \qquad (2.12)$$

where N is the number of transmitted bits, $s_k(t)$ and $c_k(t)$ are the masking chip and code word signals of the k-th user during the i-th signalling interval.

$h_0(t)$ is the flat fading process, ϕ_k the relative carrier phase, and $n(t)$ is the white noise with double sided power spectral density $N_o/2$. We assume that this receiver is synchronised to the 0-th user so $\phi_0 = 0$ and that the relative delay variable $\tau_0 = 0$.

After the 'derandomising' of the 0-th user by the modulo-2 addition of the masking sequence we have an estimate of the transmitted code sequence due to the 0-th user in vector form[2] for the i-th signalling interval written as

$$\hat{\mathbf{c}}_i = \mathrm{diag}(\mathbf{c}_i)\,\mathbf{h}_i + \boldsymbol{\gamma}_i, \tag{2.13}$$

where $\boldsymbol{\gamma}_i$ is a vector encompassing the noise and interference terms and $\mathbf{h}_i$ is a vector of the fading process from the channel state estimator (we assume here perfect channel state information) which we assume constant over the chip interval. We have dropped the superscript denoting the 0-th user for notational convenience since we need not distinguish between users in the system as the multiple access interference is lumped into the $\boldsymbol{\gamma}_i$ term. We consider the combined noise and interference term of the received signal (2.13) to be a vector of statistically independent complex Gaussian random variables [30].

A maximum likelihood (ML) decoder will select the code sequence $\mathbf{c}$ from the set of all possible sequences for which the *a posteriori* probability $\Pr(\mathbf{c}|\hat{\mathbf{c}}, \mathbf{h})$ is the largest; that is, given the estimated sequence $\hat{\mathbf{c}} = [\,\hat{\mathbf{c}}_0\,\hat{\mathbf{c}}_1\,\cdots\,\hat{\mathbf{c}}_{N-1}\,]$ and the channel state estimate sequence $\mathbf{h} = [\,\mathbf{h}_0\,\mathbf{h}_1\,\cdots\,\mathbf{h}_{N-1}\,]$, the decoder chooses the most likely transmitted sequence $\mathbf{c}$. This is equivalent to choosing the sequence $\mathbf{c}$ with the largest conditional probability density function $p(\hat{\mathbf{c}}, \mathbf{h}\,|\,\mathbf{c})$, which is jointly Gaussian since $\mathbf{c}$ and $\mathbf{h}$ are Gaussian variables [59].

Equivalently [89], the decoder chooses the sequence $\mathbf{c}$ corresponding to the smallest of 2^N path metrics formed from the probability density function. The metric corresponding to the code sequence $\mathbf{c}$ is

$$\Omega(\mathbf{c}) = (\hat{\mathbf{c}} - \mathrm{diag}(\mathbf{c})\,\mathbf{h})^{\mathrm{T}}(\hat{\mathbf{c}} - \mathrm{diag}(\mathbf{c})\,\mathbf{h}), \tag{2.14}$$

[2] $\mathrm{diag}(\mathbf{x})$ is an $N \times N$-matrix whose elements on the main diagonal are the elements of the N-length vector $\mathbf{x}$.

and can be shown to be suitable for processing by the Viterbi Algorithm where the maximisation occurs over a sum of branch metrics $\bar{\Omega}(\mathbf{c}_i)$,

$$\begin{aligned}\Omega(\mathbf{c}) &= \sum_{i=0}^{N-1} \bar{\Omega}(\mathbf{c}_i) \\ &= \sum_{i=0}^{N-1} (\hat{\mathbf{c}}_i - \mathrm{diag}(\mathbf{c}_i)\,\mathbf{h}_i)^{\mathrm{T}} (\hat{\mathbf{c}}_i - \mathrm{diag}(\mathbf{c}_i)\,\mathbf{h}_i). \end{aligned} \tag{2.15}$$

For the conventional spread spectrum system with no coding and $\kappa = 1$ the sequence receiver reduces to a symbol-based receiver.

If the transmitted code sequence is $\mathbf{c}$, the decoder will pick an erroneous sequence $\mathbf{c}'$ if $\Omega(\mathbf{c}') < \Omega(\mathbf{c})$. Defining the decision variable $\Delta = \Omega(\mathbf{c}') - \Omega(\mathbf{c})$, the probability of selecting an incorrect sequence may be written as $\Pr(\Delta < 0)$.

Following [27, 28, 89], the decision variable may be written as

$$\Delta = \mathbf{w}^{\mathrm{T}} \mathbf{F} \mathbf{w} \tag{2.16}$$

where $\mathbf{w} = [\,\hat{\mathbf{c}}\,\mathbf{h}\,]^{\mathrm{T}}$, $\Theta_{\mathbf{ww}}$ is the correlation matrix of $\mathbf{w}$, and $\mathbf{F} = \Theta_{\mathbf{ww}}^{-1}|\mathbf{c}' - \Theta_{\mathbf{ww}}^{-1}|\mathbf{c}$.

The two-sided Laplace transform of the characteristic function of the decision variable is

$$\Psi_{\Delta}(s) = \frac{1}{\det(\mathbf{I} + 2s(\Theta_{\mathbf{ww}}|\mathbf{c}\Theta_{\mathbf{ww}}^{-1}|\mathbf{c}' - \mathbf{I}))} \tag{2.17}$$

The pairwise error event probability can be found by the appropriate integration of the inverse Laplace transform of $\Psi_{\Delta}(s)$ (giving the probability density function of Δ). Following [27, 28, 89] it is simpler to calculate the probability as,

$$\Pr(\mathbf{c} \to \mathbf{c}') = \Pr(\Delta < 0) = -\sum_{\text{RP poles}} \text{Residue}\, \frac{\Psi_{\Delta}(s)}{s}, \tag{2.18}$$

where the notation 'RP poles' refers to the right-half plane poles of the (Laplace transform) characteristic function of the decision variable Δ, $\Psi_{\Delta}(s)$. The characteristic function may be written as

$$\Psi_{\Delta}(s) = \prod_{n} \frac{-p_n}{s - p_n}, \tag{2.19}$$

where the poles p_n are related to the eigenvalues λ_n of $\Theta_{\mathbf{ww}}\mathbf{F}$ by $p_n = -(2\lambda_n)^{-1}$.

In the cases of very fast and very slow fading the eigenvalues of the correlation matrices can be determined analytically. The very slow fading approximation is important since it approximates the mobile radio channel as discussed in chapter 1. The very fast fading case may be applied to the situation where we have strict timing and choose to interleave the transmitted chips.

We may obtain an analytical expression for the system performance in the special case of a system with very fast fading where the normalised Doppler frequency $f_D T \to \infty$ corresponding to a system with a channel correlation matrix $\Theta_{\mathbf{hh}} = E_c\mathbf{I}$, that is the fading between chips is independent, where E_c is the chip energy. In this case we can show that there is one pair of d-order poles of $\Psi_\Delta(s)$ where d is the Hamming distance between $\mathbf{c}$ and $\mathbf{c}'$. These are given by,

$$p_1, p_2 = \frac{1}{4\frac{E_c}{\Upsilon} \pm 4\sqrt{\left(\frac{E_c}{\Upsilon}\right)\left(1+\frac{E_c}{\Upsilon}\right)}}, \tag{2.20}$$

where $\Upsilon = \boldsymbol{\gamma}_i^{\mathrm{T}}\boldsymbol{\gamma}_i$ is the noise and interference power. Now from (2.18), [41] the pairwise probability of error is

$$\begin{aligned}\Pr(\mathbf{c}\to\mathbf{c}') &= -\frac{1}{(d-1)!}\lim_{s\to p_1}\frac{\partial^{d-1}}{\partial s^{d-1}}(s-p_1)^d\frac{p_1^d p_2^d}{s(s-p_1)^d(s-p_2)^d}\\ &= -\frac{p_1^d p_2^d}{(d-1)!}\lim_{s\to p_1}\frac{\partial^{d-1}}{\partial s^{d-1}}\frac{1}{s(s-p_2)^d}.\end{aligned} \tag{2.21}$$

By partial fraction expansion we can show that the derivative in (2.21) is

$$\frac{\partial^{d-1}}{\partial s^{d-1}}\frac{1}{s(s-p_2)^d} = (-1)^{d-1}\sum_{n=1}^{d}\frac{(d-2+n)!}{s^{d-n+1}(n-1)!(s-p_2)^{d+n-1}}. \tag{2.22}$$

Combining (2.21) and (2.22) gives the exact pairwise error probability as

$$\begin{aligned}\Pr(\mathbf{c}\to\mathbf{c}';\Upsilon) &= \frac{-p_1^d p_2^d}{(d-1)!}\sum_{n=1}^{d}\frac{(d-2+n)!}{p_2^{d-n+1}(n-1)!(p_2-p_1)^{d+n-1}}\\ &= 1-\frac{\Gamma(d+\frac{1}{2})}{2\sqrt{\pi}\Gamma(d+1)(1+\frac{E_c}{\Upsilon})^d}\ {}_2\mathrm{F}_1\left(\begin{matrix}1, 2d\\ 1+d\end{matrix}; \frac{1}{2}\left\{1+\sqrt{\frac{\frac{E_c}{\Upsilon}}{1+\frac{E_c}{\Upsilon}}}\right\}\right),\end{aligned} \tag{2.23}$$

where $\Gamma(\cdot)$ is the Euler gamma function, ${}_2\mathrm{F}_1(\cdot)$ is the hypergeometric function, and we write $\Pr(\mathbf{c} \to \mathbf{c}'; \Upsilon)$ to explicitly show that Υ is a parameter of the pairwise error probability. An approximation to (2.23) can be obtained, as shown by van Nobelen [89], and is written as

$$\Pr(\mathbf{c} \to \mathbf{c}') = \left(\frac{1}{4d\frac{E_b}{\Upsilon N_s}} \right)^d \frac{(2d-1)!}{d!(d-1)!}, \tag{2.24}$$

which is in turn an improved approximation on the upper bound from Divsalar and Simon [10]. What van Nobelen did not show, however, is that (2.24) is identical to the well known result of [59] for Rayleigh fading with d-th order diversity.

Very slow fading ($f_D T \to 0$) results in a correlation matrix $\Theta_{\mathbf{ww}}\mathbf{F}$ with only two non-zero eigenvalues giving in an expression for the pairwise error probability [89] as,

$$\Pr(\mathbf{c} \to \mathbf{c}'; \Upsilon) = \frac{1}{2 + 2d\frac{E_b}{\Upsilon N_s} + 2\sqrt{\frac{E_b}{\Upsilon N_s} d^2 + d\frac{E_b}{\Upsilon N_s}}}. \tag{2.25}$$

For high signal-to-noise and interference ratio the error probability is tightly bounded by

$$\Pr(\mathbf{c} \to \mathbf{c}') = \frac{1}{4d\frac{E_b}{\Upsilon N_s}}, \tag{2.26}$$

which has the same inverse E_b/N_o characteristic as the flat fading uncoded system. In fact we can show that in the very slow flat fading channel low rate convolutional coding performance is similar to the uncoded case. Consider the Hadamard convolutional code which has the signal flow graph transfer function [93] given by,

$$T(D, I) = \frac{ID^{\kappa 2^{\kappa-1}}(1 - D^{2^{\kappa-1}})}{1 - D^{2^{\kappa-1}}[1 + I(1 - D^{(\kappa-1)2^{\kappa-1}})]}, \tag{2.27}$$

where D is the signal-flow graph parameter whose exponent describes the Hamming weight of the branch and I indicates a branch transition in the code trellis caused by the 1-bit entering the encoder. The code weight spectra of Hadamard

codes are easily determined. If we optimistically approximate the upper bound on the probability of bit error by considering only the first term of the union bound then we may write the probability of bit error for the very slow and very fast fading channel as

$$P_b \approx \frac{1}{\frac{\kappa}{2}\frac{E_b}{N_o}}, \tag{2.28}$$

and

$$P_b \approx 4\binom{\kappa 2^{\kappa-1}-1}{\kappa 2^{\kappa-1}}\left(\frac{1}{2\kappa\frac{E_b}{N_o}}\right)^{\kappa 2^{\kappa-1}}, \tag{2.29}$$

respectively. Comparing (2.28) with the well known uncoded performance in flat fading shows that utilising the Hadamard code in the very slow fading channel requires a code with a constraint length in the neighbourhood of seven to experience no performance degradation with respect to the single user receiver. Furthermore, reviewing the foregoing reveals that the effect of MAI on the error performance of a system employing coding in the very slow fading channel is equivalent to the uncoded case.

This suggests that in the presence of very slow fading, as we expect in the mobile radio channel as discussed in chapter 1, complex convolutional codes or coding schemes are required for convolutionally coded spread spectrum systems. However, in this thesis we are concerned with reduced complexity systems—a requirement which, in light of the foregoing suggests that we should turn our attention to other methods.[3]

2.4.3 Maximum Likelihood Detector

It is shown in [59] that the vectors of correlator outputs given by $\mathbf{y}_i$ are sufficient statistics for optimum detection. The optimum receiver maximises the the *a posteriori* probability $p(\mathbf{b} \mid \mathbf{y})$ where the vectors $\mathbf{b}$ and $\mathbf{y}$ are given by

$$\mathbf{b} = [\,\mathbf{b}_0^{\mathrm{T}}\,\mathbf{b}_1^{\mathrm{T}}\,\cdots\,\mathbf{b}_{N-1}^{\mathrm{T}}\,]^{\mathrm{T}} \tag{2.30}$$

[3] It should be mentioned here that this does not preclude coding from any system design. Coding provides a means of achieving a power margin over the optimal detector.

and

$$\mathrm{y} = [\,\mathrm{y}_0^{\mathrm{T}}\,\mathrm{y}_1^{\mathrm{T}}\,\cdots\,\mathrm{y}_{N-1}^{\mathrm{T}}\,]^{\mathrm{T}} \tag{2.31}$$

respectively and where N is the number of signalling intervals. This is equivalent (by Bayes' Theorem) to selecting the vector $\mathbf{b}$ with the largest conditional probability density function $p(\mathrm{y} \mid \mathbf{b})$ since the transmitted vectors are assumed equiprobable. Assuming transmission over an AWGN channel the density function for the NK-dimensional noise vector $\mathbf{n}$ is given by,

$$p(\mathrm{y}|\mathbf{b}) = \frac{1}{(2\pi)^{K/2}|N_o\mathbf{G}|^{1/2}} \exp\left(-\frac{1}{2}(\mathrm{y}-\mathbf{G}\mathbf{b})^{\mathrm{H}}\frac{1}{N_o}\mathbf{G}^{-1}(\mathrm{y}-\mathbf{G}\mathbf{b})\right). \tag{2.32}$$

Therefore the ML decision corresponds to selecting the estimate of the transmitted vector which results in the noise realisation with minimum energy with respect to all other possible transmitted vectors. Taking the natural logarithm of (2.32) results in the log likelihood function. Noting that the first term of the log-likelihood function is independent of the transmitted vector and that the correlation matrix is Hermitian, the decision metric for the maximum likelihood receiver is proportional to the logarithm of (2.32) and may be written as,

$$\Omega(\mathbf{b}) = 2\mathrm{y}^{\mathrm{T}}\mathbf{b} - \mathbf{b}^{\mathrm{T}}\mathbf{G}\mathbf{b}. \tag{2.33}$$

The receiver then estimates the transmitted vectors given by the vectors which maximise the decision metric, or written as

$$\hat{\mathbf{b}}_i = \arg\max_{\tilde{\mathbf{b}}} \left(2\mathrm{y}_i^{\mathrm{T}}\tilde{\mathbf{b}} - \tilde{\mathbf{b}}^{\mathrm{T}}\mathbf{G}\tilde{\mathbf{b}}\right). \tag{2.34}$$

The receiver structure in the case of user synchronism is a symbol-by-symbol detector (assuming that each user's tranmitted bits are independent). As we will shown in the next chapter when we introduce asynchronous detection and the Verdú optimum receiver [91], asynchronous transmission results in an optimum receiver exhibiting a trellis structure with 2^K states[4].

[4] Verdú showed that half the states are equivalent due to a $(K-1)$-bit dependance between signalling intervals. Therefore, the complexity of the optimum receiver is proportional to 2^{K-1}

While the ML receiver is optimum in that it minimises the bit error rate, it has a complexity that is exponential in the number of users. In the following sections we summarise sub-optimal receiver structures with lower complexity.

A number of authors have proposed sub-optimal schemes based on the MLSE receiver [17], [18], [24]. The sub-optimum detectors in [24] are linear decision feedback receivers that require sorting of the survivor paths at each iteration. In [17] and [18] the authors propose a multi-trellis receiver structure, the simplest of consists of six trellis structures—three four-state, and three two-state trellises. The system is iterative in nature, and while it performs well for heavily loaded systems, the performance with imperfect power control is worse than that of the correlator at high signal to noise ratios.

2.4.4 Linear Decorrelating Detector

It is straightforward for the receiver to eliminate the inter-user interference when the receiver has knowledge of all the users' spreading sequences. The decorrelating receiver [44, 13, 14, 50] multiplies the vector of correlator outputs by the inverse of the correlation matrix $\mathbf{G}^{-1}$. The application of the Signum function to the product gives the detection result, namely

$$\begin{aligned}\hat{\mathbf{b}}_i &= \operatorname{sgn}\left(\mathbf{G}^{-1}\mathbf{y}_i\right) \\ &= \operatorname{sgn}\left(\mathbf{b}_i + \mathbf{G}^{-1}\mathbf{n}_i\right).\end{aligned} \tag{2.35}$$

The multiplication of the noise vector with the inverse correlation matrix may result in noise 'amplification'. Consequently the linear decorrelating detector is sub-optimal with respect to the maximum-likelihood detector. The degree to which the receiver is sub-optimal is a function of the matrix of sequence correlations $\mathbf{G}$ since any noise amplification is a result of this matrix. The minimum mean square error (MMSE) detector [1, 50] alleviates this problem with knowledge of the signal amplitudes and noise variance and the decorrelating detector detection output becomes, for the MMSE receiver,

$$\hat{\mathbf{b}}_i = \operatorname{sgn}\left((\mathbf{G} + N_o\mathbf{I})^{-1}\mathbf{y}_i\right), \tag{2.36}$$

where $\mathbf{I}$ is the identity matrix. For high signal to noise ratio the MMSE receiver's performance is asymptotic to the decorrelating receiver. At higher noise levels the MMSE receiver appears as the conventional correlating detector.

The complexity of the decorrelating and MMSE detectors is linear in the number of users in the system but each time the channel changes the inverse of the correlation matrix must be recalculated. In [32] an iterative structure is used avoiding the need to recalculate the correlation matrix.

2.4.5 Polynomial Expansion Detector

In [50] Moshavi describes the polynomial expansion detector which applies a polynomial expansion to the correlation matrix $\mathbf{G}$ as

$$\hat{\mathbf{b}}_i = \operatorname{sgn}\left(\left(\sum_{i=0}^{N_{pe}} w_i \mathbf{G}^i\right)\mathbf{y}_i\right), \tag{2.37}$$

producing a detector with $N_{pe}+1$ stages.

For a given $\mathbf{G}$ and polynomial degree, polynomial coefficients can be chosen to optimise the performance of the receiver. It can be shown that the detector can exactly implement the decorrelating detector for a finite message length, that is the appropriate choice of polynomial coefficients can lead to the summation approximating $\mathbf{G}^{-1}$. While for useful message lengths the number of stages is prohibitively large, good approximations are obtained for small numbers of stages [50].

2.4.6 Interference Cancellation Detectors

A large class of detectors exist which are called *interference cancellation detectors*. The principle of these receivers is the estimation of the MAI contributed by each user in order to subtract out some or all of the MAI seen by each user. Study of the maximum likelihood and polynomial expansion receivers reveals that these two receivers are in fact also kinds of interference cancellation receivers.

The first type of interference canceller is the *successive interference cancellation* (SIC) receiver [40, 94]. This results in multistage structures where at each successive stage the strongest user is detected, regenerated and removed. In this way successive stages observe fewer users and hence less MAI. The reasons for performing the cancellation on a received power level basis are three-fold—(a) it is easier to acquire and demodulate the stronger users, (b) removing the stronger users first provides greater benefit to weaker users and (c) stronger users observe relatively less MAI than weaker users. Difficulties with this type of detector include delay time since one bit of delay time occurs for each user, the requirement to re-order users when the power profile changes (which may occur frequently in a fading, dynamic channel) and the requirement for amplitude estimation.

The *parallel interference cancellation* (PIC) detector [39, 40, 90] estimates and removes all of the MAI for each user in parallel. These systems estimate the bits of all users, re-spread all estimates to form an estimate of the MAI and subtract this estimate from the received signal. These systems are often used in many stages with each stage using estimates from the previous stage [50]. The use of a decorrelating detector as the first stage has been suggested [50]. Contributions of multistage structures with soft decisions are found in [4, 50]. Weighted interference schemes with adaptive weights were proposed in [104].

Other types include hybrid structures formed with successive and parallel canceller operating on groups of users are presented in [37] and decision feedback detectors with a noise-whitening filter of [13, 14].

2.4.7 Performance

A direct performance comparision between linear and interference cancelling schemes is presented in [5] for various conditions, such as perfect power control and Rayleigh fading. The authors conclude that for receivers with power control the parallel intereferance cancellers perform best. MMSE and decorre-

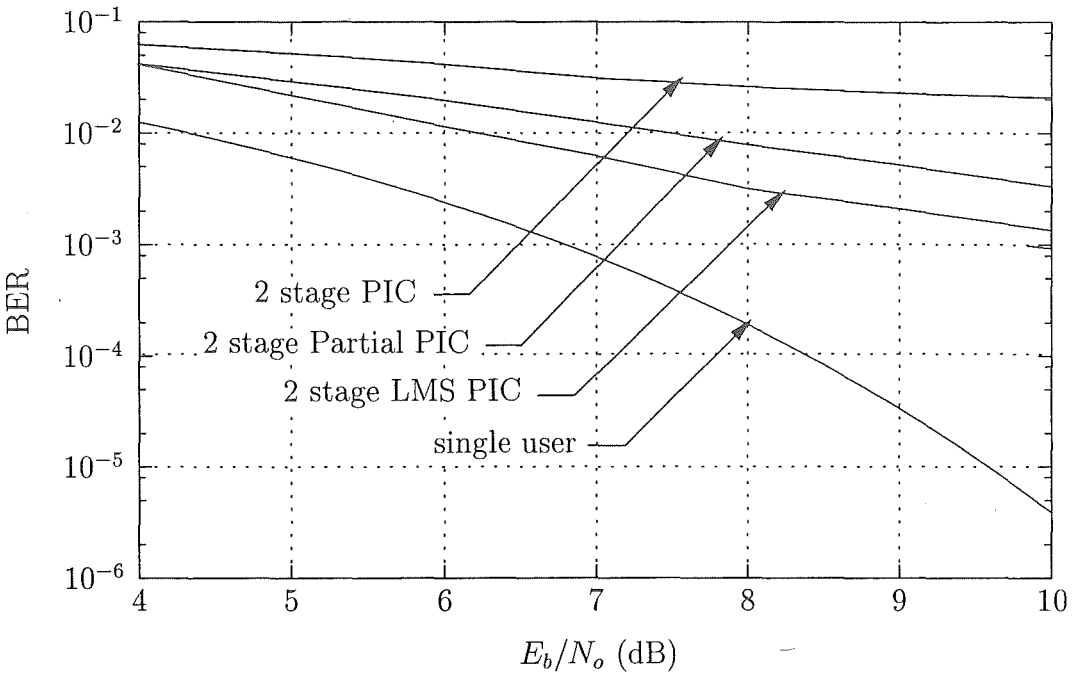

Figure 2.5: Performance comparision of various parrellel interference cancellation (PIC) schemes with 30 users in AWGN.

lating detectors have a similar performance. Linear receivers begin to perform better for bit energy to noise power spectral density ratios $E_b/N_o > 15$ dB.

In a more recent paper [33] the performance of interference cancellers was compared to the decorrelating detector in multipath Rayleigh fading channels. Their results showed that the linear detectors only had performance advantages over interference cancellers in cases where the near-far problem was particularly severe.

Comparisions between successive interference cancellers and parallel interference cancellers have also be presented [53]. The results showed that in cases where power control was used PIC detectors performed better than SIC, but in the case of a two-ray Rayleigh fading channel their performance was similar.

In Figs 2.5 and 2.6 we present performance curves for three types of PIC receivers with 30 users in AWGN and a two-ray Rayleigh fading channel.

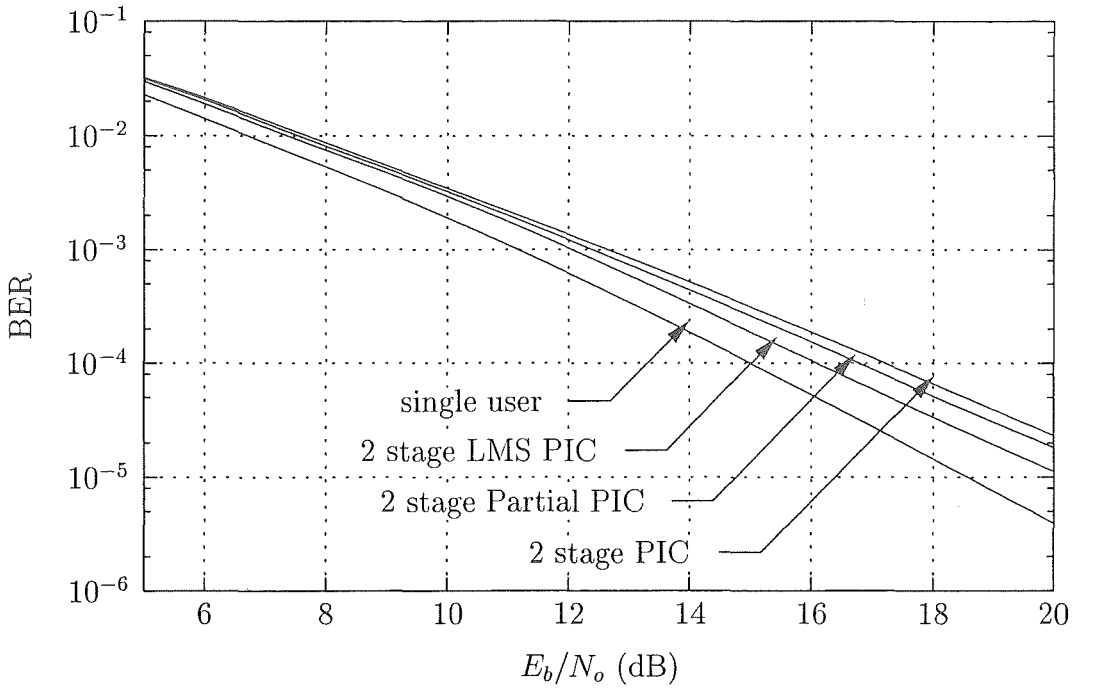

Figure 2.6: Performance comparision of various parrellel interference cancellation (PIC) schemes with 30 users in a three path Rayleigh Fading Channel.

2.5 Conclusions

In this chapter the concept of spread spectrum communications was presented. We showed how by applying a unique high rate binary spreading sequence to a users data sequence the data sequences from many users could be separated at the receiver. Properties and classes of spreading sequences were discussed and methods for the acquisition and tracking of these were summarised.

An overview of current multi-user detection techniques was presented. We showed that the conventional multi-user detector in the fading channel with forward error correcting convolutional coding requires computationally complex (high constraint length) codes in order to achieve an error rate performance similar to that of the single user receiver. This result indicates that for low complexity solutions to the multi-user detection problem we need to focus on joint detection methods.

Existing classes of joint detection methods for multi-user detection were

summarised. In the following chapters we develop three new families of joint detection based multi-user detectors based on the maximum likelihood detector.

Chapter 3

A REDUCED COMPLEXITY RECEIVER STRUCTURE

3.1 Introduction

In chapter 2 it was shown that conventional correlator spread spectrum multiple access (SSMA) systems treat multiple access interference (MAI) as white noise. The white noise assumption lumps the MAI together with the receiver's thermal noise. Performance improvements in these systems have been largely centred around finding optimal sets of spreading sequences [65]. "Smart" spread spectrum systems however, use the fact that the MAI is far from white, and multi-user systems use this knowledge to jointly detect the signals from the many users in the system [13, 92].

The asynchronous multi-user detection problem was noted by several authors [88, 69], to be a generalised intersymbol interference problem. The system proposed by Schneider involves a forward-backward processing Viterbi algorithm (VA) with 4^K states (where K is the number of users in the system). As pointed out by Schneider, the high complexity of the system limited its useful application in real time to about five users. Later, Verdú [91] presented a maximum likelihood (ML) receiver with 2^{K-1} states and suggested that ten users might be the effective processing limit of the system.

In this chapter we describe a family of reduced complexity multi-user systems based on Verdú's maximum likelihood multi-user detector (ML MUD)[91]. Similarly to the work of [91] we develop the receiver structure for the white noise asynchronous multi-user channel. We show that the new system allows the system designer to trade complexity for performance. At one extreme the

system reduces to the ML MUD while the other extreme results in a system with dramatically reduced complexity. A range of intermediate systems of varying complexity and performance are available. We present a system that with $K = 20$ users and a processing gain of $N_s = 511$ suffers at most a 0.5 dB loss with respect to the MLSE MUD at a bit error rate or BER $= 10^{-4}$. System performance degrades gracefully for systems employing lower processing gains. With respect to the previous example, when $N_s = 127$ the performance is approximately 2 dB worse than the maximum likelihood receiver.

The chapter is organised as follows. In the following section we describe the system. Performance results are presented in section 3.3. In section 3.4 analysis of the system complexity is presented. Conclusions are given in section 3.5.

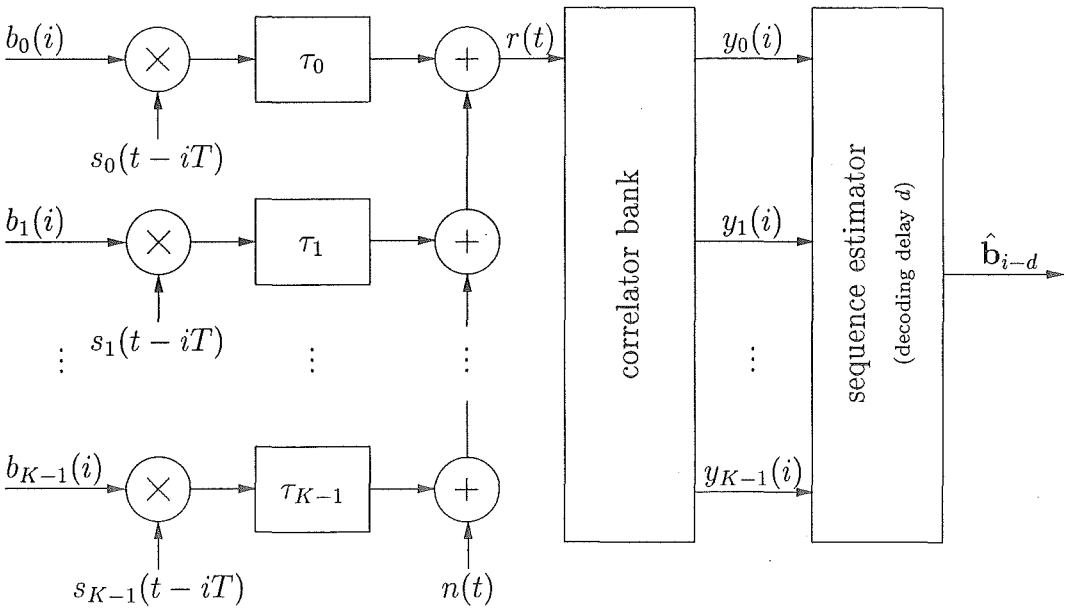

Figure 3.1: System model for asynchronous spread spectrum multiple access communication.

3.2 The System

3.2.1 Description

The asynchronous spread spectrum multiple access (SSMA) model considered here is shown in Fig. 3.1 and consists of K asynchronous transmitters, an additive white Gaussian noise channel, and the receiver. Using the notation $j = \eta(j)K + \kappa(j)$ of [91] where $\kappa(j)$ is the remainder of j mod K and $\eta(j)$ is the integer part of j/K, the received baseband signal $r(t)$ consisting of the sum of the K users' signals and the noise is written,[1]

$$r(t) = \sum_{i=0}^{N-1} \sum_{k=0}^{K-1} b_k(i)\, s_k(t - iT - \tau_k) + n(t) \tag{3.1}$$

$$= \sum_{j=0}^{NK-1} b_{\kappa(j)}(\eta(j))\, s_{\kappa(j)}(t - \eta(j)T - \tau_{\kappa(j)}) + n(t), \tag{3.2}$$

where N is the length of the transmitted sequence, $n(t)$ is AWGN with double-sided power spectral density $N_o/2$, $b_k(i)$ is the i-th data bit of the k-th user, $s_k(t - iT - \tau_k)$ is the k-th user's spreading sequence (equal to 0 outside the interval [0,T)), T is the bit duration and τ_k is the time delay of the k-th user. If $\{\underline{s}_k(c)\}$ is the sequence of spreading sequence chips of period N_s for the k-th user then we write $s_k(t)$ as

$$s_{\kappa(j)}(t - \eta(j)T - \tau_\kappa(j)) = \sum_{c=0}^{N_s-1} \underline{s}_{\kappa(j)}(c)\, p(t - \eta(j)T - \frac{cT}{N_s} - \tau_{\kappa(j)}), \tag{3.3}$$

where $p(t)$ is the rectangular chip waveform.

While many of the results presented here can be extended to arbitrary input alphabets, we restrict ourselves to binary alphabets, $b_k(i) \in \{\pm 1\}$. We

[1] Throughout this thesis we assume for the sake of notational simplicity that all users transmit using a carrier signal of the same phase. This can be assumed without loss of generality because in the general case where inter-user phase offsets exist, the phase offsets can be included in the matrix of user spreading sequence cross correlations to be presented later in this section. The carrier phases of all users are obtained through techniques such as those discussed in [26] and [59]. As a consequence, the results which we present here are also valid for carrier asynchronism as well was spreading sequence asynchronism.

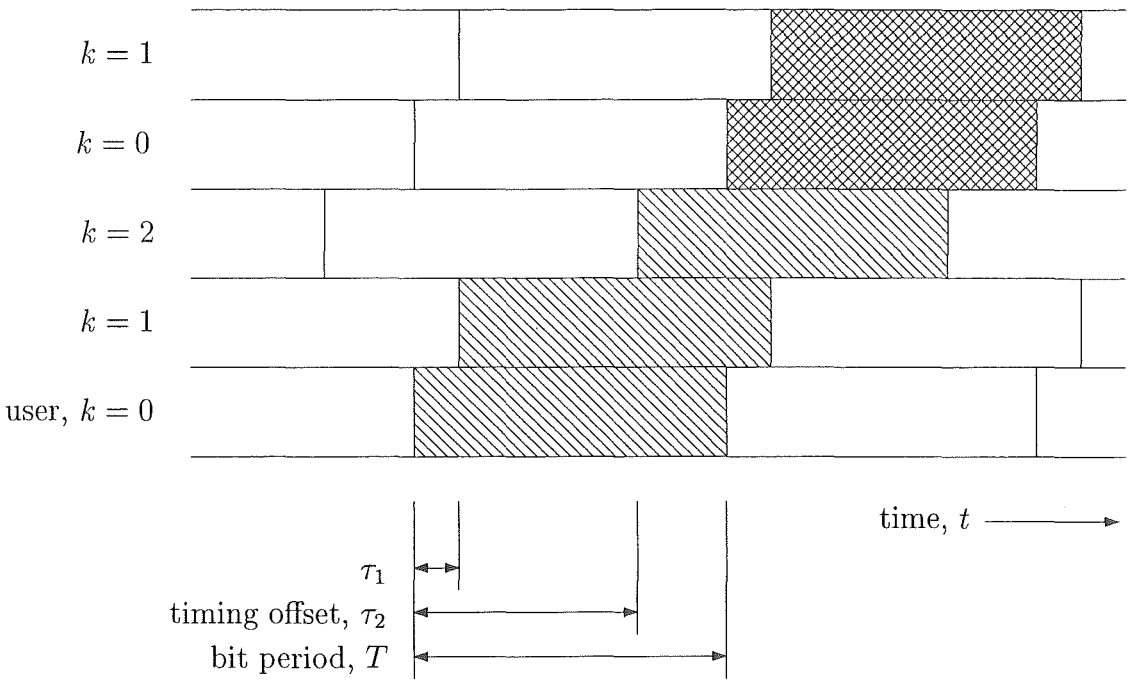

Figure 3.2: Interuser interference in asynchronous SSMA system with $K = 3$ users. One signalling interval is shown by the diagonal fill pattern, the next is shown as a criss-cross pattern. Each transmitted bit in the system interferes with $2(K-1)$ other bits.

assume, without loss of generality, that the users are numbered such that their relative delays τ_k are ordered as $0 \leq \tau_0 \leq \cdots \leq \tau_{K-1} < T$. All transmitted symbols are assumed equiprobable and independent.

The asynchronous channel means that the transmitted bits of the users not only interfere with the transmitted bits of other users in the current signalling interval, but interfere with the previous and following bits of the other users in the system as well. This is illustrated in Fig. 3.2. In the figure each row represents the consecutive transmitted bits of a user with respect to the different signalling intervals shown by the two different hash patterns used in the figure.

The receiver matched filters (or correlates) the received signal $r(t)$ with each of the users' spreading sequences $s_k(t-iT-\tau_k)$. We assume that the number of users K and their spreading sequences are known. In practice this may involve a correlation type search of the received signal using a predetermined set of

spreading sequences [11] as discussed in section 2.3. In general, the timing offset for the k-th user τ_k is an undefined quantity estimated for each user by conventional spread spectrum acquisition and tracking techniques [59]. The K matched filter outputs are given by,

$$\begin{aligned} y_{\kappa(j)}(\eta(j)) = {} & b_{\kappa(j)}(\eta(j))\, g_{\kappa(j),\kappa(j)}(\eta(j),\eta(j)) \\ & + \sum_{l=1}^{K-1} b_{\kappa(j-l)}(\eta(j-l))\, g_{\kappa(j-l),\kappa(j)}(\eta(j-l),\eta(j)) \\ & + \sum_{l=1}^{K-1} b_{\kappa(j+l)}(\eta(j+l))\, g_{\kappa(j+l),\kappa(j)}(\eta(j+l),\eta(j)) + n_{\kappa(j)}(\eta(j)), \end{aligned} \tag{3.4}$$

where $g_{k,k'}(i,i')$ is the spreading sequence partial cross correlation between the k-th and k'-th users at the i-th and i'-th data symbol (bit) intervals,

$$g_{k,k'}(i,i') = \int_{-\infty}^{\infty} s_k(t - iT - \tau_k) s_{k'}(t - i'T - \tau_{k'})\, dt, \tag{3.5}$$

with $g_{k,k}(i,i) = E_b$, the bit energy of the k-th user, and where $n_{\kappa(j)}(\eta(j))$ is the sampled noise at the output of the matched filters given by

$$n_{\kappa(j)}(\eta(j)) = \int_{-\infty}^{\infty} n(t) s_k(t - iT - \tau_k)\, dt. \tag{3.6}$$

Because of the partial cross correlations of the users' spreading sequences the resulting sequence of sampled noise is correlated. The correlation may be written as

$$\mathrm{E}[n_{\kappa(j)}(\eta(j))\, n_{\kappa(j')}(\eta(j'))] = \frac{N_o}{2} g_{\kappa(j),\kappa(j')}(\eta(j),\eta(j')). \tag{3.7}$$

The matched filter outputs of each for the K users and their corresponding transmitted bits at time $t = iT$ in (3.4) may be contained in vectors written as

$$\mathbf{y}_i = [\, y_0(i)\, y_1(i)\, \cdots\, y_{K-1}(i)\,]^{\mathrm{T}}, \tag{3.8}$$

and

$$\mathbf{b}_i = [\, b_0(i)\, b_1(i)\, \cdots\, b_{K-1}(i)\,]^{\mathrm{T}}, \tag{3.9}$$

respectively where i denotes the signalling interval.

The MLSE receiver selects the sequence that maximises the *a posteriori* probability $\Pr(\mathbf{b} \mid \mathbf{y})$; that is, given the sequences of matched filter outputs,

$$\mathbf{y} = [\,\mathbf{y}_0^{\mathrm{T}} \cdots \mathbf{y}_{N-2}^{\mathrm{T}}\,\mathbf{y}_{N-1}^{\mathrm{T}}\,]^{\mathrm{T}}, \tag{3.10}$$

the decoder chooses the most likely transmitted sequence,

$$\mathbf{b} = [\,\mathbf{b}_0^{\mathrm{T}} \cdots \mathbf{b}_{N-2}^{\mathrm{T}}\,\mathbf{b}_{N-1}^{\mathrm{T}}\,]^{\mathrm{T}}. \tag{3.11}$$

This is equivalent (by Bayes' Theorem) to selecting the sequence $\mathbf{b}$ with the largest conditional probability density function $p(\mathbf{y} \mid \mathbf{b})$ since the transmitted sequences of symbols are assumed equiprobable. This probability density function (pdf) is Gaussian since $n(t)$ is Gaussian so the maximum likelihood criterion is a minimum distance rule [59]. The ML receiver selects the sequence that maximises the metric

$$\begin{aligned}\Omega(\mathbf{b}) = 2 \sum_{j=0}^{NK-1} b_{\kappa(j)}(\eta(k)) \int_{-\infty}^{\infty} r(t) s_{\kappa(j)}(t - \eta(j)T - \tau_{\kappa(j)})\, dt \\ - \Big\{ \sum_{j=0}^{NK-1} b_{\kappa(j)}(\eta(j)) \int_{-\infty}^{\infty} s_{\kappa(j)}(t - \eta(j)T - \tau_{\kappa(j)})\, dt \Big\}^2.\end{aligned} \tag{3.12}$$

Using the identity $\left(\sum_{i=a}^{b} c_i\right)^2 = \sum_{i=a}^{b}\{c_i^2 + 2\sum_{j=1}^{b-a-1} c_i c_{i-j}\}$ used in [91] the metric becomes,

$$\begin{aligned}\Omega(\mathbf{b}) = \sum_{j=0}^{NK-1} \Big\{ & b_{\kappa(j)}(\eta(j))\, y_{\kappa(j)}(\eta(j)) - b_{\kappa(j)}^2(\eta(j))\, g_{\kappa(j),\kappa(j)}(\eta(j), \eta(j)) \\ & - \sum_{l=1}^{K-1} b_{\kappa(j)}(\eta(j))\, b_{\kappa(j-l)}(\eta(j-l))\, g_{\kappa(j),\kappa(j-l)}(\eta(j), \eta(j-l)) \Big\},\end{aligned} \tag{3.13}$$

and is equivalent in vector notation to

$$\begin{aligned}\Omega(\mathbf{b}) &= \sum_{i=0}^{N-1} \bar{\Omega}(\mathbf{b}_i) \\ &= \sum_{i=0}^{N-1} \mathbf{b}_i^{\mathrm{T}} \left(\mathbf{y}_i - \operatorname{diag} \mathbf{X}_i \mathbf{G}\right),\end{aligned} \tag{3.14}$$

where $\bar{\Omega}(\mathbf{b}_i)$ may be regarded as a branch metric, the matrix $\mathbf{G}$ is a $(K-1)\times K$ matrix whose m-th column is the correlation of the m-th and $\kappa(m-i)$-th users' spreading sequences, where $i = 1, 2, \cdots K-1$,

$$\mathbf{G} \; : \; G_{n,m} = g_{\kappa(n),\kappa(n-m)}(\eta(n), \eta(n-m)). \tag{3.15}$$

We will refer to the $\kappa(m-i)$, where $i = 1, 2, \cdots K-1$ users, as the previous $K-1$ users of m. The $K \times (K-1)$ matrix $\mathbf{X}_i$ contains the previous $K-1$ hypothesised bits (in rows) for each of the users,

$$\mathbf{X}_i \; : \; X^{(i)}_{n,m} = b_{\kappa(Ki+n-m)}(\eta(Ki+n-m)). \tag{3.16}$$

Note that $\mathbf{X}_i$ is not a constant for a given i but is a function of $\mathbf{b}$ due to the serial dependence of bits as illustrated in Fig. 3.2.

The path metric in (3.14) allows the definition of a state sequence and the maximum likelihood detection of the transmitted bits by means of the Viterbi algorithm. The 2^K states of the VA are each of the possible length K vectors $\mathbf{b}_i$ of (3.9). At each signalling interval the trellis is advanced by the computation of branch metrics (the addend in (3.14) for each hypothesised $\mathbf{b}_i$) from each originating state to each succeeding state. The branch metrics are *added* to the path metric at the originating state; the competing path metrics entering each of the succeeding states are *compared* and the path corresponding to the largest path metric is *selected*—this is known as the Add-Compare-Select process of the Viterbi algorithm [59]. Note that as shown in [91], and again in (3.13), there is only a $K-1$ previous bit dependence on the branch metric calculations so half the path metrics are equivalent and the ML detector using the VA requires 4^{K-1} path metric calculations per signalling interval. The exponential complexity of the ML receiver employing the Viterbi algorithm limits the number of users to about ten [91].

The complexity of the ML detector is a result of the large number of states in the trellis. To reduce the complexity we seek to reduce the number of states

that need to be processed by the VA at any instant of time. To do this we employ a partitioning process that leads to a sequentially expanded trellis with significantly fewer states operated on during each of a sequence of sub-intervals.

The partitioning segments the vector containing each of the K-users bits transmitted in the i-th data signalling interval $\mathbf{b}_i$, into $N_p = \lceil K/K_s \rceil$ K_s-length sub-vectors[2] $\mathbf{b}_{i,p}$, where the subscript p denotes the sub-interval and $p = 0, 1, \cdots, N_p - 1$ such that,

$$\mathbf{b}_i = [\, \mathbf{b}_{i,0}^{\mathrm{T}} \, \mathbf{b}_{i,1}^{\mathrm{T}} \, \cdots \, \mathbf{b}_{i,N_p-1}^{\mathrm{T}} \,]^{\mathrm{T}}. \tag{3.17}$$

This produces reduced sets of 2^{K_s} states which are mapped to a sequentially expanded time-varying trellis such that $N_p = \lceil K/K_s \rceil$ sub-intervals of the reduced trellis are processed during each data symbol interval with each sub-interval used to processes one of the sub-vectors. Extending the modulo notation introduced in the first section to account for the sub-interval partitioning we define $\rho(j) = \lfloor \kappa(j)/K_s \rfloor$ to specify to which subset the $\kappa(j)$-th user belongs. Each state in the reduced trellis is labelled $\mathbf{b}^s$, with $s = 0, 1, \cdots, 2^{K_s} - 1$ and corresponds to a length K_s vector representing the possible values of the received sub-vector $\mathbf{b}_{i,p}$. The set of all states $B = \{\mathbf{b}^s \,;\, s = 0, 1, \cdots, 2^{K_s} - 1\}$ represents all possible 2^{K_s} values of the sub-vectors $\mathbf{b}_{i,p}$. The ML receiver uses states that are labelled with the 2^K hypothesised values of $\mathbf{b}_i$. The reduced complexity receiver employs a trellis which is N_p branches deep within each signalling interval and where each of the N_p stages has states labelled with the 2^{K_s} hypothesised values of the corresponding sub-vector $\mathbf{b}_{i,p}$. That is, the first advance through the trellis of the reduced complexity receiver during the i-th signalling interval updates the path metrics corresponding to the sub-vector $\mathbf{b}_{i,0}$, and N_p advances through the trellis must be performed during each bit interval in order to consider all N_p sub-vectors $\mathbf{b}_{i,0}, \mathbf{b}_{i,1}, \cdots, \mathbf{b}_{i,N_p-1}$. Note that the ordering of the subsets as described must be maintained throughout the processing because of the dependence on $K - 1$ previous hypothesised bits.

[2] $\lceil x \rceil$ is the next integer greater than or equal x, and $\lfloor x \rfloor$ is the integer component of x.

As the N_p advances are made through the trellis during the i-th signalling interval, N_p estimates $\hat{\mathbf{b}}_{i-d,p}$, $p = 0, 1, \cdots N_p - 1$ are output by the Viterbi Algorithm (with decision depth d symbol periods). The N_p estimates are concatenated to form the estimate of the bits transmitted by all K users d signalling intervals in the past as

$$\hat{\mathbf{b}}_{i-d} = [\,\hat{\mathbf{b}}^{\mathrm{T}}_{i-d,0}\,\hat{\mathbf{b}}^{\mathrm{T}}_{i-d,1}\,\cdots\,\hat{\mathbf{b}}^{\mathrm{T}}_{i-d,N_p-1}\,]^{\mathrm{T}}. \tag{3.18}$$

The partitioning into subsets does not limit K_s to factors of K. When K and K_s are relatively prime the final subset contains $R = K - N_p K_s$ users, where $R \neq 0$. In this case each of the 2^R state labels are represented $2^{K_s - R}$ times in the 2^{K_s} state trellis. This is purely an implementation nicety and the redundancy may be removed by equivalently employing a trellis structure where the final stage in each signalling interval contains fewer states than those of previous stages.

The reduced state trellis allows for significant complexity reduction due to the sequential decoding of the sub-vectors within each interval. As we will show later this is because reducing the number of users per state K_s reduces the complexity *exponentially* while the corresponding increase due to sequential decoding of the sub-vectors increases the complexity only *geometrically*.

Rewriting (3.14) to account for the partitioning, we obtain the suboptimum overall path metric as the sum of the branch metrics $\bar{\Omega}(\mathbf{b}_{i,p})$,

$$\begin{aligned}\tilde{\Omega}(\mathbf{b}) &= \sum_{i=0}^{N-1}\sum_{p=0}^{N_p-1}\bar{\Omega}(\mathbf{b}_{i,p}) \\ &= \sum_{i=0}^{N-1}\sum_{p=0}^{N_p-1}\mathbf{b}^{\mathrm{T}}_{i,p}\left(\mathbf{y}_{i,p} - \operatorname{diag}\mathbf{X}_{i,p}\mathbf{G}^{pK_s+1,(p+1)K_s}\right),\end{aligned} \tag{3.19}$$

where $\mathbf{X}_{i,p}$ is the $K_s \times (K-1)$ matrix of previous bits, corresponding to the p-th subset. It is formed by considering the $K-1$ surviving inputs by tracing back N_p branches through the trellis along the surviving paths. $\mathbf{G}^{pK_s+1,(p+1)K_s}$ is a $(K-1) \times K_s$ sub-matrix of $\mathbf{G}$ where the superscript notation gives the range of columns from $\mathbf{G}$ in (3.15). The sequence $\mathbf{b} =$

$[\,\mathbf{b}^{\mathrm{T}}_{\eta(0),\rho(0)}\,\mathbf{b}^{\mathrm{T}}_{\eta(1),\rho(1)}\,\cdots\,\mathbf{b}^{\mathrm{T}}_{\eta(NK-1),\rho(NK-1)}\,]^{\mathrm{T}}$ which maximises (3.19) is an estimate of the most likely sequence within the reduced trellis.

In each sub-interval the path metric $\Omega^{\mathbf{b}^s}_{i,p}$, $s = 0, 1, \cdots, 2^{K_s} - 1$ at each state in the Viterbi algorithm is updated by a one-step application of (3.19) (that is, the inner term) as,

$$\Omega^{\mathbf{b}^s}_{i,p} = \max_{s'} \Omega^{\mathbf{b}^{s'}}_{\eta(j-1),\rho(j-1)} + \bar{\Omega}^{\mathbf{b}^{s'}}(\mathbf{b}^s_{i,p}), \tag{3.20}$$

where $\Omega^{\mathbf{b}^s}_{i,p}$ is the path metric in the $\mathbf{b}^s$-state at the p-th sub-interval of the i-th signalling interval, $\Omega^{\mathbf{b}^{s'}}_{\eta(j-1),\rho(j-1)}$, is the path metric from the previous sub-interval, and $\bar{\Omega}^{\mathbf{b}^{s'}}(\mathbf{b}^s_{i,p})$ is the branch metric at the p-th sub-interval of the i-th signalling interval from the $\mathbf{b}^{s'}$-state to the $\mathbf{b}^s$-state, namely,

$$\bar{\Omega}^{\mathbf{b}^{s'}}(\mathbf{b}^s_{i,p}) = \mathbf{b}^{s\mathrm{T}}(\mathbf{y}_{i,p} - \operatorname{diag} \mathbf{X}^{\mathbf{b}^{s'},\mathbf{b}^s}_{i,p} \mathbf{G}^{pK_s+1,(p+1)K_s}), \tag{3.21}$$

The path dependence on the matrix of previous bits $\mathbf{X}$ is shown by the superscripts.

3.2.2 Example

Consider the four user example in Fig. 3.3 for the transition from the $(i_o - 1)$-th to the i_o-th signalling interval. The ML receiver has the trellis shown in Fig. 3.3(a). It has 16 states and each state has 16 possible branches to a state in the next signalling interval (although Verdú showed half the metric calculations are equivalent because of the $K-1$ previous bit dependence shown in (3.13)).

The trellis of a reduced complexity receiver with $K_s = 2$ users per state and $N_p = 2$ sub-intervals per symbol is shown in Fig. 3.3(b). $N_p = 2$ advances through this reduced trellis must be made to compute the path metrics for the transition from the $(i_o - 1)$-th to the i_o-th signalling interval. The path metrics at each of the four states, $\Omega^{\mathbf{b}^0}_{i,p}$, $\Omega^{\mathbf{b}^1}_{i,p}$, $\Omega^{\mathbf{b}^2}_{i,p}$, and $\Omega^{\mathbf{b}^3}_{i,p}$ for the p-th sub-interval of the i-th signalling interval, are estimates of the decision metric shown in (3.19). A correct path may be prematurely discarded in an earlier

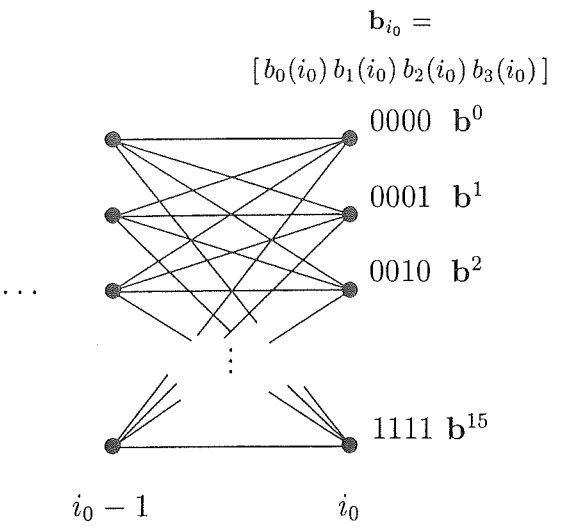

(a) Four user MLSE trellis. The states represent the hypothesised bits of all K users at each signalling interval.

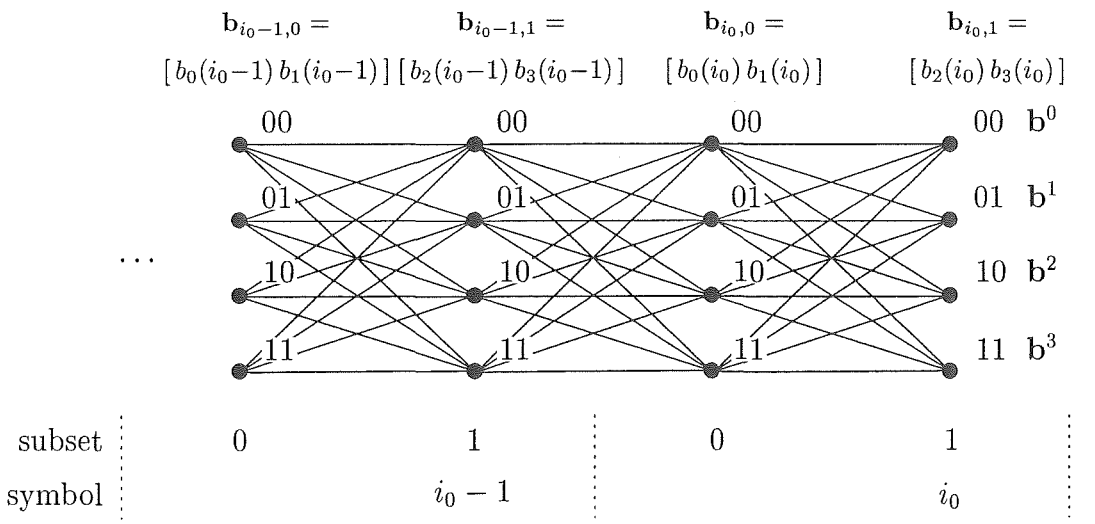

(b) Four user trellis partitioned into two users per state. The states are labelled with the hypothesised $K_s = 2$ length sub-vectors. $N_p = 2$ advances through the trellis are required for each signalling interval.

Figure 3.3: A four user receiver example.

comparison, where if all possible sub-interval transitions were considered the discarded path would be still in contention; this error behaviour is discussed in the next section when system performance is analysed. The first sub-interval is responsible for contributing to the path metrics from the first two users, the second sub-interval contributes from the third and fourth users. The output of the bank of correlators at time $i = i_o$ is represented by the vector,

$$\mathbf{y}_{i_o} = [\, y_0(i_o)\, y_1(i_o)\, y_2(i_o)\, y_3(i_o)\,]^{\mathrm{T}}.$$

At each state in the reduced trellis four paths from previous states compete to be the surviving path. The branch metrics from each state at $i = i_o - 1$, $p = 1$ are calculated using the addend of (3.19) and the first set of outputs from the correlator bank $\mathbf{y}_{i_o,0} = [\, y_0(i_o)\, y_1(i_o)\,]^{\mathrm{T}}$. Consider one case where the competing paths enter the $\mathbf{b}^0$-state at $i = i_o$, $p = 0$. The receiver discards three of the four paths by choosing the most likely (surviving) path from the four contenders as in (3.20). The correlation matrix $\mathbf{G}^{1,2}$ is a constant during the calculations at any sub-interval and is a subset of the matrix of all user correlations $\mathbf{G}$ from (3.15). The matrix of surviving inputs $\mathbf{X}_{i_o,0}$ is formed row-wise by tracing back from each state at $i = i_o$, $p = 0$ by $N_p = 2$ branches in the trellis filling rows of $\mathbf{X}_{i_o,0}$ with the surviving bits along the path represented by the state labels. Note that each branch metric calculation requires a different $\mathbf{X}_{i_o,0}$ since the $K - 1$ previous bits in each path are different. To illustrate, suppose a competing path arriving at the $\mathbf{b}^0$-state at $i = i_o$, $p = 0$, had at $i = i_o - 1$, $p = 1$ passed through the $\mathbf{b}^2$-state, and had at $i = i_o - 1$, $p = 0$ passed through the $\mathbf{b}^1$-state, then,

$$\mathbf{X}_{i_o,0}^{\mathbf{b}^2,\mathbf{b}^0} = \begin{bmatrix} -1 & 1 & 1 \\ -1 & -1 & 1 \end{bmatrix},$$

and the branch metric $\bar{\Omega}^{\mathbf{b}^2}(\mathbf{b}_{i_0,0}^0)$ corresponding to the path entering the $\mathbf{b}^0$-state from the $\mathbf{b}^2$-state at $i = i_0$, $p = 0$ is,

$$\bar{\Omega}^{\mathbf{b}^2}(\mathbf{b}_{i_0,0}^0) = \mathbf{b}^{0\mathrm{T}} \left(\mathbf{y}_{i_o,0} - \operatorname{diag} \mathbf{X}_{i_o,0}^{\mathbf{b}^2,\mathbf{b}^0} \mathbf{G}^{1,2} \right).$$

Path metrics for each of the remaining three paths entering the $\mathbf{b}^0$-state are calculated, each with a different matrix of previous bits, $\mathbf{X}_{i_o,0}^{\mathbf{b}^0,\mathbf{b}^0}$, $\mathbf{X}_{i_o,0}^{\mathbf{b}^1,\mathbf{b}^0}$, and $\mathbf{X}_{i_o,0}^{\mathbf{b}^3,\mathbf{b}^0}$. The path corresponding to the greatest of the four path metrics is selected as the surviving path and the remainder are discarded as given by (3.20). The same technique is applied to each of the remaining states at $i = i_o$, $p = 0$. When all branches to states at $i = i_o$, $p = 0$ have been calculated the Viterbi algorithm searches through all four states for the largest path metric and follows the path corresponding to the greatest metric through the decision depth of the VA. The originating state of this path determines the most likely transmitted bits (from d signalling intervals earlier) for the first two users, $\hat{\mathbf{b}}_{i_o-d,0} = [\,\hat{b}_0(i_o-d)\,\hat{b}_1(i_o-d)\,]^{\mathrm{T}}$.

The second sub-vector is processed by considering the second set of outputs from the correlator bank, $\mathbf{y}_{i_o,0} = [\,y_2(i_o)\,y_3(i_o)\,]^{\mathrm{T}}$. The matrix of surviving inputs $\mathbf{X}_{i_o,1}$ includes bits in the paths at the previous sub-interval, $i = i_o$, $p = 0$; as an example suppose a competing path arriving at the $\mathbf{b}^2$-state at $i = i_o$, $p = 1$, had at $i = i_o$, $p = 0$ passed through the $\mathbf{b}^0$-state, and had at $i = i_o - 1$, $p = 1$ passed through the $\mathbf{b}^1$-state, then,

$$\mathbf{X}_{i_o,1}^{\mathbf{b}^0,\mathbf{b}^2} = \begin{bmatrix} -1 & -1 & 1 \\ 1 & -1 & -1 \end{bmatrix}.$$

The correlation matrix for the second sub-interval is the sub-matrix of $\mathbf{G}$ with columns corresponding to the third and fourth users, namely $\mathbf{G}^{3,4}$. The same add, compare, select processes are applied to the branch metrics and the estimated bits $\hat{\mathbf{b}}_{i_o-d,1} = [\,\hat{b}_2(i_o-d)\,\hat{b}_3(i_o-d)\,]^{\mathrm{T}}$ are returned by the VA by examining the originating state of the path with the greatest path metric. Note that in this example with $N_p = 2$ sub-intervals per symbol, two iterations of the Viterbi algorithm are required to estimate the bits for all the users and this requires two sets of add, compare, and select operations. The vector $\hat{\mathbf{b}}_{i_o-d}$ representing all the decoded user bits is a concatenation of the vectors obtained by the reduced VA during processing of each sub-interval, and may be written

as

$$\begin{aligned}\hat{\mathbf{b}}_{i_o-d} &= [\hat{\mathbf{b}}^{\mathrm{T}}_{i_o-d,0}\,\hat{\mathbf{b}}^{\mathrm{T}}_{i_o-d,1}]^{\mathrm{T}} \\ &= [\,\hat{b}_0(i_o-d)\,\hat{b}_1(i_o-d)\,\hat{b}_2(i_o-d)\,\hat{b}_3(i_o-d)\,]^{\mathrm{T}}.\end{aligned}$$

3.2.3 Performance

The exact error performance of the system is not easy to determine. We begin with a description of the error events due to the sequential-type decoding within the system resulting from the serial partitioning described in the previous section.

Consider again the four user system with two users per sub-interval shown in Fig. 3.3. At each sub-interval all but the most likely path leading to each state are discarded. The partitioning effectively forces the decoder to make early decisions within each sub-interval—the more sub-intervals per symbol interval, the more early decisions are required.

In each symbol interval the maximum likelihood receiver extends each of the surviving paths from the previous symbol interval by considering 2^{K-1} branch metrics from each state, that is there are 2^{K-1} branches entering each state. In the reduced complexity receiver, the partitioning of the symbol vector $\mathbf{b}_i$ into sub-vectors whose possible values label the states in the reduced trellis reduces the total number of state sequences to be tested by the receiver over each symbol interval. Consider the 2^{Ks} path metrics arriving at a given state. The receiver chooses the most likely and discards the remainder. However, the reduced complexity receiver performance is degraded with respect to the ML receiver if one of the discarded paths turns out to be the most likely path if the *whole* symbol interval were to be considered as in the ML case. Clearly this sort of error propagation is more acute for receivers employing a larger number of sub-intervals with fewer users per state (since there are more opportunities for error) and there is a larger degradation in performance.

To obtain a measure of the performance of the system we consider a K-

user system with one user per state. The resulting performance is effectively an upper bound on system performance for reasons previously outlined. To obtain a reasonably simple, approximate derivation of system performance we make some assumptions which will be tested by simulation in the next section—(a) we assume that the dominant error event is one in which the most likely path, as determined by the receiver, deviates from the correct path at only one sub-interval, that is minimum distance events are dominant; (b) we neglect the effect of error propagation dues to the discarding of the correct path; and (c) the error events are independent. In this case the two paths (the correct path and the path in error) merge one sub-interval later.

Assuming without loss of generality that the all-zeros path is the correct path, then from (3.20) the path metrics for the correct path and incorrect path for the system with one user per state are $\Omega_{i,p}^{\mathbf{b}^0}$ and $\Omega_{i,p}^{\mathbf{b}^1}$ respectively, that is the path metrics of the two competing paths entering the $\mathbf{b}^0$-state. The probability that the incorrect path is chosen over the correct path is $\Pr(\Omega_{i,p}^{\mathbf{b}^1} - \Omega_{i,p}^{\mathbf{b}^0} > 0)$. Both path metrics are equal before the paths diverged two sub-intervals earlier, so the difference $\Omega_{i,p}^{\mathbf{b}^1} - \Omega_{i,p}^{\mathbf{b}^0}$ is the difference between the sum of the two branch metrics along each path,

$$\begin{aligned}\Omega_{i,p}^{\mathbf{b}^1} - \Omega_{i,p}^{\mathbf{b}^0} &= \bar{\Omega}^{\mathbf{b}^0}(\mathbf{b}^1_{\eta(j-1),\rho(j-1)}) + \bar{\Omega}^{\mathbf{b}^1}(\mathbf{b}^0_{\eta(j),\rho(p)}) - \\ &\quad (\bar{\Omega}^{\mathbf{b}^0}(\mathbf{b}^0_{\eta(j-1),\rho(j-1)}) + \bar{\Omega}^{\mathbf{b}^0}(\mathbf{b}^0_{\eta(j),\rho(j)})) \\ &= \bar{\Omega}^{\mathbf{b}^0}(\mathbf{b}^1_{\eta(j-1),\rho(j-1)}) - \bar{\Omega}^{\mathbf{b}^0}(\mathbf{b}^0_{\eta(j-1),\rho(j-1)}) + \\ &\quad \bar{\Omega}^{\mathbf{b}^0}(\mathbf{b}^1_{\eta(j),\rho(j)}) - \bar{\Omega}^{\mathbf{b}^0}(\mathbf{b}^0_{\eta(j),\rho(j)}). \end{aligned} \tag{3.22}$$

From (3.19)

$$\begin{aligned}&\bar{\Omega}^{\mathbf{b}^0}(\mathbf{b}^1_{\eta(j-1),\rho(j-1)}) - \bar{\Omega}^{\mathbf{b}^0}(\mathbf{b}^0_{\eta(j-1),\rho(j-1)}) \\ &\quad = -2\Big\{ g_{\kappa(j-1),\kappa(j-1)}(\eta(j-1),\eta(j-1)) \\ &\qquad - \sum_{l=1}^{K-1} g_{\kappa(j-1),\kappa(j-1-l)}(\eta(j-1),\eta(j-1-l)) + n_{\kappa(j-1)}(\eta(j-1))\Big\}\end{aligned} \tag{3.23}$$

and

$$\bar{\Omega}^{\mathbf{b}^0}(\mathbf{b}^1_{\eta(j),\rho(j)}) - \bar{\Omega}^{\mathbf{b}^0}(\mathbf{b}^0_{\eta(j),\rho(j)}) = -2g_{\kappa(j-1),\kappa(j)}(\eta(j-1),\eta(j)). \tag{3.24}$$

The probability of choosing the incorrect path is written as,

$$\begin{aligned}\Pr(\Omega^{\mathbf{b}^1}_{i,p} - \Omega^{\mathbf{b}^0}_{i,p} > 0) \approx \Pr\Big(& - g_{\kappa(j-1),\kappa(j-1)}(\eta(j-1),\eta(j-1)) \\ & - \sum_{l=1}^{K-1} g_{\kappa(j-1),\kappa(j-1+l)}(\eta(j-1),\eta(j-1+l)) \\ & + n_{\kappa(j-1)}(\eta(j-1)) > 0\Big) \\ = \Pr\Big(& - g_{\kappa(j-1),\kappa(j-1)}(\eta(j-1),\eta(j-1)) - \gamma > 0\Big).\end{aligned} \tag{3.25}$$

where γ is the combined noise and interference term given by the summation of the second and third terms of the first line. Note that the right-hand side of (3.25) is given in terms of $j-1$ since the paths diverge at $j-1$ and re-merge one branch later.

The mean of the noise and interference term is zero while the variance is [60],

$$\begin{aligned}\mathrm{V}[\gamma] &= \frac{E_b N_o}{2} + \sum_{l=1}^{K-1} \int_0^T g^2_{\kappa(j-1),\kappa(j-1+l)}(\eta(j-1),\eta(j-1+l))\, d\tau_{\kappa(j-1)} \\ &= \frac{E_b N_o}{2} + \sum_{l=1}^{K-1}\sum_{m=0}^{N-1} \int_{mT/N_s}^{(m+1)T/N_s} g^2_{\kappa(j-1),\kappa(j-1+l)}(\eta(j-1),\eta(j-1+l))\, d\tau_{\kappa(j-1)} \\ &= \frac{E_b N_o}{2} + \frac{E_b}{3N_s^3} \sum_{l=1}^{K-1}\sum_{m=0}^{N-1} \Big\{ C^2_{\kappa(j_1),\kappa(j_1+l)}(m+1) \\ &\qquad + C_{\kappa(j_1),\kappa(j_1+l)}(m+1) C_{\kappa(j_1),\kappa(j_1+l)}(m) + C^2_{\kappa(j_1),\kappa(j_1+l)}(m)\Big\}\end{aligned} \tag{3.26}$$

$$= \frac{E_b N_o}{2} + \frac{E_b^2}{3} \sum_{l=1}^{K-1} g_v(l). \tag{3.27}$$

In (3.27)

$$C_{k,k'}(m) = \sum_{i=0}^{N_s-1-m} \underline{s}_k(i)\underline{s}_{k'}(i+m) \qquad 0 \le m \le N_s - 1, k \ne k'. \tag{3.28}$$

where $C_{k,k'}(m)$ is the discrete aperiodic cross-correlation function of the spreading sequences given by (2.8).

Calculations for $g_v(l)$ can be made for any set of spreading sequences. We numerically calculate $g_v(l)$ for random sequences from sets of m-sequences of different lengths given in Table 2.1 resulting in a parameter g_v which is independent of l and dependant only on sequence length. The noise and interference variance can be written

$$\mathrm{V}[\gamma] = \frac{E_b N_o}{2} + \frac{E_b^2 g_v (K-1)}{3}. \tag{3.29}$$

A simple expression is obtained by modelling the noise and interference term as a Gaussian process, with the above mean and variance. Making the substitution $x \triangleq -g_{\kappa(j_1),\kappa(j_1)}(\eta(j_1),\eta(j_1)) - \gamma$ an approximation to the bit error rate for a K user system with one user per state can written simply as,

$$\begin{aligned} P_b &\approx \Pr(x > 0) \\ &= \frac{1}{\sqrt{2\,\mathrm{V}[x]\pi}} \int_0^\infty \exp\left(-\frac{(x-\mathrm{E}[x])^2}{2\,\mathrm{V}[x]}\right) dx \\ &= \frac{1}{2}\,\mathrm{erfc}\left(\sqrt{\frac{E_b}{N_o + 2g_v E_b (K-1)/3}}\right) \end{aligned} \tag{3.30}$$

where $\mathrm{E}[x] = -g_{\kappa(j_1),\kappa(j_1)}(\eta(j_1),\eta(j_1))$, and $\mathrm{V}[x] = \mathrm{V}[\gamma]$ as defined above. This expression is similar in form to the classical approximation of conventional correlator-type spread spectrum performance. In the following section we calculate g_v for different sequence lengths and compare the approximation with simulation results.

In conventional spread spectrum, the absence of power control, so that a stronger user tends to flood the spectrum, is a limiting factor on system performance. The ML receiver is known to be near-far resistant in that users whose signals are stronger than other users' signals do not adversely effect the performance of the weaker users. The receiver structures presented here are formed from a transformation of the near-far resistant ML receiver. However, it can be seen from (3.30) that the reduced complexity receiver structure has reduced

near-far resistance. The second term in the denominator can be considered a *leakage* term and is a function of the relative power levels among the users' signals. Users with greater power levels contribute more to the leakage term and the performance worsens; it appears as if more users are in the system. In the next section we present performance results for a range of user numbers and spreading sequence lengths.

3.3 Performance Results

We have performed extensive Monte Carlo simulations using the metric in (3.19) and the Viterbi algorithm with K equiprobable asynchronous binary sources with equal powers and rectangular spreading sequence waveforms over a AWGN channel.

The results of the first simulations are shown in Fig. 3.4 and Fig. 3.5. In the figures we compare the analytical performance result from (3.30) with simulation results. The systems employ maximal length sequences (m-sequences) with $N_s = 127$ and $N_s = 511$ chips per bit respectively from Table 2.1. Results are shown for 10, 20, and 30 asynchronous users with uniformally distributed relative delays τ_k. Note that (3.30) provides an excellent measure of the performance of systems with $K_s = 1$ user per state.

To determine the performance of systems for $K_s > 1$ we rely purely on simulation results. The performance for $K = 10$ users with processing gain $N_s = 127$ is shown in Fig. 3.6. The performance of conventional (correlator) spread spectrum [30] is also shown in the figure as a reference. The reduced complexity receiver with one user per state suffers approximately 0.7 dB in performance for BER $= 10^{-4}$. In the next section we will quantify the computational complexity reduction, for now we merely state that the complexity has been reduced from being exponential in the number of users to being polynomial for the case of $K_s = 1$ user per state.

Fig. 3.7 shows the same system but with $K = 20$ users. While the performance is worse than the system with 10 users, note that the conventional

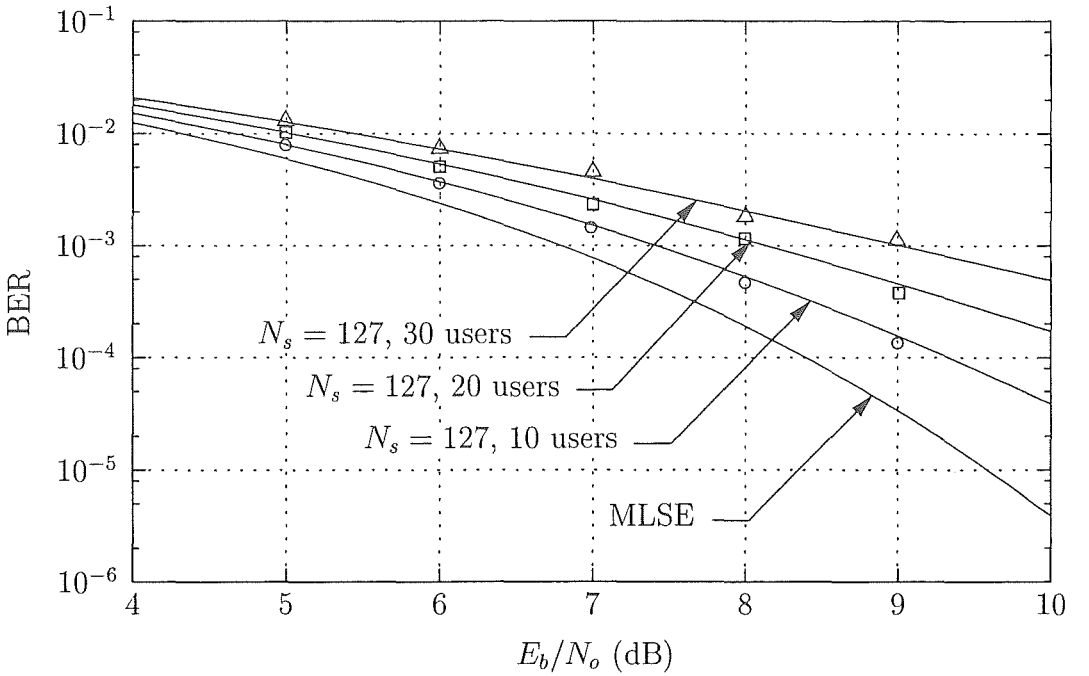

Figure 3.4: Performance of the reduced complexity receiver with $K_s = 1$ user per state with processing gain $N_s = 127$ and K users. Simulation results are shown as points.

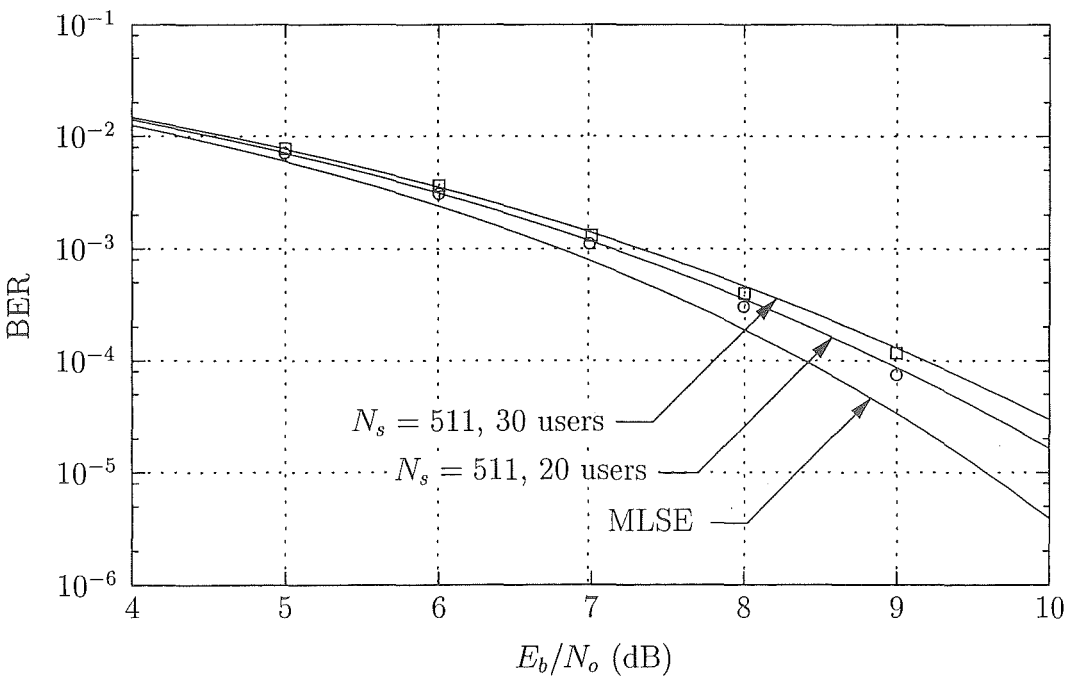

Figure 3.5: Performance of the reduced complexity receiver with $K_s = 1$ user per state with processing gain $N_s = 511$ and K users. Simulation results are shown as points.

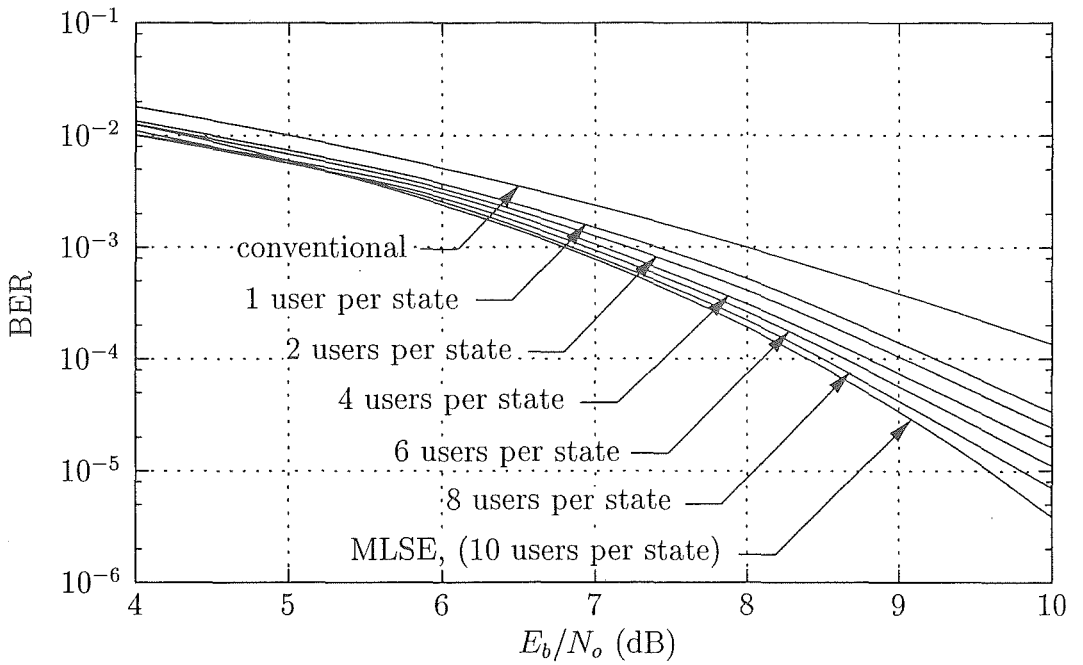

Figure 3.6: Simulated performance of the reduced complexity receiver (users per state, K_s is parameterised) with $K = 10$ users and processing gain $N_s = 127$. Performance of conventional correlation spread spectrum and the MLSE receivers are shown as a reference.

receiver has fared far worse by the increase of 10 users to 20.

Fig. 3.8 shows the effect of increasing the number of users to $K = 30$. Obtaining a BER $= 10^{-4}$ requires more than $K_s = 8$ users per state or a significant reduction in efficiency (E_b/N_o increase) compared with the ML receiver. In this case to avoid more than 3 dB degradation, the receiver must use $K_s \geq 10$ users per state. The complexity and power requirements on acceptable performance for large numbers of users may be alleviated by increasing the processing gain of the system. This is shown in Fig. 3.9 where we show performance results for the same $K = 30$ user system, but with a processing gain of $N_s = 511$.

The simulation results indicate that (3.30) provides a good estimate of the performance of the whole family of receivers for a given processing gain since the $K_s = 1$ user per state receiver bounds, in an increasingly loose fashion as K_s increases, the performance of the higher users per state systems. Of particular interest is that for medium/wide-band spread spectrum systems the

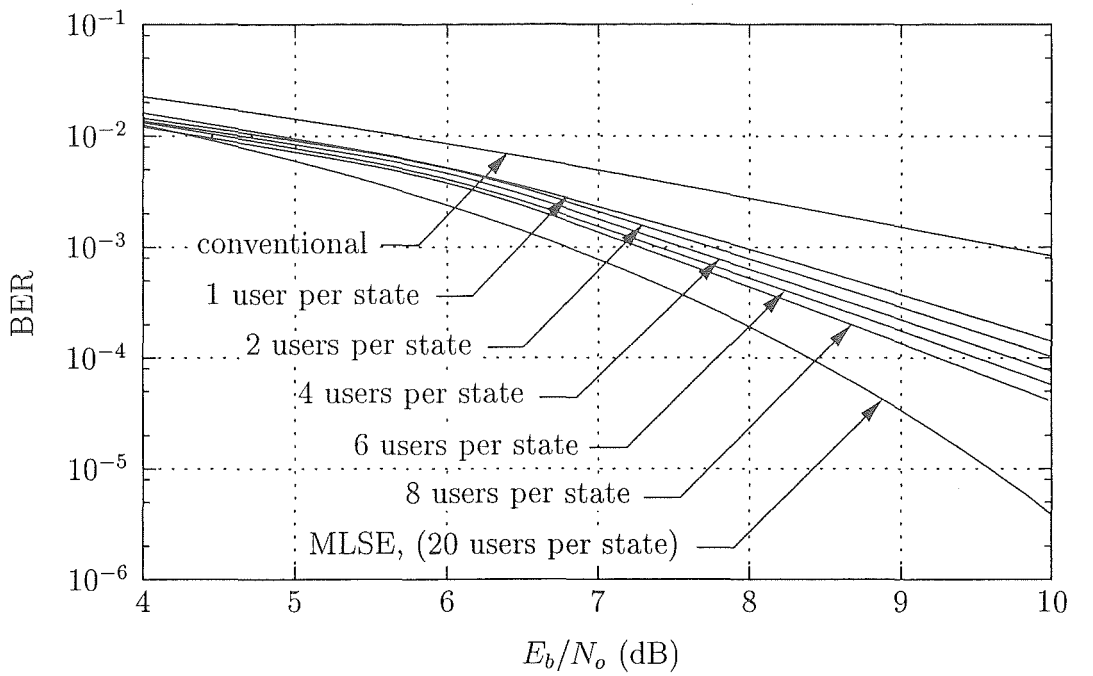

Figure 3.7: Simulated performance of the reduced complexity receiver (users per state, K_s is parameterised) with $K = 20$ users and processing gain $N_s = 127$. Performance of conventional correlation spread spectrum and the MLSE receivers are shown as a reference.

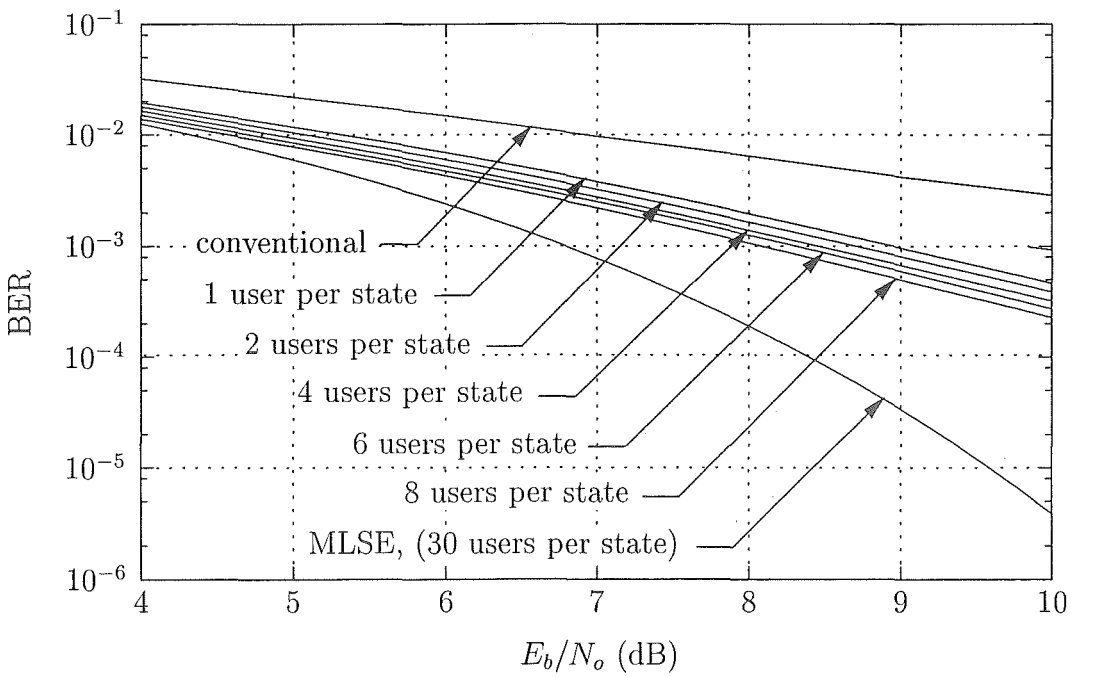

Figure 3.8: Simulated performance of the reduced complexity receiver (users per state, K_s is parameterised) with $K = 30$ users and processing gain $N_s = 127$. Performance of conventional correlation spread spectrum and the MLSE receivers are shown as a reference.

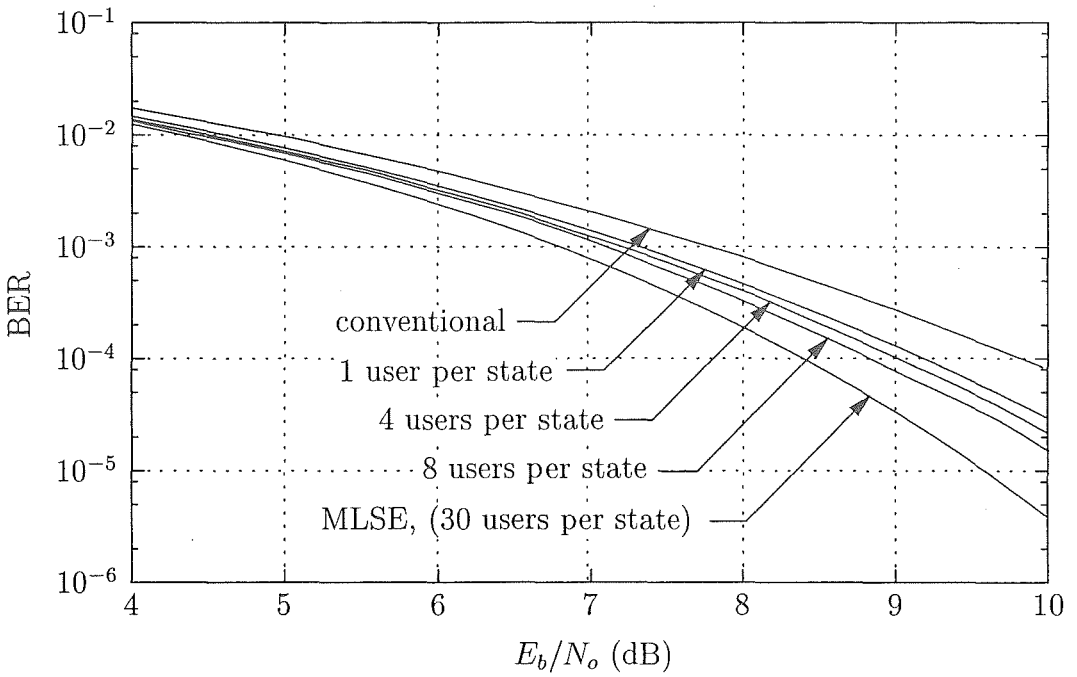

Figure 3.9: Simulated performance of the reduced complexity receiver (users per state, K_s is parameterised) with $K = 30$ users and processing gain $N_s = 511$. Performance of conventional correlation spread spectrum and the MLSE receivers are shown as a reference.

performance is only marginally worse than the ML performance even for quite large numbers of users. In this case for processing gain $N_s = 511$ and a $K = 30$ users system, performance about the region of interest for quality voice communications, BER $= 10^{-4}$, is approximately 0.7 dB worse than the ML case, but at $N_s = 127$ this penalty increases to approximately 2.4 dB. Performance in the case of unequal power levels can be determined by finding the 'equivalent number of users' transmitting with the nominal signal power. For example, a system with K users where one user transmits with a signal power of $2E_b/T$ exhibits an error rate performance equivalent to a $(K + 1)$ user system with performance given by (3.30). It should be noted that this type of system is not near-far resistant as is the case for the maximum likelihood receiver. However, neither is the system as near-far intolerant as the conventional correlator type system since $g_v << 1$ in (3.27) and (3.30). As a result we suggest that power control algorithms and protocols can be significantly relaxed with respect to the conventional receiver.

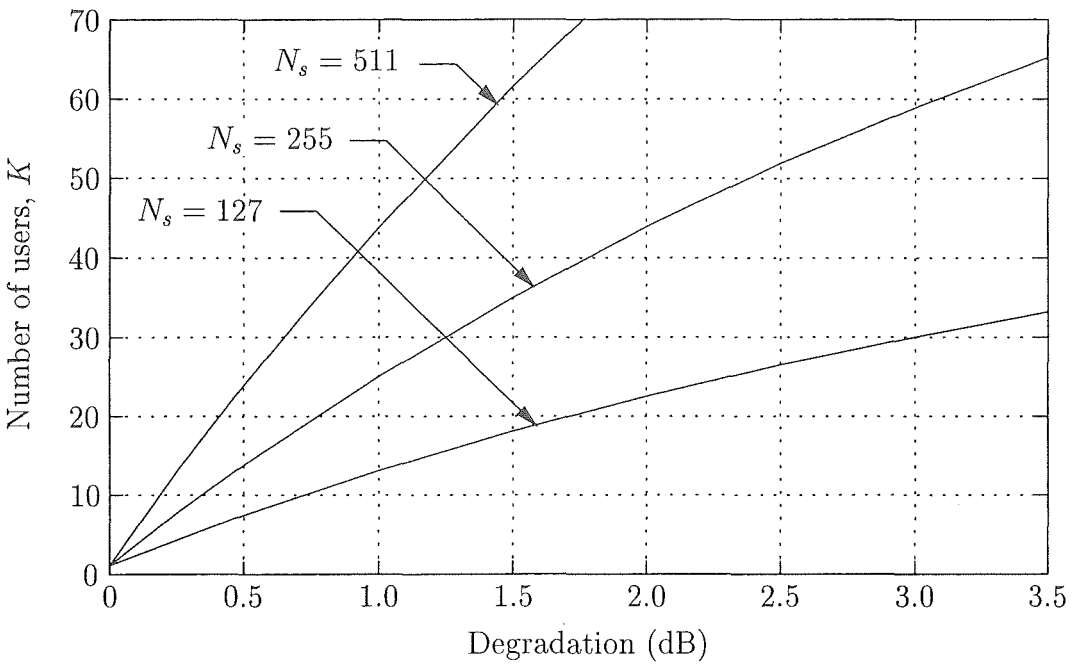

Figure 3.10: Number of supported users in a $K_s = 1$ user per state system for BER $= 10^{-4}$ as a function of processing gain and required increase in signal-to-noise ratio with respect to the maximum likelihood multi-user detector to maintain the same error rate.

Fig. 3.10 shows the number of users that can be supported by a $K_s = 1$ user per state system operating with an error rate of BER $= 10^{-4}$ as a function of processing gain and the necessary increase in signal-to-noise ratio required with respect to the ML MUD to maintain the error performance. The reduced complexity receiver can support more than 10 users with a processing gain of $N_s = 127$, more than 20 users for $N_s = 255$ and more than 40 users for $N_s = 511$ at BER $= 10^{-4}$ with a bit energy to noise power spectral density ratio 1 dB greater than that required by the ML detector.

3.4 Complexity

In this section we quantify the computational complexity of the family of reduced complexity multi-user receivers presented in this chapter. The reduction in computation over the maximum likelihood receiver is due to ML complexity being exponential in the number of states so that reducing the number of

states in the trellis by partially sequentially decoding the user signals replaces exponential complexity with geometric complexity.

Consider again the four user example in Fig. 3.3. With two users per state the number of states reduces from sixteen to four for each of the two subsets, that is, the computation burden is approximately halved. The greater the number of users in the system, the greater is the improvement in complexity for a given K/K_s.

Generally, a K user receiver with K_s users per reduced state has 2^{K_s} states in each subinterval from each of which 2^{K_s} branch metrics must be calculated. The system has N_p subsets requiring a total of $C_{bm} = N_p 4^{K_s}$ branch metric calculations per symbol interval. Note that in the case of the maximum likelihood receiver with Viterbi processing C_{bm} (with $N_p = 1$ and $K_s = K$) is an upper bound since there is a $K-1$ bit dependence, in the maximum likelihood case the branch metrics from half the states are equal so $C_{bm}^{ML} = 4^K/2$.

From the metric given by (3.19) we can determine the arithmetic cost for progress along the trellis by one subset. We assume that addition and multiplication operations are equally costly. From (3.19) the arithmetic cost per branch metric calculation is $A_{bm} = K_s(2K+1)$ leading to the total number of arithmetic operations for each user's decoded bit as

$$\begin{aligned} A_b &= \frac{1}{K} N_p 4^{K_s} K_s (2K+1) \\ &\approx 4^{K_s}(2K+1), \end{aligned} \tag{3.31}$$

since $K = N_p K_s$. This clearly shows the value of the new reduced complexity receivers. The number of arithmetic operations per bit is exponential in the number of users per state, K_s and reducing K_s has a dramatic effect on reducing the complexity of the system. The number of operations per bit of the ML receiver is $A_b^{ML} = 4^K(2K+1)/2$.

The number of storage elements required by the algorithm is exponential in K_s since there are 2^{K_s} paths through the reduced trellis. While the decision depth of the algorithm is increased by a factor N_p the exponential term

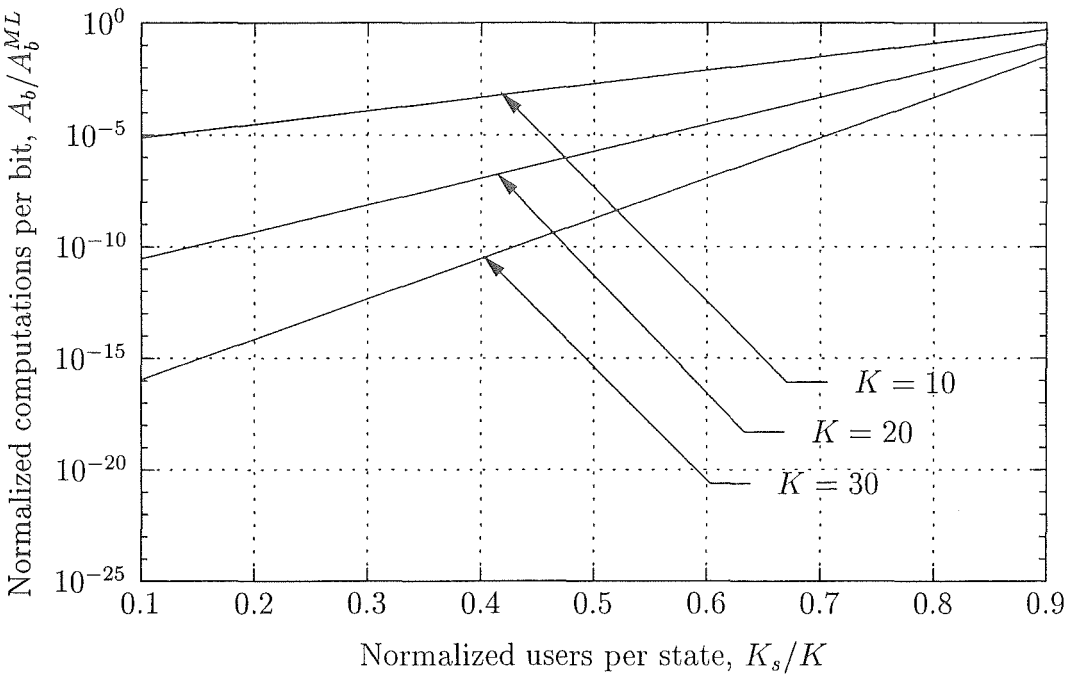

Figure 3.11: Relative computational complexity of the reduced complexity receivers with respect to the maximum likelihood receiver.

clearly dominates and shows the reduced storage requirements of the reduced complexity receivers.

As discussed in earlier sections the reduced complexity receiver requires N_p advances through the trellis during each signalling interval. This requires a Viterbi algorithm processor to be clocked at a higher rate than that used in the ML receiver. This over-clocking requirement is easily offset by the reduction of the computational burden on the VA processor in the reduced complexity receiver.

In Fig. 3.11 we plot the relative number of arithmetic operations per bit A_b/A_b^{ML} (where A_b^{ML} is the number of operations per bit of the ML receiver) as a function of the number of users per state. The effect of reducing the number of users per state on the computational complexity of the receiver is evident. Moreover, since complexity is dominated by the number of users per state K_s the relative computation reduction is greater for systems serving larger numbers of users.

A reduced complexity system with $K = 30$ users and $K_s = 8$ users per state requires fewer arithmetic operations per bit than the ML receiver supporting ten users. As shown in the previous section this system employing sequences with $N_s = 511$ chips per bit has no worse than a 0.7 dB drop in performance with respect to the ML receiver for a BER of 10^{-4} and up to 30 simultaneous users.

3.5 Conclusions

We have presented and evaluated a family of reduced complexity receivers for detecting K asynchronous spread spectrum multiple access users in white noise. The range of receivers available to the system designer allows for the trade off between complexity and performance. The system is based on the maximum likelihood multi-user detector with a serial expansion of the maximum likelihood trellis reducing the number of states to be processed at each instant by the Viterbi algorithm.

It was shown that at one extreme the system reduces to the maximum likelihood multi-user detector while the other extreme results in a system with dramatically reduced complexity. A range of intermediate systems of varying complexity and performance are available. We showed that a system with $K = 20$ users and a processing gain of $N_s = 511$ suffers at most a 0.5 dB loss with respect to the MLSE MUD at a bit error rate of BER $= 10^{-4}$. System performance degrades gracefully for systems employing lower processing gains. With respect to the previous example, when $N_s = 127$ the performance is approximately 2 dB worse than that of the maximum likelihood receiver.

Chapter 4

A REDUCED STATE SEQUENCE ESTIMATION BASED MULTI-USER RECEIVER

4.1 Introduction

Reduced state sequence estimation (RSSE) is a technique in which trellis states are grouped into a single state called a super-state. With this method the number of states can be reduced since at each time interval the a super-state can represent any of its candidate states. This introduces decision feedback into the trellis structure since multiple transitions exist between states during the add and compare stages of the Viterbi algorithm. RSSE techniques were originally applied to the inter-symbol interference problem [19]. The similarities between the intersymbol interference problem and the asynchronous multi-user detection problem are well known and it might be considered surprising that no work has been published that applies RSSE to the multi-user problem. However, if we consider a RSSE system based on the maximum likelihood multi-user detector where all 2^{K-1} states are contained within one super-state, then during the add and compare processes of the Viterbi algorithm there exist 2^{K-1} transitions between states and the number of users does not need to be very large before the number of branch metric calculations becomes prohibitively large. This situation may be alleviated if the serial expansion of the trellis as described in the previous chapter is first applied to the trellis—in this case the number of states is a system parameter and the number of calculations can be reduced to manageable levels for greater numbers of users in the system.

In this chapter RSSE techniques are applied to the family of receivers developed in the previous chapter to form a new family with two degrees of

freedom. We show that the resulting error performance is effectively independent of the number of states per super state giving a performance characteristic asymptotic to the performance of the previous receiver.

4.2 The System

The receiver development continues from the receiver structure presented in the previous chapter. The receiver model is shown in Fig. 3.1 and given by (3.2). The partitioning technique of serial trellis expansion presented in chapter 3 results in a sub-optimal, but significantly reduced complexity receiver structure with an overall path metric given by,

$$\begin{aligned}\tilde{\Omega}(\mathbf{b}) &= \sum_{i=0}^{N}\sum_{p=0}^{N_p-1}\bar{\Omega}(\mathbf{b}_{i,p}) \\ &= \sum_{i=0}^{N}\sum_{p=0}^{N_p-1}\mathbf{b}_{i,p}^{\mathrm{T}}\left(\mathbf{y}_{i,p} - \operatorname{diag}\mathbf{X}_{i,p}\mathbf{G}^{pK_s+1,(p+1)K_s}\right), \end{aligned} \tag{4.1}$$

where $\bar{\Omega}(\mathbf{b}_{i,p})$ is the branch metric for the p-th sub-interval of the i-th signalling interval, the matrix of previous bits $\mathbf{X}_{i,p}$ is,

$$\mathbf{X}_{i,p} \;:\; X_{n,m}^{(i,p)} = b_{\kappa(iK+pK_s+n-m)}(\eta(iK+pK_s+n-m)), \tag{4.2}$$

and $\mathbf{G}^{pK_s+1,(p+1)K_s}$ is a $(K-1)\times K_s$ matrix where the superscript notation gives the range of columns from $\mathbf{G}$ in (3.15). The sequence $\mathbf{b} = [\,\mathbf{b}_{\eta(0),\rho(0)}^{\mathrm{T}}\ \mathbf{b}_{\eta(1),\rho(1)}^{\mathrm{T}} \cdots \mathbf{b}_{\eta(NK-1),\rho(NK-1)}^{\mathrm{T}}\,]^{\mathrm{T}}$ which maximises (4.1) is an estimate of the most likely sequence, under the constraint of the serial expanded and reduced trellis.

As shown in the previous chapter, in each sub-interval the path metrics $\Omega_{i,p}^{\mathbf{b}^s}$, $s = 0, 1, \cdots, 2^{K_s}-1$ at each state in the Viterbi algorithm are updated by a one-step application of (4.1) to obtain

$$\Omega_{i,p}^{\mathbf{b}^s} = \max_{s'}\left[\Omega_{\eta(j-1),\rho(j-1)}^{\mathbf{b}^{s'}} + \bar{\Omega}^{\mathbf{b}^{s'}}(\mathbf{b}_{i,p}^{s})\right] \tag{4.3}$$

where $\Omega_{i,p}^{\mathbf{b}^s}$ is the path metric at the $\mathbf{b}^s$-state at the p-th sub-interval of the i-th signalling interval, $\Omega_{\eta(j-1),\rho(j-1)}^{\mathbf{b}^{s'}}$, is the path metric from the previous sub-interval, and $\bar{\Omega}^{\mathbf{b}^{s'}}(\mathbf{b}_{i,p}^{s})$ is the branch metric in the p-th sub-interval of the i-th

signalling interval from the $\mathbf{b}^{s'}$-state to the $\mathbf{b}^{s}$-state, namely

$$\bar{\Omega}^{\mathbf{b}^{s'}}(\mathbf{b}^{s}_{i,p}) = \mathbf{b}^{s\mathrm{T}}(\mathbf{y}_{i,p} - \operatorname{diag} \mathbf{X}^{\mathbf{b}^{s'},\mathbf{b}^{s}}_{i,p} \mathbf{G}^{pK_s+1,(p+1)K_s}), \tag{4.4}$$

where the path dependence on the matrix of previous bits $\mathbf{X}$ is shown by the superscripts.

This reduced trellis structure is shown in Fig. 4.1(a) for $K = 4$ users with $K_s = 2$ users per state. We call this type of receiver the *sequentially reduced complexity receiver.* Applying RSSE techniques to this trellis results in a new family of receiver structures which we call *RSSE reduced complexity receivers.* Following the example in the figure, at each subset the four states can be merged into a number of super-states, S, where $1 \leq S \leq 2^{K_s}$ and the number of states per super state $S_s \leq 2^{K_s}/S$. While the theory may be generalised, we limit S to be a factor of 2^{K_s} so that S_s is constant for all super-states.

This process is shown in Fig. 4.1(b) for $S = 2$ super-states and in Fig. 4.1(c) for $S = 1$. In both cases the RSSE partitioning of the trellis allows for each state in the reduced trellis to represent more than one sub-vector—each of the S super-states has a number of candidate states as members. We will show later that the optimal criterion for the grouping of states into super-states is a rule of maximum distance between constituent super-state members. This ensures that the probability of choosing the incorrect state as the value assumed by the super-state is minimised. The partitioning is such that the set of candidate states in each super-state is $B^s \subset B$ with $B^s \cap B^{s'} = \emptyset$ for $s, s' = 0, 1, \cdots, 2^{K_s} - 1$ and $s \neq s'$, and $\bigcup_{s=0}^{2^{K_s}-1} B^s = B$ where B is the set of all possible vectors $\mathbf{b}$ defined in section 3.2. That is, all states of the reduced trellis are represented, and represented only once in the super-state grouping process. This process introduces delayed decision feedback [13] into the receiver structure. The receiver makes S coarse estimates of a different subset of the set of bit estimates and uses the trellis structure to refine the estimate by considering more of the transmitted sequences.

In each sub-interval the S path metrics $\Omega^{\mathbf{b}^s}_{i,p}$ of the super-states are updated

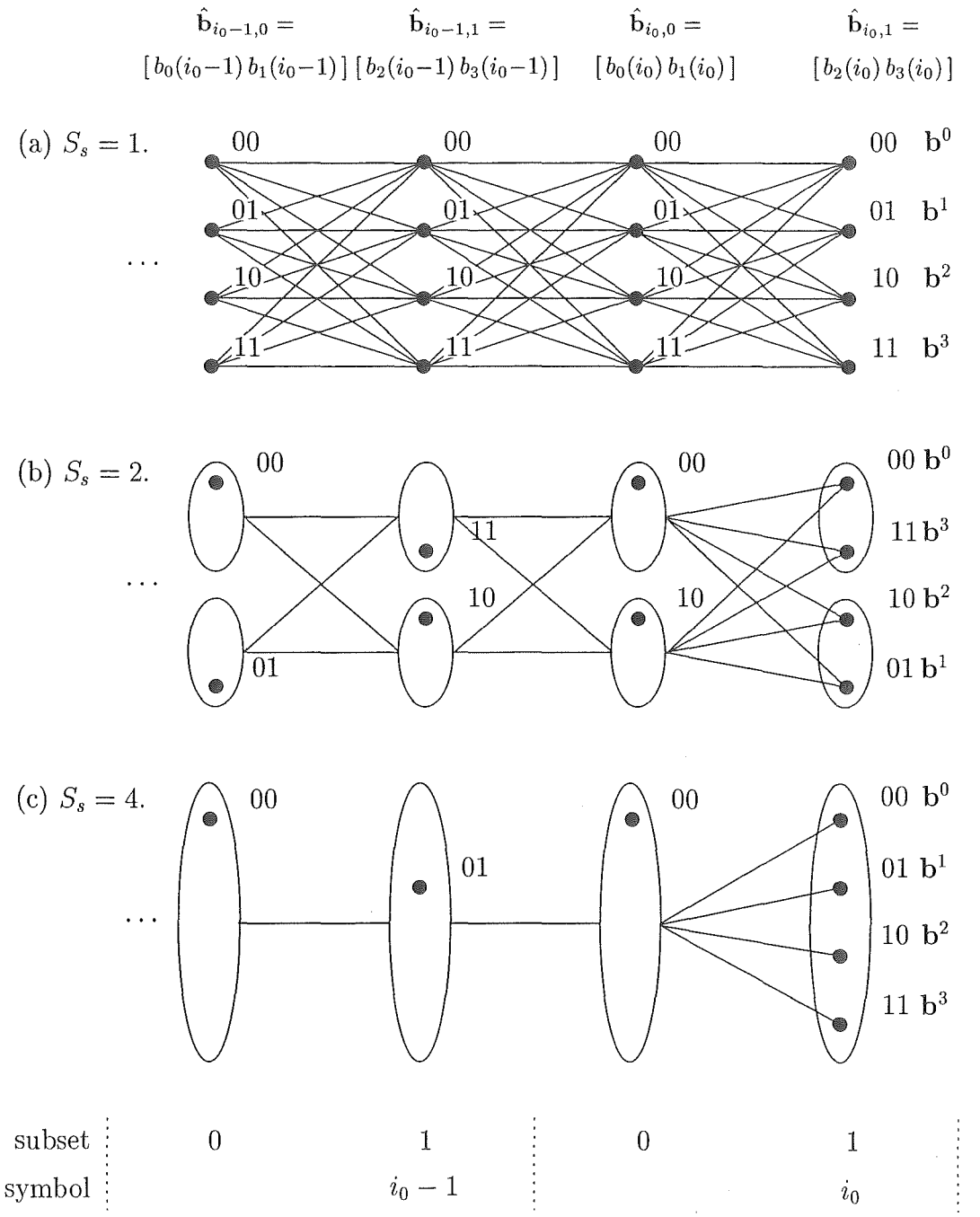

Figure 4.1: $K = 4$ user reduced complexity trellis with $K_s = 2$ users per state, S super-states, S_s states per super-state and $N_p = 2$ sub-intervals per bit.

by choosing the greatest path metric from each of the S_s candidate states,

$$\Omega_{i,p}^{\mathbf{b}^s} = \max_{\mathbf{b}^{s'} \in B^s} \Omega_{i,p}^{\mathbf{b}^{s'}}, \tag{4.5}$$

where $\Omega_{i,p}^{\mathbf{b}^{s'}}$ is the path metric at the $\mathbf{b}^{s'}$ state in the p-th sub-interval of the i-th symbol period given by

$$\Omega_{i,p}^{\mathbf{b}^{s'}} = \max_{s} \left[\Omega_{\eta(iK+pN_p-1),\rho(iK+pN_p-1)}^{\mathbf{b}^s} + \bar{\Omega}^{\mathbf{b}^s}(\mathbf{b}_{i,p}^{s'}) \right], \tag{4.6}$$

and the super-state at that sub-interval $\mathbf{b}_{i,p}^s$ assumes the value corresponding to the surviving path metric entering the super-state,

$$\mathbf{b}_{i,p}^j = \arg \Omega_{i,p}^{\mathbf{b}^s}. \tag{4.7}$$

In the special case where all states are candidate states for one super-state ($S = 1$ and $S_s = 2^{K_s}$) the maximisation in (4.6) is only over one state since the trellis has collapsed to one path with one state. The receiver then becomes a pure decision feedback structure which is observed in the dependency of the path metric (4.6) on the previous bits as shown in (4.1). We call this special case of the RSSE reduced complexity receiver the *decision feedback reduced complexity receiver*. In this case, combining (4.5) and (4.6) gives the path metric written as,

$$\Omega_{i,p}^{\mathrm{DF}} = \max_{\mathbf{b}^{s'} \in B} \bar{\Omega}(\mathbf{b}_{i,p}^{s'}), \tag{4.8}$$

and the value assumed by the super-state at each sub-interval is,

$$\mathbf{b}_{i,p}^0 = \arg \Omega_{i,p}^{\mathrm{DF}}. \tag{4.9}$$

The decision feedback receiver structure is shown in Fig. 4.2 and consists of a decision device utilising the metric of (4.8), and an length N_p, K_s-dimensional shift register to store the previous $N_p K_s = K$ estimates in order to form $\mathbf{X}_{i,p}$.

4.2.1 Example

Consider the four user example in Fig. 4.1 for the transition from the (i_0-1)-th to the i_0-th signalling interval. The trellis of a reduced complexity receiver with

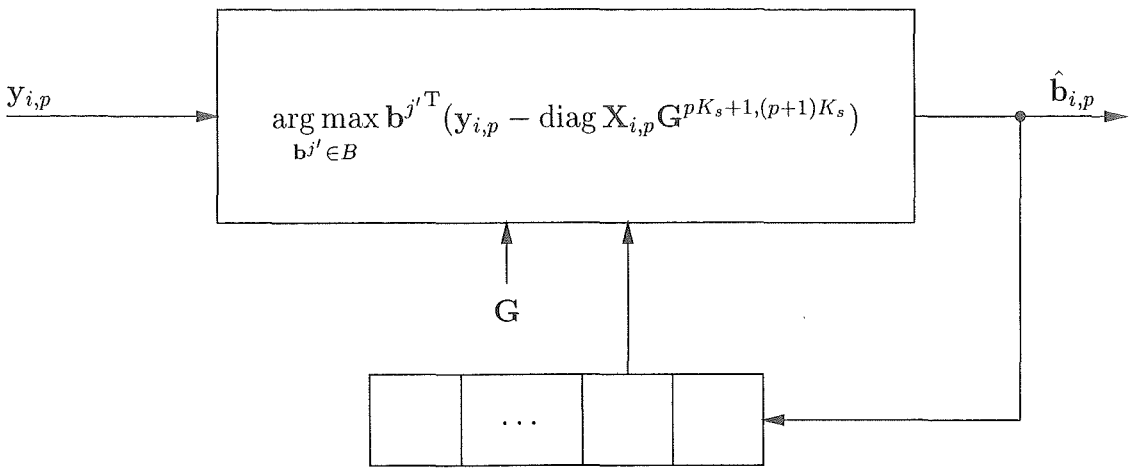

Figure 4.2: A Decision Feedback RSSE Reduced Complexity Receiver.

$K_s = 2$ users per state, $S_s = 2$ states per super-state and $N_p = 2$ sub-intervals per symbol is shown in Fig. 4.1(b). $N_p = 2$ transitions through the trellis must be made to compute the path metrics for the transition from the $(i_0 - 1)$-th to the i_0-th signalling interval. The first subset is responsible for contributing to the path metrics from the first two users, the second subset contributes from the third and fourth users. The output of the bank of correlators at symbol time $i = i_0$ is represented by the vector,

$$\mathbf{y}_{i_0} = [\, y_0(i_0)\, y_1(i_0)\, y_2(i_0)\, y_3(i_0)\,]^{\mathrm{T}}.$$

At each state in the reduced trellis, four paths from previous states compete to be the surviving path. The path metrics entering each state at $i = i_0$, $p = 0$ are calculated using (4.6) and the first set of outputs from the correlator bank, $\mathbf{y}_{i_0,0} = [\, y_0(i_0)\, y_1(i_0)\,]^{\mathrm{T}}$. Consider the case where the competing paths enter the $\mathbf{b}^0$-state at $i = i_0$, $p = 0$, in this case $\mathbf{b}_{i_0,0} = [\,-1\ -1\,]^{\mathrm{T}}$. The receiver discards three of the four paths by choosing the most likely (surviving) path from the four contenders. The correlation matrix $\mathbf{G}^{1,2}$ is a constant during the calculations at any sub-interval and is a subset of the matrix of all user correlations $\mathbf{G}$ from (3.15). The matrix of previous bits $\mathbf{X}_{i_0,0}$ is formed row-

wise by tracing back from each state at $i = i_0$, $p = 0$ by $N_p = 2$ branches in the trellis, filling rows of $\mathbf{X}_{i_0,0}$ with the surviving bits along the path represented by the state labels $\mathbf{b}^{s'}$. Note that each branch metric calculation requires a different $\mathbf{X}_{i_0,0}$ since the $K-1$ previous bits in each path are different. To illustrate, suppose a competing path arriving at the $\mathbf{b}^0$-state at $i = i_0$, $p = 0$, had at $i = i_0 - 1$, $p = 1$ passed through the $\mathbf{b}^2$-state, and had at $i = i_0 - 1$, $p = 0$ passed through the $\mathbf{b}^1$-state, then,

$$\mathbf{X}_{i_0,0}^{\mathbf{b}^2,\mathbf{b}^0} = \begin{bmatrix} -1 & 1 & 1 \\ -1 & -1 & 1 \end{bmatrix},$$

and the branch metric $\bar{\Omega}^{\mathbf{b}^2}(\mathbf{b}_{i_0,0}^0)$ corresponding to the first path entering the $\mathbf{b}^0$-th state is,

$$\bar{\Omega}^{\mathbf{b}^2}(\mathbf{b}_{i_0,0}^0) = \mathbf{b}^{0\mathrm{T}} \left(\mathbf{y}_{i_0,0} - \operatorname{diag} \mathbf{X}_{i_0,0}^{\mathbf{b}^2,\mathbf{b}^0} \mathbf{G}^{1,2} \right).$$

The other path entering the $\mathbf{b}^0$-state is calculated with another $\mathbf{X}_{i_0,0}$ matrix representing the previous bits from the other path in the trellis entering the $\mathbf{b}^0$-state. The surviving path entering the $\mathbf{b}^0$-state is calculated from (4.6). The same process is applied to determine the surviving path entering the other contending state $\mathbf{b}^3$ in the first super-state. The greater of the two metrics gives the surviving path entering the first super-state by (4.5) and the value assumed by the super-state at $i = i_0$, $p = 0$ is given directly by (4.7). Similar calculations are made to determine survivors entering the candidate states $\mathbf{b}^1$ and $\mathbf{b}^2$ in the second super-state, the surviving path entering the super-state and its assumed value.

The Viterbi Algorithm searches through the two super-states for the largest path metric and follows the path corresponding to the greatest metric through the decision depth of the VA. The assumed value of the originating state of this path gives the most likely transmitted bits (from d signalling intervals earlier) for the first two users, $\hat{\mathbf{b}}_{i_0-d,0} = [\, \hat{b}_0(i_0 - d)\, \hat{b}_1(i_0 - d)\,]^{\mathrm{T}}$.

The second sub-interval is decoded considering the second set of outputs from the correlator bank, $\mathbf{y}_{i_0,0} = [\, y_2(i_0)\, y_3(i_0)\,]^{\mathrm{T}}$. The matrix of surviving

inputs $\mathbb{X}_{i_0,1}$ includes bits in the paths at $i = 0$, $p = 0$; as an example suppose a competing path arriving at the $\mathbf{b}^3$-state at $i = i_0$, $p = 1$, had at $i = i_0$, $p = 0$ passed through the $\mathbf{b}^0$-state, and had at $i = i_0 - 1$, $p = 1$ passed through the $\mathbf{b}^3$-state, then

$$\mathbb{X}_{i_0,1}^{\mathbf{b}^0,\mathbf{b}^3} = \begin{bmatrix} -1 & -1 & 1 \\ 1 & -1 & -1 \end{bmatrix}.$$

The correlation matrix for the second sub-interval is the sub-matrix of $\mathbf{G}$ with columns corresponding to the third and fourth users, namely $\mathbf{G}^{3,4}$. The same add, compare, select process is applied to the branch metrics and the estimated bits $\hat{\mathbf{b}}_{i_0-d,1} = [\,\hat{b}_2(i_0-d)\,\hat{b}_3(i_0-d)\,]^{\mathrm{T}}$ are returned by the VA by examining the originating state of the path with the greatest path metric. Note that in this example with $N_p = 2$ subsets, two iterations of the Viterbi Algorithm are required to estimate all the users and this requires two sets of add, compare, and select operations. The vector $\hat{\mathbf{b}}_{i_0-d}$ representing all the decoded users is a concatenation of the vectors obtained by the reduced VA during processing of each subset, and may be written as

$$\begin{aligned} \hat{\mathbf{b}}_{i_0-d} &= [\,\hat{\mathbf{b}}_{i_0-d,0}^{\mathrm{T}}\,\hat{\mathbf{b}}_{i_0-d,1}^{\mathrm{T}}\,]^{\mathrm{T}} \\ &= [\,\hat{b}_0(i_0-d)\,\hat{b}_1(i_0-d)\,\hat{b}_2(i_0-d)\,\hat{b}_3(i_0-d)\,]^{\mathrm{T}}. \end{aligned}$$

The decision feedback reduced complexity receiver for the same $K = 4$ users, $K_s = 2$ users per state system selects the state to be assumed by the super-state through (4.9). In this case the estimate of the transmitted vector of user bits for the i_0-th symbol interval is

$$\hat{\mathbf{b}}_{i_0} = [\,\hat{\mathbf{b}}_{i_0,0}^{0^{\mathrm{T}}}\,\hat{\mathbf{b}}_{i_0,1}^{0^{\mathrm{T}}}\,]^{\mathrm{T}},$$

where $\hat{\mathbf{b}}_{i_0,0}^0$ and $\hat{\mathbf{b}}_{i_0,1}^0$ are the values assumed by the super-state during the two sub-intervals of the i_0-th symbol interval given directly by (4.9) as

$$\hat{\mathbf{b}}_{i_0,0}^0 = \underset{\mathbf{b}^{s'} \in B}{\arg\max}\, \mathbf{b}^{s'^{\mathrm{T}}}_{i_0,0} \left(\mathbf{y}_{i_0,0} - \operatorname{diag} \mathbb{X}_{i_0,0}\mathbf{G}^{1,2}\right),$$

and

$$\hat{\mathrm{b}}^{0}_{i_0,1} = \arg\max_{\mathrm{b}^{s'} \in B} \mathrm{b}^{s'\,\mathrm{T}}_{i_0,1} \left(\mathrm{y}_{i_0,1} - \operatorname{diag} \mathrm{X}_{i_0,1} \mathrm{G}^{3,4} \right).$$

That is, the decision feedback receiver also requires that $N_p = 2$ sub-intervals be processed in order to estimate the transmitted bit of all $K = 4$ users.

4.2.2 Performance

In this section performance measures for the RSSE reduced complexity receiver family are developed in a similar fashion to the simple reduced complexity receiver of the previous chapter. Throughout the derivation it is assumed that the transmitted bits of different users are independent and that the effects of error propagation are small. The error propagation assumption allows the received errored path to be considered as a one sub-interval deviation from the transmitted path, which is assumed without loss of generality to be the all-zeros path through the trellis. The probability that the most likely of the estimated paths diverges from the transmitted path at one sub-interval and re-merges one sub-interval later, P_e, will be used to estimate the probability of bit error P_b.

Considering the metric in (4.6) the error event probability may be written as,

$$P_e = \frac{1}{K_s} \sum_{j'=0}^{2^{K_s}-1} \Pr\left(\Omega^{\mathrm{b}^0} < \Omega^{\mathrm{b}^{j'}} \right), \tag{4.10}$$

where the probability that the receiver chooses the wrong candidate state to be assumed by the super-state is

$$\begin{aligned} \Pr\left(\Omega^{\mathrm{b}^0} < \Omega^{\mathrm{b}^{j'}} \right) &= \Pr\left(\Omega^{\mathrm{b}^0} - \Omega^{\mathrm{b}^{j'}} < 0 \right) \\ &= \Pr\Big(\mathrm{b}^{0\,\mathrm{T}}_{i,p} (\mathrm{y}_{i,p} - \operatorname{diag} \mathrm{X}_{i,p} \mathrm{G}^{pK_s+1,(p+1)K_s}) - \\ &\qquad \mathrm{b}^{j'\,\mathrm{T}}_{i,p} (\mathrm{y}_{i,p} - \operatorname{diag} \mathrm{X}_{i,p} \mathrm{G}^{pK_s+1,(p+1)K_s}) < 0 \Big). \end{aligned} \tag{4.11}$$

Expanding the vector notation, (4.11) becomes

$$\begin{aligned}\Pr\left(\Omega^{\mathbf{b}^0} < \Omega^{\mathbf{b}^{j'}}\right) = \\ \Pr\Bigg(\sum_{k=0}^{K_s-1} \Big\{ & b^{j'}_{\kappa(a)}(\eta(a))\, b^0_{\kappa(a)}(\eta(a))\, g_{\kappa(a),\kappa(a)}(\eta(a),\eta(a)) \\ & + b^{j'}_{\kappa(a)}(\eta(a)) \sum_{l=1}^{K-1} b^0_{\kappa(a+l)}(\eta(a+l))\, g_{\kappa(a),\kappa(a+l)}(\eta(a),\eta(a+l)) \\ & + b^{j'}_{\kappa(a)}(\eta(a))\, n_{\kappa(a)}(\eta(a)) - g_{\kappa(a),\kappa(a)}(\eta(a),\eta(a)) \\ & - b^0_{\kappa(a)}(\eta(a)) \sum_{l=1}^{K-1} b^0_{\kappa(a+l)}(\eta(a+l))\, g_{\kappa(a),\kappa(a+l)}(\eta(a),\eta(a+l)) \\ & - b^0_{\kappa(a)}(\eta(a))\, n_{\kappa(a)}(\eta(a)) \Big\} < 0\Bigg), \end{aligned} \tag{4.12}$$

where the straight-forward substitution $a = iK + pK_s + k$ is made. Recognising in (4.12) that if $w_{j'}$ is the Hamming weight of the $\mathbf{b}^{j'}$-state then there are $K - w_{j'}$ equal bits (and $w_{j'}$ unequal) in the correct path and the error path, the error event probability is written as,

$$\begin{aligned}\Pr\left(\Omega^{\mathbf{b}^0} < \Omega^{\mathbf{b}^{j'}}\right) = \Pr\Bigg(& \sum_{k\in K_1} \sum_{l\in L} g_{\kappa(a),\kappa(a+l)}(\eta(a),\eta(a+l)) \\ & + \sum_{k\in K_2} \Big\{ g_{\kappa(a),\kappa(a)}(\eta(a),\eta(a)) - n_{\kappa(a)}(\eta(a)) \\ & - \sum_{l=1}^{K-1} g_{\kappa(a),\kappa(a+l)}(\eta(a),\eta(a+l)) \Big\} < 0\Bigg), \end{aligned} \tag{4.13}$$

where the sets K_1, K_2, and L are defined as,

$$\begin{aligned} K_1 &= \left\{k : b^{j'}_{\kappa(a+l)}(\eta(a+l)) = b^0_{\kappa(a+l)}(\eta(a+l))\right\}, \\ K_2 &= \left\{k : b^{j'}_{\kappa(a+l)}(\eta(a+l)) \neq b^0_{\kappa(a+l)}(\eta(a+l))\right\}, \end{aligned}$$

and

$$L = \left\{l : b^{j'}_{\kappa(a+l)}(\eta(a+l)) \neq b^0_{\kappa(a+l)}(\eta(a+l))\right\}.$$

Combining the noise and interference terms, (4.13) becomes,

$$\Pr\left(\Omega^{b^0} < \Omega^{b^{j'}}\right) = \Pr\Big(\sum_{k\in K_2} \Big\{ g_{\kappa(a),\kappa(a)}(\eta(a),\eta(a)) - n_{\kappa(a)}(\eta(a)) - \sum_{l=1}^{K-1} g_{\kappa(a),\kappa(a+l)}(\eta(a),\eta(a+l)) + \frac{1}{w_{j'}} \sum_{k\in K_1}\sum_{l\in L} g_{\kappa(a),\kappa(a+l)}(\eta(a),\eta(a+l)) \Big\} < 0 \Big)$$

$$= \Pr\Big(\sum_{k\in K_2} \big\{ g_{\kappa(a),\kappa(a)}(\eta(a),\eta(a)) - \gamma \big\} < 0 \Big), \tag{4.14}$$

where γ is the combined noise and interference with zero mean and variance given by,

$$\begin{aligned} \mathrm{V}[\gamma] &= \frac{E_b N_o}{2} + \sum_{l=1}^{K-1} \int_0^T g^2_{\kappa(a),\kappa(a+l)}(\eta(a),\eta(a+l)) \; , d\tau_{\kappa(a)} \\ &\quad - \frac{1}{w_j} \sum_{k\in K_1}\sum_{l\in L} \int_0^T g^2_{\kappa(a),\kappa(a+l)}(\eta(a),\eta(a+l))\, d\tau_{\kappa(a)} \\ &= \frac{E_b N_o}{2} + \sum_{l=1}^{K-1}\sum_{m=0}^{N_s-1} \int_{mT/N_s}^{(m+1)T/N_s} g^2_{\kappa(a),\kappa(a+l)}(\eta(a),\eta(a+l))\, d\tau_{\kappa(a)} \\ &\quad - \frac{1}{w_j} \sum_{k\in K_1}\sum_{l\in L}\sum_{m=0}^{N_s-1} \int_{mT/N_s}^{(m+1)T/N_s} g^2_{\kappa(a),\kappa(a+l)}(\eta(a),\eta(a+l))\, d\tau_{\kappa(a)} \\ &= \frac{E_b N_o}{2} + \frac{E_b^2}{3} \sum_{l=1}^{K-1} g_v(l) - \frac{E_b^2}{3w_j} \sum_{k\in K_1}\sum_{l\in L} g_v(l). \end{aligned} \tag{4.15}$$

In (4.15) the interference term $g_v(l)$ may be written as

$$g_v(l) = \frac{1}{N_s^3} \sum_{m=0}^{N_s-1} \Big\{ C^2_{\kappa(a),\kappa(a+l)}(m+1) + C_{\kappa(a),\kappa(a+l)}(m+1) C_{\kappa(a),\kappa(a+l)}(m) + C^2_{\kappa(a),\kappa(a+l)}(m) \Big\}, \tag{4.16}$$

in terms of the discrete aperiodic cross-correlation function $C_{k,k'}(m)$ of (2.8).

Calculations for $g_v(l)$ can be made for any set of spreading sequences using (4.16). Again we calculate $g_v(l)$ for random spreading sequences giving the parameter g_v which is independent of l and dependant only on sequence length. The noise and interference variance can then be written as

$$\mathrm{V}[\gamma] = \frac{E_b N_o}{2} + \frac{E_b^2 g_v (K - K_s + w_{j'} - 1)}{3}. \tag{4.17}$$

Modelling the noise and interference as a Gaussian process with the mean and variance as written above, a simple expression for the bit error probability follows. Making the substitution $x \triangleq -g_{\kappa(a'),\kappa(a')}(\eta(a'),\eta(a')) + \gamma$ gives the error event probability written as,

$$\begin{aligned} P_e &= \frac{1}{K_s}\sum_{j'=0}^{2^{K_s}-1} \Pr\Big(\sum_{k\in K_2} x > 0\Big) \\ &= \frac{1}{K_s}\sum_{j'=0}^{2^{K_s}-1} \frac{1}{\sqrt{2w_{j'}\,\mathrm{V}[x]\pi}} \int_0^{\infty} \exp\left(-\frac{(x - w_{j'}\,\mathrm{E}[x])^2}{2w_{j'}\,\mathrm{V}[x]}\right) dx \\ &= \frac{1}{2K_s}\sum_{j'=0}^{2^{K_s}-1} \operatorname{erfc}\left(\sqrt{\frac{w_{j'}E_b}{N_o + 2g_v E_b(K - K_s + w_{j'} - 1)/3}}\right). \end{aligned} \tag{4.18}$$

The probability of bit error at medium to high E_b/N_o for the decision feedback reduced complexity receiver is well approximated by $P_b = P_e$ since for moderate to high E_b/N_o the effects of error propagation are small and there is only one path in the trellis. For the general RSSE receivers (4.18) can be used to calculate the approximate probability of any error path through the trellis and thus determine an approximation of the bit error probability by union bound techniques. However, for medium to high E_b/N_o the error events are dominated by minimum distance error events and an approximation to the bit error probability is also $P_b \approx P_e$.

Since the super-state in each sub-interval in the decision feedback RSSE reduced complexity receiver contains all possible 2^{K_s} binary vectors the bit error probability can be written in terms of the binomial coefficient as

$$P_b = \frac{1}{2K_s}\sum_{j=1}^{K_s} \binom{K_s}{j} \operatorname{erfc}\left(\sqrt{\frac{jE_b}{N_o + 2g_v E_b(K - K_s + j - 1)/3}}\right). \tag{4.19}$$

Note that the first summation term in (4.19) is the bit error probability for the receiver family with the number of users per state set to $K_s = 1$, that is the sequentially reduced complexity receiver of chapter 3 and [79]. For medium to high E_b/N_o, the first summation term dominates, and the performance of the RSSE reduced complexity receiver, for any number of users per state

K_s, approaches that of the simple receiver but with a further reduction in complexity. We analyse the complexity of this receiver family in section 4.4.

As discussed in chapter 3 the second term in the denominator of the complimentary error function argument in (4.19) can be considered to be a leakage term and is a function of the relative power levels among the users' signals. Users transmitting with greater power levels contribute more to the leakage term and the average performance worsens. The nature of this behaviour is similar to that of conventional spread spectrum systems without power control except on two points—(a) the level of interference is smaller than that of conventional spread spectrum because of joint detection and (b) the level of interference may be controlled through the number of users per state K_s. These two points suggest that a relaxation of power control regimes is possible and that complexity in the detector can be traded for complexity in the power control algorithm and control channel protocol.

4.3 Performance Results

Monte Carlo simulations have been performed for the whole family of RSSE reduced complexity receivers employing K equiprobable asynchronous binary sources with equal powers, uniformally distributed relative delays τ_k and rectangular m-sequence spreading waveforms in an AWGN channel. For the case of unequal signal powers, an 'equivalent number of users' can be determined and the approximate performance determined from (4.19).

In Figs. 4.3 and 4.4 we compare simulation results with the theoretical results developed in the previous section for systems employing processing gains of $N_s = 127$, a range of users per state K_s and $K = 10, 30$ respectively. The performance results for the receiver with $S = 2^{K_s}$ super-states corresponding to the simple reduced complexity receiver are from chapter 3. The results show that the effect of grouping states into super-states has little effect on system error performance. In the figures we have plotted simulation results for the simple reduced complexity receiver and the decision feedback receiver; other

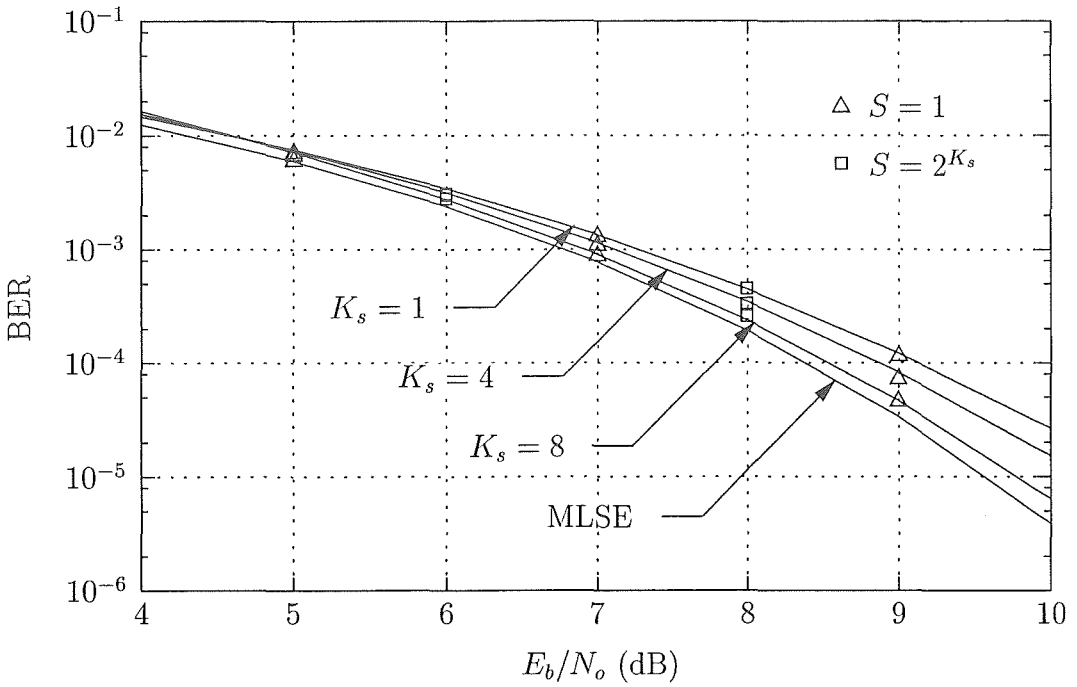

Figure 4.3: Performance of the decision feedback reduced complexity receiver with $K = 10$ users and processing gain $N_s = 127$. Simulation results for the decision feedback receiver ($S = 1$) and the sequentially reduced complexity receiver ($S = 2^{K_s}$) are shown as points.

values of S produce similar results. The results show that the simulation and theoretical results are a close match and that there is little performance change, at least at medium to high E_b/N_o, for changes in the number of super-states S. Hence, the decision feedback reduced complexity receiver is representative, performance-wise, of the whole family of RSSE reduced complexity receivers for a given K_s.

In Fig. 4.5 the performance of the decision feedback receiver is shown for a processing gain of $N_s = 255$. For a BER $= 10^{-4}$ the receiver performance for $K_s = 8$ users per state is a fraction of a dB from the ML receiver for $K = 10$ and less than 1 dB for $K = 30$. For $K_s = 1$ user per state, the receiver requires about 0.3 dB higher E_b/N_o than the ML detector for $K = 10$, and approximately 1.3 dB more when the number of users increases to $K = 30$.

Fig. 4.6 presents performance results for the same system but with a processing gain of $N_s = 511$. In this case the degradation from the ML receiver

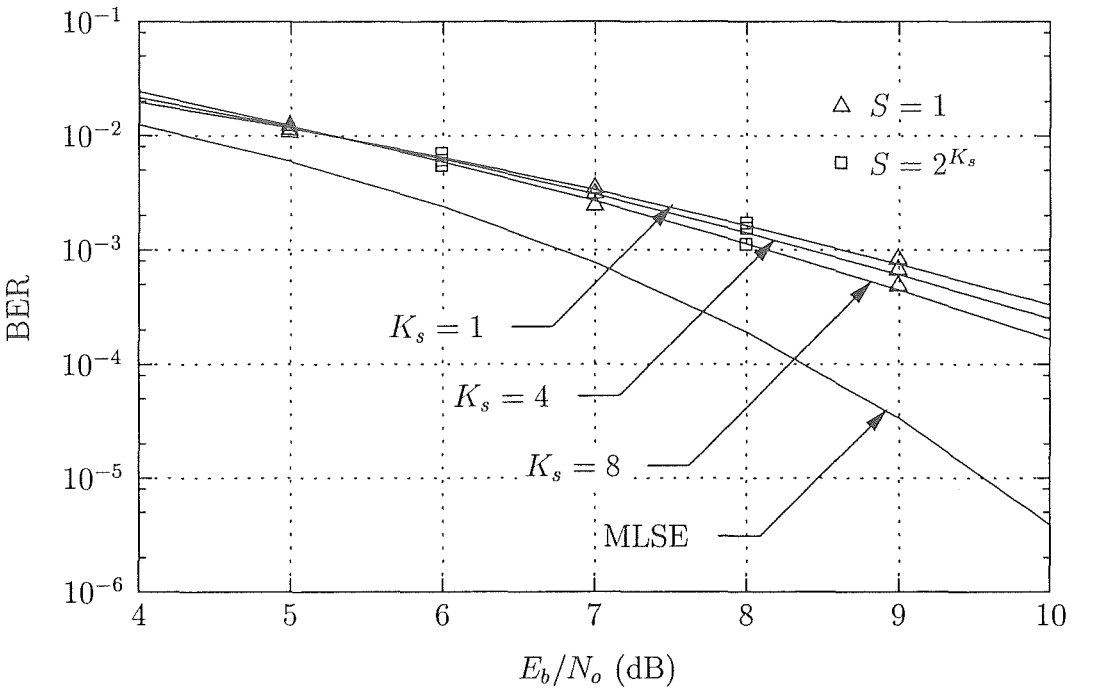

Figure 4.4: Performance of the decision feedback reduced complexity receiver with $K = 30$ users and processing gain $N_s = 127$. Simulation results for the decision feedback receiver ($S = 1$) and the sequentially reduced complexity receiver ($S = 2^{K_s}$) are shown as points.

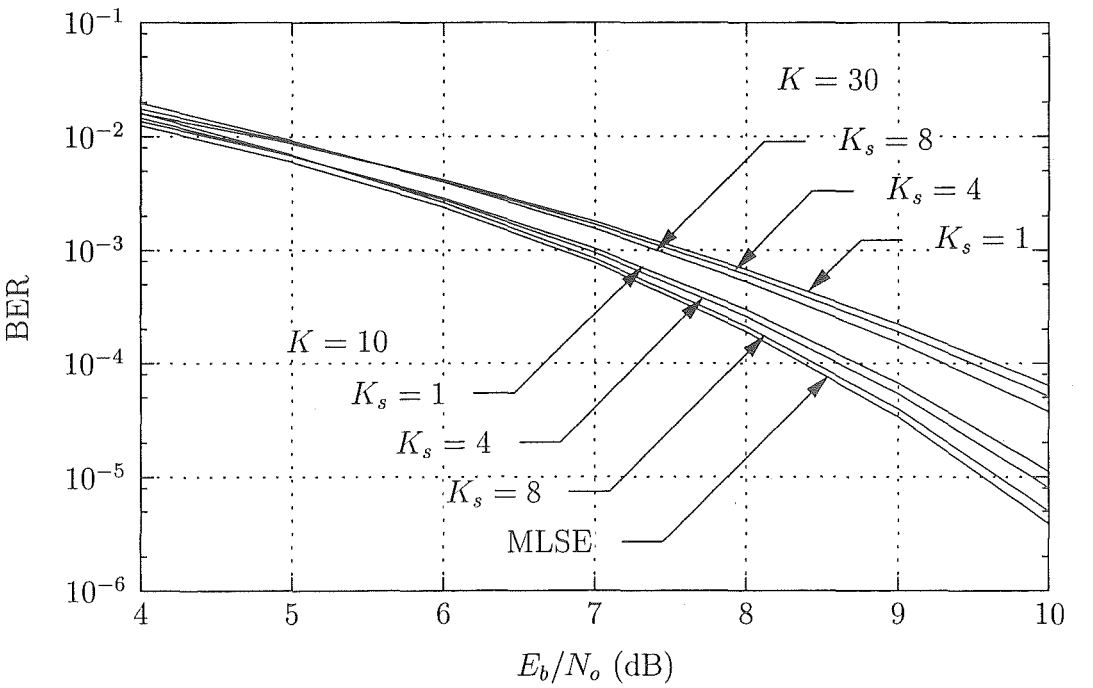

Figure 4.5: Performance of the decision feedback reduced complexity receiver with $K = 10, 30$ users and processing gain $N_s = 255$.

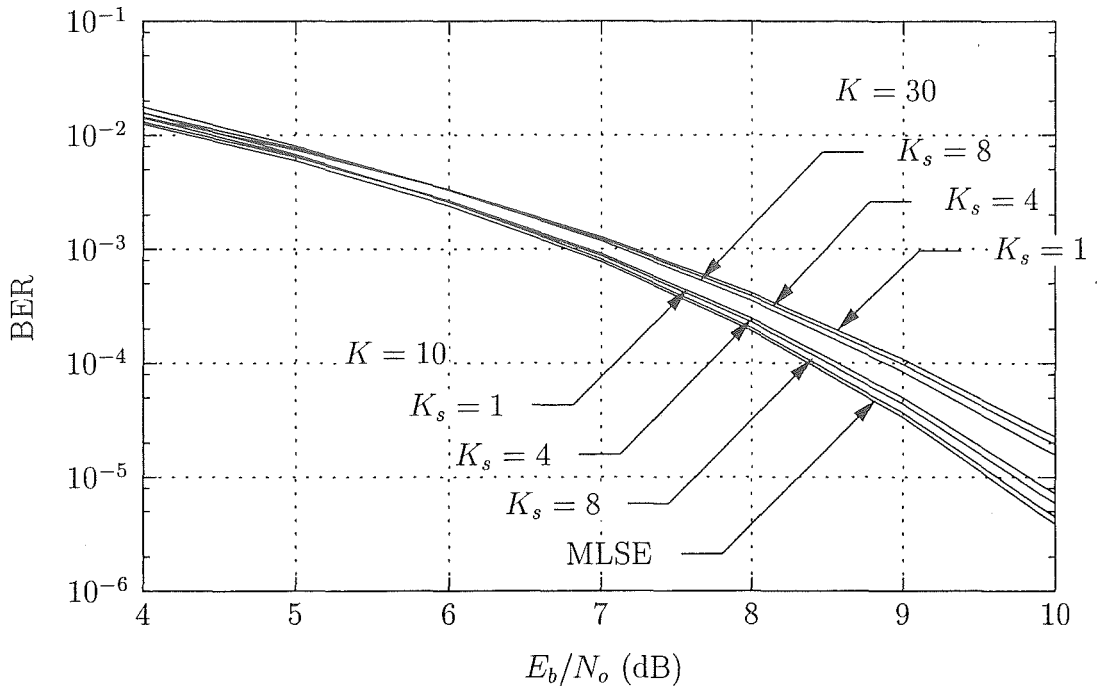

Figure 4.6: Performance of the decision feedback reduced complexity receiver with $K = 10, 30$ users and processing gain $N_s = 511$.

is reduced. For $K = 10$ the performance for the decision feedback receiver is comparable to the ML receiver for $K_s = 8$, and the degradation with respect to the ML receiver is approximately 0.5 dB for $K = 30$.

The degradation with respect to the ML detector for a BER $= 10^{-4}$ is shown in Fig. 4.7 as a function of processing gain and the number of users per state. For a degradation of 0.5 dB with respect to the ML receiver, the decision feedback receiver with $K_s = 8$ supports $K = 14, 20, 30$ users for processing gains of $N_s = 127, 255, 511$ respectively. For a 1 dB performance degradation the number of supported users at the same error rate BER 10^{-4} increases to $K = 20, 31, 50$ users. The figure shows the range of supported users for other E_b/N_o degradation levels withN_s and K_s as parameters.

Comparing the performance of the RSSE reduced complexity receivers with the performance curves for the PIC detector in Fig. 2.5 it is clear that the RSSE reduced complexity receivers perform much closer to the optimum receiver as do the PIC receivers. For a bit error rate of BER=10^{-3}, the decision feedback

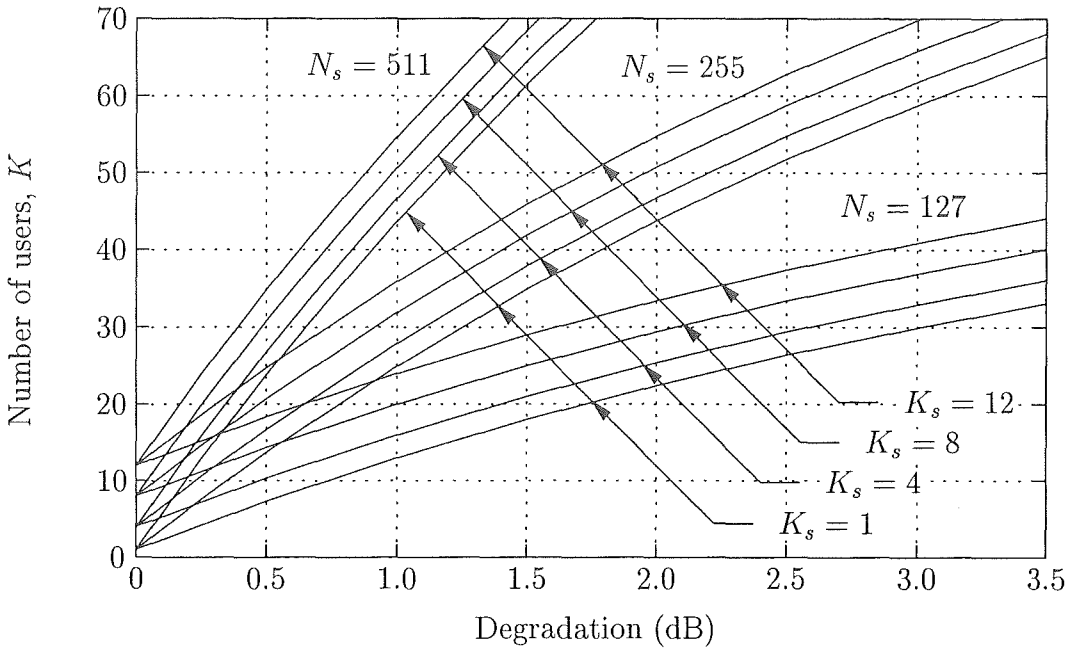

Figure 4.7: Number of supported users for BER = 10^{-4} as a function of processing gain N_s, the number of users per state K_s and the required increase in E_b/N_o with respect to the MLSE receiver in order to maintain the same error rate.

receiver with $K = 30$ users perform 1 dB better that the PIC receivers. For higher numbers of states the situation improves; with $K_s = 8$, the RSSE detector is 2.5 dB better than the PIC detector.

In Fig. 4.8 a more heavily loaded system is presented. In this case the receiver has a processing gain of $N_s = 127$ and $K = 64$ users. As expected, the error performance for a given bit energy to noise power spectral density ratio is worse than that of a system which is not as heavily loaded. However, as shown in the figure, increasing the number of users per state K_s improves the error performance of the system. We have modelled a system exhibiting the near-far

phenomenom where the average received power levels of users observed by the receiver are distributed uniformally. In Figs 4.9 and 4.10 the ratio of maximum observed users signal power to nominal is 3 dB, in Figs 4.11 and 4.12 the ratio is 10 dB. In both cases the resultant degradion is less than 0.5 dB.

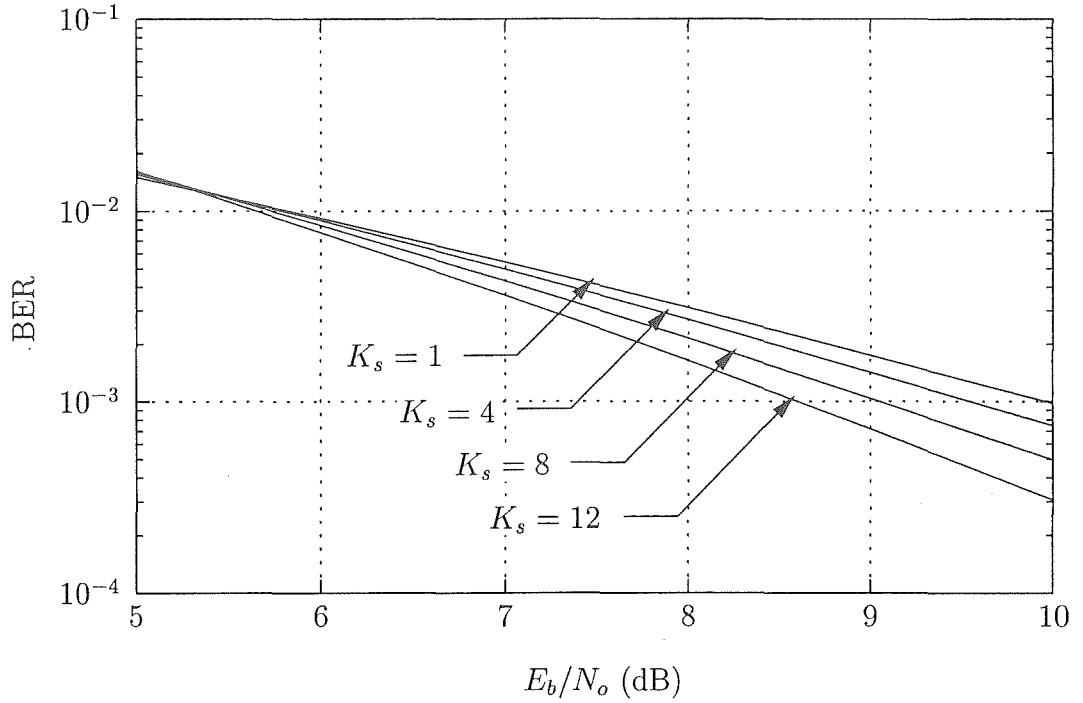

Figure 4.8: Receiver performance for varying users per state K_s with $K = 64$ users with a procesing gain $N_s = 127$.

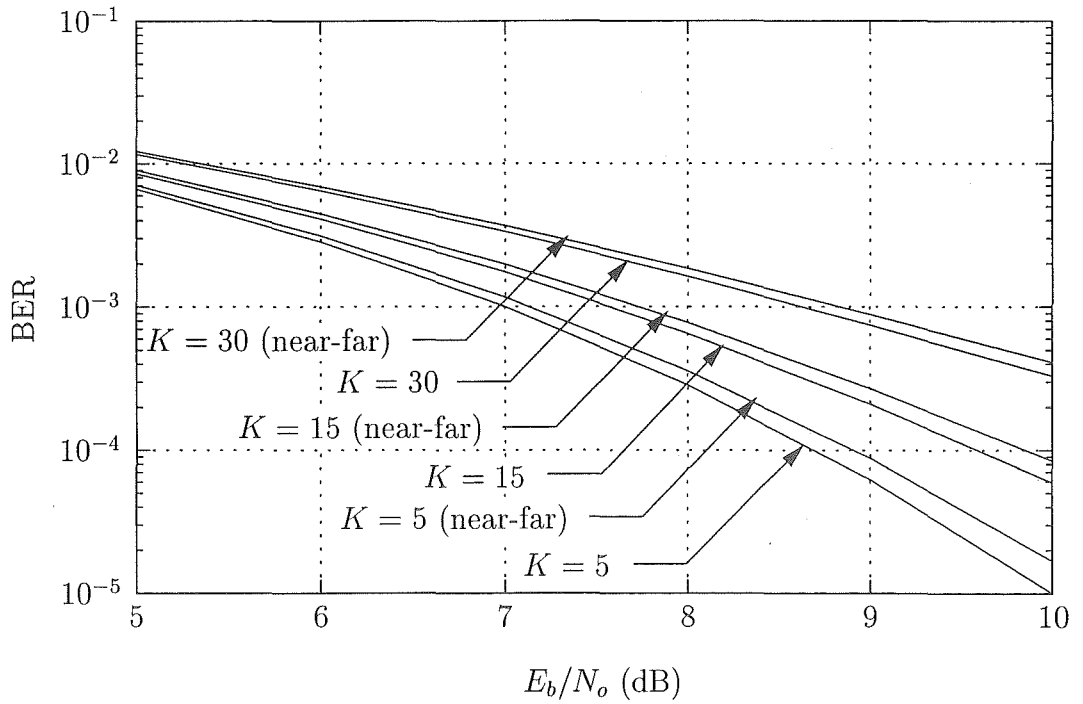

Figure 4.9: Simulation of a decision feedback receiver with $N_s = 127$ in communications environment exhibiting the near-far phenomenom. The K user's power levels are distributed uniformally. The ratio of maximum observed power to nominal is 3 dB.

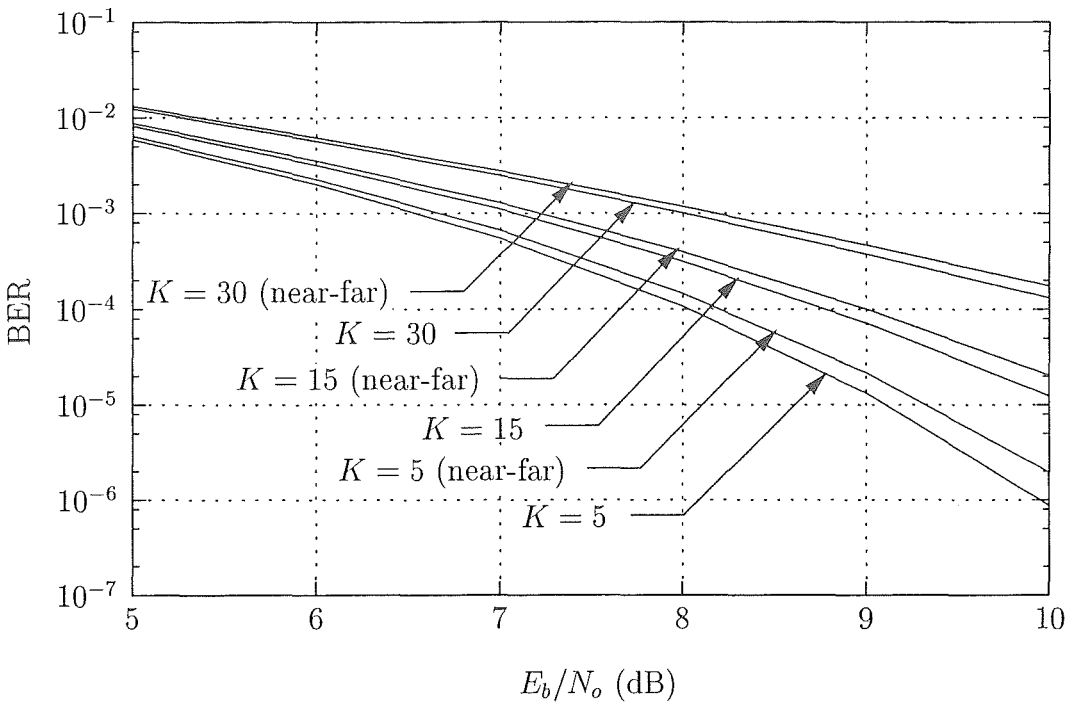

Figure 4.10: Simulation of an RSSE receiver with $N_s = 127$ and $K_s = 10$ in communications environment exhibiting the near-far phenomenom. The K user's power levels are distributed uniformally. The ratio of maximum observed power to nominal is 3 dB.

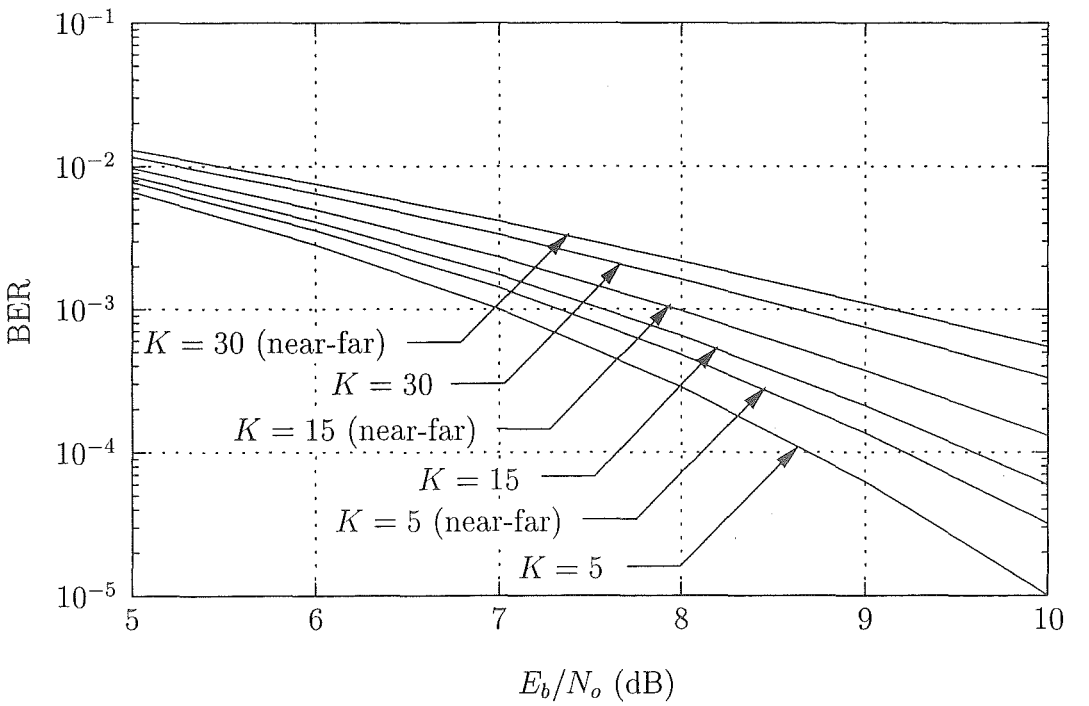

Figure 4.11: Simulation of a decision feedback receiver with $N_s = 127$ in communications environment exhibiting the near-far phenomenom. The K user's power levels are distributed uniformally. The ratio of maximum observed power to nominal is 10 dB.

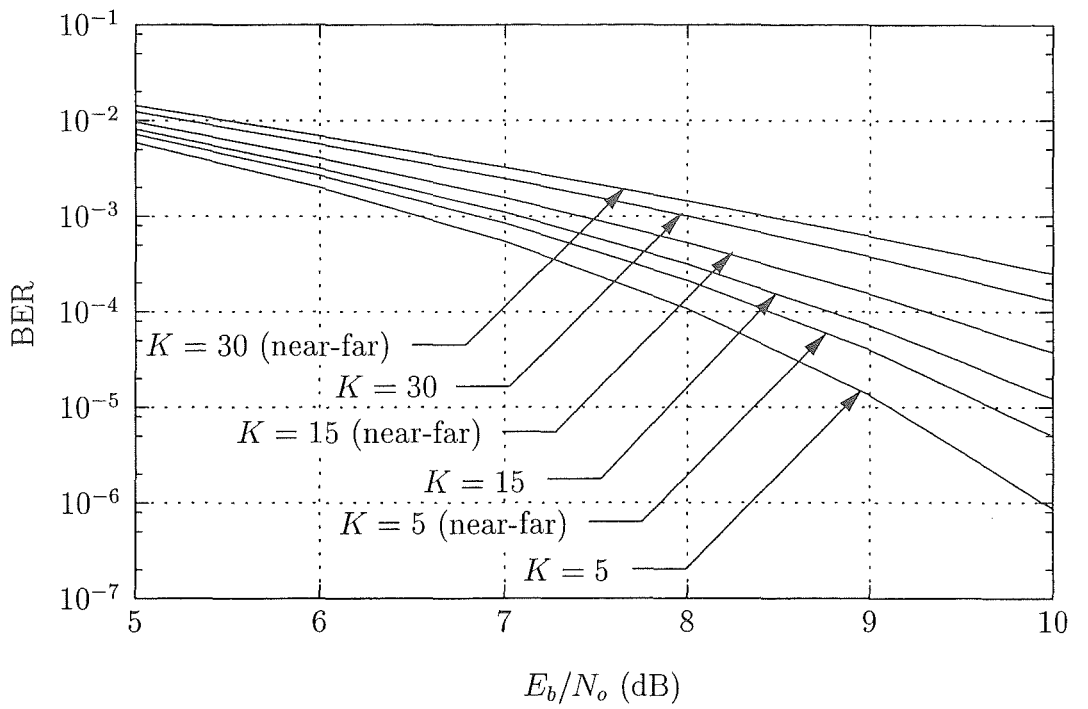

Figure 4.12: Simulation of an RSSE receiver with $N_s = 127$ and $K_s = 10$ in communications environment exhibiting the near-far phenomenom. The K user's power levels are distributed uniformally. The ratio of maximum observed power to nominal is 10 dB.

4.4 Complexity

Consider again the $K = 4$, $K_s = 2$, $S = 2$ trellis structure in Fig. 4.1(b). During the Add-Compare-Select process of the Viterbi Algorithm for each sub-interval in the trellis, each state compares the S path metrics arriving from previous states. The receiver has 2^{K_s} states per sub-interval so in each sub-interval there are a total of $S2^{K_s}$ Add-Compare-Select processes. Over a bit period, there are N_p sub-intervals and the number of branch metric calculations is $C_{bm} = N_p S 2^{K_s}$.

The maximum likelihood receiver with the Viterbi Algorithm requires $C_{bm}^{ML} = 4^K/2$ branch metric calculations because of a $(K-1)$ bit dependence on the path metric [91].

For the RSSE receiver metric in (4.1) the arithmetic cost for progress along the trellis by one subset can be determined. Assuming that addition and multiplication operations are equally costly, the number of arithmetic operations

per branch metric calculation is $A_{bm} = K_s(2K+1)$. This leads to the total number of arithmetic operations for each user's decoded bit which we write as

$$\begin{aligned} A_b &= \frac{1}{K} N_p S 2^{K_s} K_s (2K+1) \\ &\approx S 2^{K_s} (2K+1), \end{aligned} \tag{4.20}$$

where the equality is exact when $K = N_p K_s$. Note that for the sequentially reduced complexity receiver $S = 2^{K_s}$ and (4.20) becomes $A_b \approx 4^{K_s}(2K+1)$ as shown in [79]. The number of operations per bit for the ML receiver is $A_b^{ML} = 4^K(2K+1)/2$.

As in chapter 3 and [79] the performance of the RSSE reduced complexity receivers is exponential in the number of users per state K_s. Unlike the simple reduced complexity receivers, grouping states in each sub-interval into S super-states reduces the computational complexity. As shown in the previous section the performance of the family of receivers is effectively independent of S, which may be chosen to reduce the computational complexity resulting in the decision feedback reduced complexity receiver.

In Fig. 4.13 the relative number of arithmetic operations per bit A_b/A_b^{ML} is presented as a function of the number of users per state K_s, number of super-states S and the processing gain N_s of the system. The effect of reducing the number of users per state is clear. Since complexity is dominated by the number of users per state, the complexity reduction is greater for a given normalised number of users per state, for a greater number of users and a greater number of super-states.

4.5 Conclusions

We have presented a family of reduced complexity multi-user detectors for asynchronous spread spectrum multiple access in AWGN. The system may be augmented to operate in a multi-path fading environment by replacing the correlator bank with a bank of RAKE filters . The receiver structure was formed by applying reduced state sequence estimation techniques to the

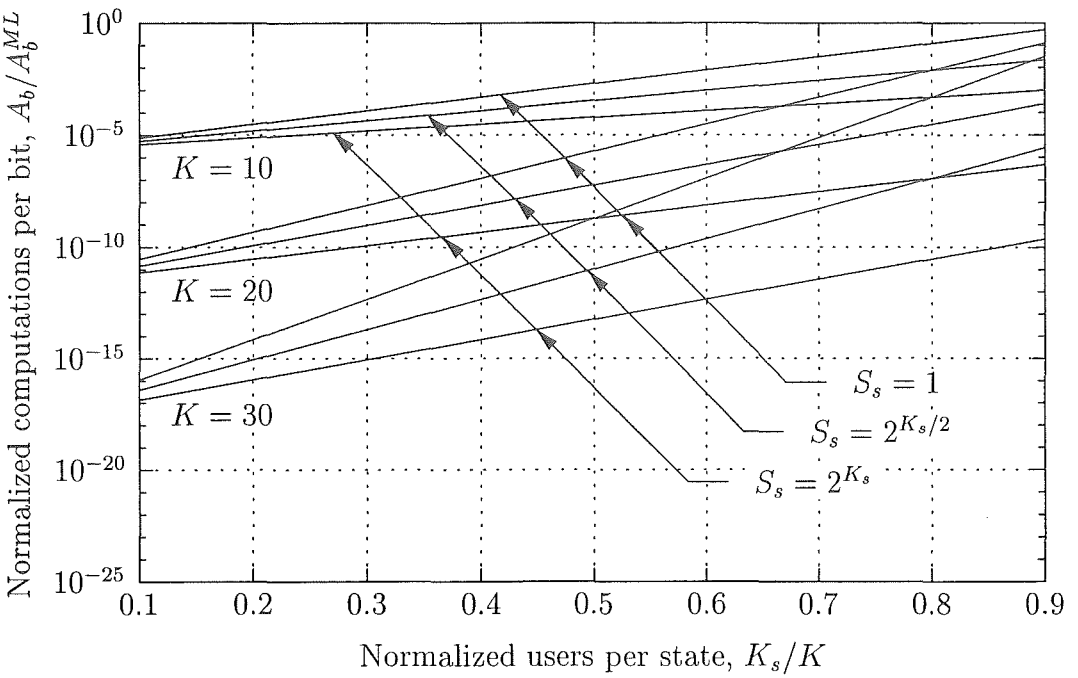

Figure 4.13: Relative computational complexity of the RSSE reduced complexity receivers with respect to the maximum likelihood receiver.

sequentially reduced complexity receivers presented in chapter 3. The new receiver structure allows the system designer to make performance/complexity tradeoffs with two degrees of freedom; one of which was shown to have a near negligible effect on error performance and in the limit of one super-state, results in a simple decision feedback structure.

It was demonstrated that the asymptotic performance of the new RSSE reduced complexity receivers approaches the performance of the simple receivers from chapter 3, but with a greater reduction in complexity. A system with $K = 30$ users, $K_s = 8$ and a processing gain $N_s = 511$ suffers less than 0.5 db loss with respect to the maximum likelihood receiver. A graceful degradation in system performance is observed for lower processing gains. The same system with a processing gain of $N_s = 255$ suffers a 0.9 dB loss, while with $N_s = 127$ the loss is 2.0 dB. This 30 user system has a computational complexity approximately equivalent to the maximum likelihood receiver with only six users.

Chapter 5

REDUCED COMPLEXITY RECEIVERS FOR THE MULTI-PATH FADING CHANNEL

5.1 Introduction

Spread Spectrum multi-user detectors use the second order statistics of the users' spreading sequences to obtain improved error performance over the conventional correlator (or matched filter) type spread spectrum systems [91]. We have seen that when the users are asynchronous the complexity of the receiver increases and different approaches to receiver design have produced structures which exhibit exponential or polynomial complexity in the number of users. The maximum likelihood (ML) receiver [91] is exponentially complex in the number of users. The decorrelating receivers are polynomial but require a new matrix inversion with each change in channel state.

In chapter 3 we presented a family of reduced complexity receivers which allow for a tradeoff in performance versus complexity. The receiver structure consists of a partial serialisation of the ML algorithm operating over a reduced state trellis. The receiver is sub-optimal in that some bit combinations are not considered. At one extreme the system reduces to the maximum likelihood multi-user detector while the other extreme results in a system with dramatically reduced complexity.

Reduced state sequence estimation (RSSE) techniques [19] were applied to the reduced complexity receiver in chapter 4 producing receiver structures with varying degrees of decision feedback by the grouping of states into super-states. We showed that the number of super-states has little effect on the error performance of the receivers.

In this chapter we develop a reduced complexity receiver for the fading multi-path asynchronous spread spectrum multiple access channel. The new receiver is a maximal-ratio combination based receiver [59] with self-noise reduction. The receiver is developed and analysed for the limiting case of very slow fading. For faster fade rates we present error rate performance curves obtained through simulation and show that error rate performance is dominated by the diversity of the channel.

The chapter is organised as follows. In the following section we describe the system. Performance results are presented in section 5.4. Conclusions are given in section 5.5.

5.2 *The System*

5.2.1 Description

Consider the spread spectrum multiple access (SSMA) model shown in Fig. 5.1. The model consists of K asynchronous transmitters, an L-path fading channel, and the receiver.

Using the notation $j = \eta(j)K + \kappa(j)$ of [91] where $\kappa(j)$ is the remainder of j mod K and $\eta(j)$ is the integer part of j/K, the received complex baseband signal $r(t)$ consisting of the sum of the K users' signals and the noise is written as,

$$r(t) = \sum_{i=0}^{N-1} \sum_{r=0}^{L-1} \sum_{k=0}^{K-1} b_k(i) h_r(t) s_k(t - iT - \tau_k - \xi_r) + n(t), \tag{5.1}$$

$$= \sum_{j=0}^{NK-1} \sum_{r=0}^{L-1} b_{\kappa(j)}(\eta(j)) h_r(t) s_{\kappa(j)}(t - \eta(j)T - \tau_{\kappa(j)} - \xi_r) + n(t), \tag{5.2}$$

where $n(t)$ is AWGN with double-sided power spectral density $N_o/2$, $b_k(i)$ is the i-th data bit of the k-th user, $s_k(t - iT - \tau_k)$ is the k-th user's spreading signal (equal to 0 outside the interval $[0,T)$), T is the bit duration and τ_k is the time delay of the k-th user. The complex fading components $h_r(t)$ are defined below. If $\{\underline{s}_{\kappa(j)}(c)\}$ represents the sequence of spreading sequence chips

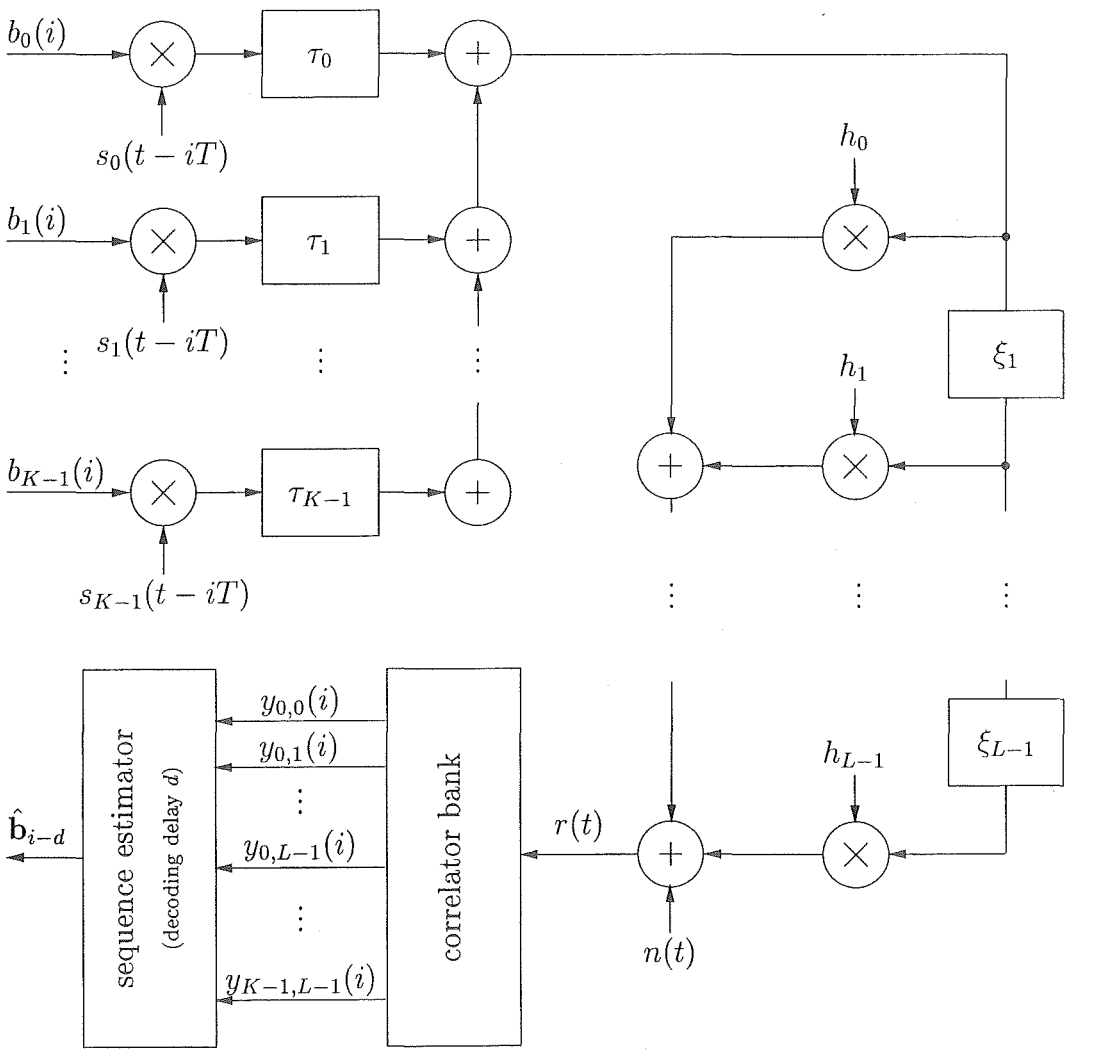

Figure 5.1: System model for asynchronous spread spectrum multiple access communication over a multi-path fading channel.

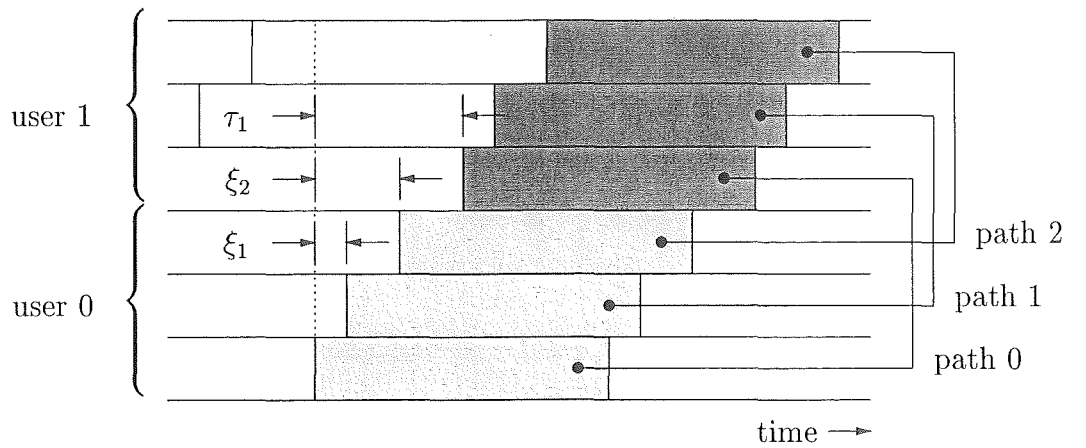

Figure 5.2: The asynchronous SSMA multi-path channel for two users and three paths. User 1 is delayed by τ_1 and the second and third paths are delayed by ξ_1 and ξ_2 respectively.

of period N_s for the $\kappa(j)$-th user then we write $s_{\kappa(j)}(t)$ as

$$s_{\kappa(j)}(t-\eta(j)T-\tau_\kappa(j)-\xi_r)=\sum_{c=0}^{N_s-1}\underline{s}_{\kappa(j)}(c)\,p_r(t-\eta(j)T-\frac{cT}{N_s}-\tau_{\kappa(j)}-\xi_r), \tag{5.3}$$

where $p_r(t)$ is the rectangular chip waveform.

The multi-path channel model is modelled as consisting of an L-tap tapped delay line with delays ξ_r for $r=0,1,\cdots,L-1$. We assume that the fading effect is dominated by scatters in the neighbourhood of the receiver so that each user experiences the same fading. Each of the paths in the channel model has a complex valued fading coefficient $h_r(t)$ for $r=0,1,\cdots,L-1$ of zero mean and variance σ_r^2. The time-varying impulse response (see chapter 1) is given by

$$c(t)=\sum_{r=0}^{L-1}h_r(t-\xi_r) \tag{5.4}$$

The set of variances of the fading coefficients is known as the *delay power spectrum* [59] of the channel and gives the relative strengths of each of the faded paths as a function of their relative arrival times as discussed in chapter 1. We assume a discrete delay power spectrum with a minimum inter-path arrival time greater than the chip period T/N_s so that all paths are resolvable by the

receiver. Furthermore, the delay spectrum is normalised so that $\sum_{r=0}^{L-1} \sigma_r^2 = 1$, and the paths are numbered such that $\xi_0 < \xi_1 < \cdots < \xi_{L-1}$ and that $\xi_0 = 0$ and $\xi_{L-1} < T$. The receiver may be generalised so the the last requirement is removed and it should be noted that it is retained here only for notational simplicity. The fading paths are considered to be independent so that they are uncorrelated, $\mathrm{E}[h_r(t)h_{r'}^*(t)] = 0$, for $r \neq r'$. The fading processes in each of the paths are assumed to have an autocorrelation given by [83] $\mathrm{E}[h_r(t)h_r^*(t - iT)] = 2\,\mathrm{J}_0(2\pi i f_D T)$ where f_D is the maximum Doppler frequency and $\mathrm{J}_0(\cdot)$ is the zero order Bessel function. The quantity $f_D T$ is called the *normalised Doppler frequency* and is a measure of the ratio of the maximum Doppler shift experienced by the mobile's carrier frequency to the symbol rate. In the formulation of the receiver, very slow fading is assumed so that the fading process can be considered constant over the bit period so the $\eta(j)$-th sample of the r-th path response is $h_r(\eta(j)) = h_r(t - \eta(j)T)$.

While many of the results presented here can be extended to arbitrary input alphabets, we again restrict ourselves to binary alphabets, $b_k(i) \in \{\pm 1\}$. We assume, without loss of generality, that the users are numbered such that their relative delays τ_k are ordered as $0 \leq \tau_0 \leq \cdots \leq \tau_{K-1} < T$. All transmitted symbols are assumed equiprobable and independent.

The receiver correlates (or matched filters) the received signal $r(t)$ with each of the users' spreading sequences at each of the path arrival times $s_k(t - iT - \tau_k - \xi_r)$. The correlator bank (see Fig. 5.3) consists of K sets of correlators, one for each user. Each set has L correlators each with the k-th user's spreading sequence delayed by the appropriate multi-path delay time ξ_r. This type of filter structure employing matched filters at delays equal to each path delay is known as a RAKE receiver structure [59]. In the present case we employ an array of matched filters for each of the L paths, one for each of the K users. We assume that the number of paths L, users K and their spreading sequences are known. In practice this may involve a correlation-type search of the received signal using a predetermined set of spreading sequences (see

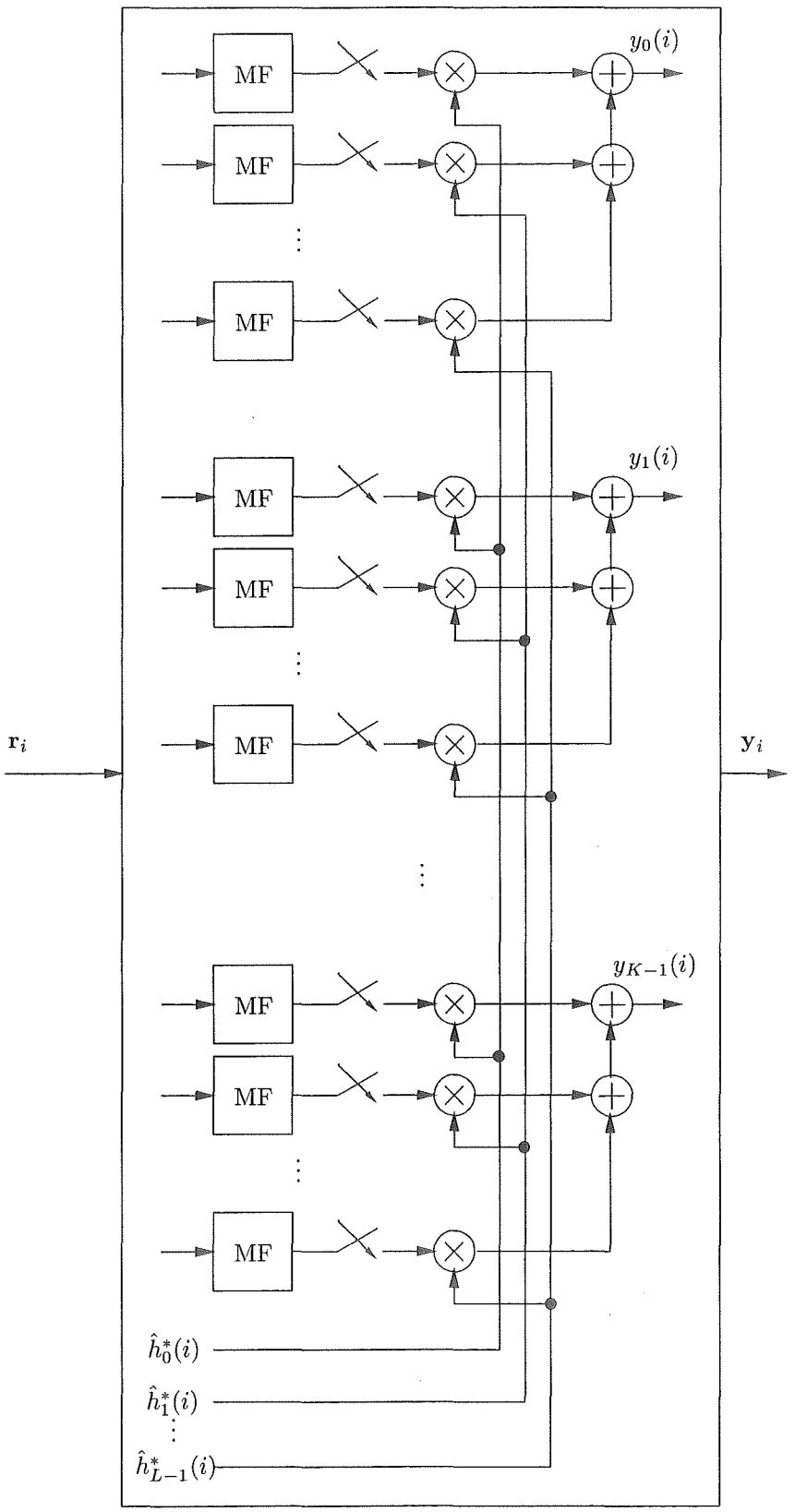

Figure 5.3: Matched filter and combiner structure for receivers for the multi-path fading channel.

chapter 2 and [11]). In general, the timing offset for the k-th user and r-th path $\tau_k + \xi_r$ is an undefined quantity that is estimated by conventional spread spectrum acquisition and tracking techniques [59]. We assume that channel information obtained through well-known estimation methods such as those of [96] is available and provides estimates of the fading components. The KL matched filter outputs for each of the users and received paths during the $\kappa(j)$-th signalling interval are given by

$$\begin{aligned} y_{\kappa(j),r}(\eta(j)) &= b_{\kappa(j)}(\eta(j))\, h_r(\eta(j))\, g_{\kappa(j),\kappa(j)}(\eta(j), r\,;\eta(j), r) \\ &\quad + \sum_{r'=0,\, r'\neq r}^{L-1} b_{\kappa(j)}(\eta(j))\, h_{r'}(\eta(j))\, g_{\kappa(j),\kappa(j)}(\eta(j), r'\,;\eta(j), r) \\ &\quad + \sum_{r'=0}^{L-1}\sum_{l=1}^{K-1} b_{\kappa(j-l)}(\eta(j-l))\, h_{r'}(\eta(j))\, g_{\kappa(j-1),\kappa(j)}(\eta(j-l), r'\,;\eta(j), r) \\ &\quad + \sum_{r'=0}^{L-1}\sum_{l=1}^{K-1} b_{\kappa(j+l)}(\eta(j+l))\, h_{r'}(\eta(j))\, g_{\kappa(j+1),\kappa(j)}(\eta(j+l), r'\,;\eta(j), r) \\ &\quad + n_{\kappa(j),r}(\eta(j)) \end{aligned} \tag{5.5}$$

where $g_{k,k'}(i, r\,; i', r)$ is the spreading sequence partial cross correlation between the k-th and k'-th users at the i-th and i'-th data symbol (bit) intervals and r-th and r'-th paths,

$$g_{k,k'}(i, r\,; i', r') = \int_{-\infty}^{\infty} s_k(t - iT - \tau_k - \xi_r) s_{k'}(t - i'T - \tau_{k'} - \xi_{r'})\, dt, \tag{5.6}$$

with $g_{k,k}(i, r\,; i, r) = E_b$, the bit energy of the k-th user, and where $n_{\kappa(j),r}(\eta(j))$ is the sampled noise at the output of the matched filters given by

$$n_{\kappa(j),r}(\eta(j)) = \int_{-\infty}^{\infty} n(t) s_k(t - iT - \tau_k - \xi_r)\, dt. \tag{5.7}$$

The resulting sequence of sampled noise is correlated due to the partial correlations of users' spreading sequences. This correlation may be written as

$$\mathrm{E}[n_{\kappa(j),r}(\eta(j))\, n_{\kappa(j'),r'}(\eta(j'))] = \frac{N_o}{2} g_{\kappa(j),\kappa(j')}(\eta(j), r\,;\eta(j'), r'). \tag{5.8}$$

The transmitted bits for the K users in (5.5) may be contained in a vector written as

$$\mathbf{b}_i = [\, b_0(i)\, b_1(i)\, \cdots\, b_{K-1}(i)\,]^{\mathrm{T}}. \tag{5.9}$$

Combining the L terms corresponding to the multi-path components for each user in a linear combination of weighted signals gives the combined matched filter outputs for the K users. The L components are each weighted by multiplication by the conjugate of the path estimate $\hat{h}_r^*$ to compensate for the phase shift introduced by the path and to weight the signal in proportion to the received signal strength. This form of linear combination is called a *maximal ratio combination* and can be shown to be optimum for diversity systems [59]. The maximal ratio combination may be written as,

$$y_{\kappa(j)}(\eta(j)) = \sum_{r=0}^{L-1} \hat{h}_r^* \, y_{\kappa(j),r}(\eta(j)), \tag{5.10}$$

which may also be contained in a vector written as,

$$\mathbf{y}_i = [\, y_0(i)\, y_1(i) \cdots y_{K-1}(i)\,]^{\mathrm{T}}, \tag{5.11}$$

where i denotes the i-th signalling interval, $(i-1) \leq t \leq iT$.

The maximal ratio combiner is performance limited by the cross correlation between the signals in each received path [59] as shown by the summations over the path index r' in the second, third and fourth addends of (5.5). This *self-noise* is signal dependant and is identical in form to the multiple access interference occurring in conventional correlator-type spread spectrum systems. Therefore, we may treat the self-noise terms as extra users in the system.

The decision metric is an extension of the maximum likelihood decision metric for the AWGN channel but with maximal-ratio combining self-noise cancellation. The receiver selects the sequence $\mathbf{b} = [\, \mathbf{b}_0^{\mathrm{T}}\, \mathbf{b}_1^{\mathrm{T}} \cdots \mathbf{b}_{N-1}^{\mathrm{T}}\,]$ that maximises the metric,

$$\Omega(\mathbf{b}) = \sum_{i=0}^{N-1} \mathbf{b}_i^{\mathrm{T}} \, \mathrm{Re}(\mathbf{y}_i - \mathrm{diag}\, \mathbf{X}_i \mathbf{G}). \tag{5.12}$$

where the matrix $\mathbf{G}$ is a $K \times K$ matrix whose m-th column is a set of submatrices representing the correlation of the m-th and $\kappa(m-n)$-th users' spread-

ing sequences for each of the L paths,

$$\mathbf{G} = \begin{bmatrix} \mathbf{G}_{0,0} & \mathbf{G}_{0,1} & \cdots & \mathbf{G}_{0,K-1} \\ \mathbf{G}_{1,0} & \mathbf{G}_{1,1} & & \vdots \\ \vdots & & \ddots & \vdots \\ \mathbf{G}_{K-1,0} & \mathbf{G}_{K,1} & \cdots & \mathbf{G}_{K-1,K-1} \end{bmatrix}. \tag{5.13}$$

In (5.13) the sub-matrices $\mathbf{G}_{n,m}$ give the partial cross-correlation between the m-th and $\kappa(m-n)$-th user for each of the received paths,

$$\mathbf{G}_{n,m} \; : \; G_{i,j}^{n,m} = g_{\kappa(m),\kappa(m-n)}(\eta(m), j\,; \eta(m-n), i). \tag{5.14}$$

The sub-matrices $\mathbf{G}_{n,m}$ are $L \times L$-dimensional except for the sub-matrices of the first row of (5.13) which are $(L-1) \times L$ dimensional—the matrix element $i = j$ in (5.14) does not appear. The first row of the correlation matrix in (5.13) is responsible for the maximal-ratio self noise cancellation of the current bit under consideration—the diagonal elements of (5.14) for matrices in the first row of (5.13) correspond to these desired terms and so only the terms from other paths interfering with the desired terms are removed.

The matrix of hypothesised bits and channel estimates $\mathbf{X}_i$ is given by,

$$\mathbf{X}_i = \begin{bmatrix} \mathbf{X}_{0,0}^{(i)} & \mathbf{X}_{0,1}^{(i)} & \cdots & \mathbf{X}_{0,K-1}^{(i)} \\ \mathbf{X}_{1,0}^{(i)} & \mathbf{X}_{1,1}^{(i)} & & \vdots \\ \vdots & & \ddots & \vdots \\ \mathbf{X}_{K-1,0}^{(i)} & \mathbf{X}_{K,1}^{(i)} & \cdots & \mathbf{X}_{K-1,K-1}^{(i)} \end{bmatrix}, \tag{5.15}$$

where the sub-matrices $\mathbf{X}_{n,m}^{(i)}$ are written as,

$$\mathbf{X}_{n,m}^{(i)} = b_{\kappa(Ki+n-m)}(\eta(Ki+n-m)) \begin{bmatrix} \hat{h}_0^* \hat{h}_0^p & \hat{h}_0^* \hat{h}_1^p & \cdots & \hat{h}_0^* \hat{h}_{L-1}^p \\ \hat{h}_1^* \hat{h}_1^p & \hat{h}_1^* \hat{h}_1^p & & \hat{h}_1^* \hat{h}_{L-1^p} \\ \vdots & & \ddots & \vdots \\ \hat{h}_{L-1}^* \hat{h}_0^p & \hat{h}_{L-1}^* \hat{h}_1^p & \cdots & \hat{h}_{L-1}^* \hat{h}_{L-1}^p \end{bmatrix}. \tag{5.16}$$

In (5.16) we have written $\hat{h}_r^*(\eta(Ki))$ as $\hat{h}_r^*$ and $\hat{h}_r(\eta(Ki+n-m))$ as $\hat{h}_r^p$ for notational simplicity. The conjugated channel estimates are the estimates of the

channel during the current signalling interval; the non-conjugated estimates are those from previous intervals and are denoted by the superscript p. Similarly, to the formation of the correlation sub-matrices, the sub-matrices in the first column of (5.16) are $(L-1) \times L$-dimensional—the diagonal elements of (5.15) do not appear. As with the correlation matrix, the first column of (5.16) is used to cancel the self-noise from the maximal-ratio combination of the L paths.

The receiver with the decision metric given in (5.12) has a complexity which is exponential in the number of users in the system. In chapter 3 reduced complexity was achieved by reducing the number of states that need to be processed by the Viterbi Algorithm (VA) at any instant of time through a partitioning process that leads to a sequentially expanded reduced state trellis. The complexity was further reduced in chapter 4 by the grouping of states into super-states resulting in a trellis structure with fewer states each assuming the value of one of many member states. Similar processes may be employed here.

The partitioning process leads to a sequentially expanded trellis with significantly fewer states operated on during each of a sequence of N_p sub-intervals within each symbol period. The length K vectors $\mathbf{b}_i$ of (5.9) are partitioned into N_p sub-vectors of length K_s such that,

$$\mathbf{b}_i = [\, \mathbf{b}_{i,0}^{\mathrm{T}} \, \mathbf{b}_{i,1}^{\mathrm{T}} \, \cdots \, \mathbf{b}_{i,N_p-1}^{\mathrm{T}} \,]^{\mathrm{T}}. \tag{5.17}$$

Each component vector $\mathbf{b}_{i,j}$ in (5.17) corresponds to a 2^{K_s} sub-trellis. These are grouped into a sequentially expanded 2^{K_s}-state trellis in that $N_p = \lceil K/K_s \rceil$ sub-intervals of the reduced trellis are processed during each data symbol interval with each sub-interval processing one of the sub-vectors as shown in chapter 3.

As the N_p advances are made through the trellis during the i-th signalling interval, N_p estimates $\hat{\mathbf{b}}_{i-d,p}$, $p = 0, 1, \cdots N_p - 1$ are output by the Viterbi Algorithm (with decision depth d symbol periods). The N_p estimates are concatenated to form the estimate of the bits transmitted by all K users d

signalling intervals in the past as

$$\hat{\mathbf{b}}_{i-d} = [\,\hat{\mathbf{b}}_{i-d,0}^{\mathrm{T}}\,\hat{\mathbf{b}}_{i-d,1}^{\mathrm{T}}\,\cdots\,\hat{\mathbf{b}}_{i-d,N_p-1}^{\mathrm{T}}\,]^{\mathrm{T}}. \tag{5.18}$$

As shown in earlier chapters this partitioning technique results in a sub-optimal, but significantly reduced complexity receiver structure with an overall path metric given by,

$$\begin{aligned}\tilde{\Omega}(\mathbf{b}) &= \sum_{i=0}^{N}\sum_{p=0}^{N_p-1}\bar{\Omega}(\mathbf{b}_{i,p}) \\ &= \sum_{i=0}^{N}\sum_{p=0}^{N_p-1}\mathbf{b}_{i,p}^{\mathrm{T}}\,\mathrm{Re}\left(\mathbf{y}_{i,p} - \mathrm{diag}\,\mathbf{X}_{i,p}\mathbf{G}_p\right).\end{aligned} \tag{5.19}$$

where N is the sequence length.

In each sub-interval the path metrics $\Omega_{i,p}^{\mathbf{b}^s}$, $s = 0, 1, \cdots, 2^{K_s} - 1$ at each state in the Viterbi algorithm are updated by a one-step application of (5.19) to obtain

$$\Omega_{i,p}^{\mathbf{b}^s} = \max_{s'}\left[\Omega_{\eta(j-1),\rho(j-1)}^{\mathbf{b}^{s'}} + \bar{\Omega}^{\mathbf{b}^{s'}}(\mathbf{b}_{i,p}^{s})\right] \tag{5.20}$$

where $\Omega_{i,p}^{\mathbf{b}^s}$ is the path metric at the $\mathbf{b}^s$-state at the p-th sub-interval of the i-th signalling interval, $\Omega_{\eta(j-1),\rho(j-1)}^{\mathbf{b}^{s'}}$, is the path metric from the previous sub-interval, and $\bar{\Omega}^{\mathbf{b}^{s'}}(\mathbf{b}_{i,p}^{s})$ is the branch metric at the p-th sub-interval of the i-th signalling interval from the $\mathbf{b}^{s'}$-state to the $\mathbf{b}^s$-state, namely

$$\bar{\Omega}^{\mathbf{b}^{s'}}(\mathbf{b}_{i,p}^{s}) = \mathbf{b}^{s\mathrm{T}}\,\mathrm{Re}(\mathbf{y}_{i,p} - \mathrm{diag}\,\mathbf{X}_{i,p}^{\mathbf{b}^{s'},\mathbf{b}^s}\mathbf{G}_p), \tag{5.21}$$

where the path dependence on the matrix of previous bits $\mathbf{X}$ is shown by the superscripts.

In each sub-interval the S path metrics $\Omega_{i,p}^{\mathbf{b}^s}$ of the super-states are updated by choosing the greatest path metric from each of the S_s candidate states,

$$\Omega_{i,p}^{\mathbf{b}^s} = \max_{\mathbf{b}^{s'}\in B^s}\Omega_{i,p}^{\mathbf{b}^{s'}}, \tag{5.22}$$

where $\Omega_{i,p}^{\mathbf{b}^{s'}}$ is the path metric at the $\mathbf{b}^{j'}$ state in the p-th sub-interval of the i-th symbol period given by

$$\Omega_{i,p}^{\mathbf{b}^{s'}} = \max_{s}\left[\Omega_{\eta(iK+pN_p-1),\rho(iK+pN_p-1)}^{\mathbf{b}^{s}} + \bar{\Omega}^{\mathbf{b}^{s}}(\mathbf{b}_{i,p}^{s'})\right], \tag{5.23}$$

and the super-state at that sub-interval $\mathbf{b}_{i,p}^{s}$ assumes the value corresponding to the surviving path metric entering the super-state,

$$\mathbf{b}_{i,p}^{j} = \arg \Omega_{i,p}^{\mathbf{b}^s}. \tag{5.24}$$

In the special case where all states are candidate states for one super-state ($S = 1$ and $S_s = 2^{K_s}$) the maximisation in (5.23) is only over one state since the trellis has collapsed to one path with one state. We called this special case of the RSSE reduced complexity receiver the *decision feedback reduced complexity receiver* in chapter 4. In this case, combining (5.22) and (5.23) gives the path metric written as,

$$\Omega_{i,p}^{\mathrm{DF}} = \max_{\mathbf{b}^{s'} \in B} \bar{\Omega}(\mathbf{b}_{i,p}^{s'}), \tag{5.25}$$

and the value assumed by the super-state at each sub-interval is,

$$\mathbf{b}_{i,p}^{0} = \arg \Omega_{i,p}^{\mathrm{DF}}. \tag{5.26}$$

The decision feedback receiver structure for the multi-path fading channel is shown in Fig. 5.4 and consists of a decision device utilising the metric of (5.25), and an length N_p, K_s-dimensional shift register to store the hypothesised bits and channel estimates in order to form $\mathbf{X}_{i,p}$.

5.2.2 Example

Consider the four user example in Fig. 4.1 for the transition from the (i_0-1)-th to the i_0-th signalling interval. In this example we assume a three ray multi-path channel. The trellis of a reduced complexity receiver with $K_s = 2$ users per state, $S_s = 2$ states per super-state and $N_p = 2$ sub-intervals per symbol is shown in Fig. 4.1(b). $N_p = 2$ transitions through the trellis must be made to compute the path metrics for the transition from the $(i_0 - 1)$-th to the i_0-th signalling interval. The first subset contributes to the path metrics for the first two users, the second subset contributes for the third and fourth users. The

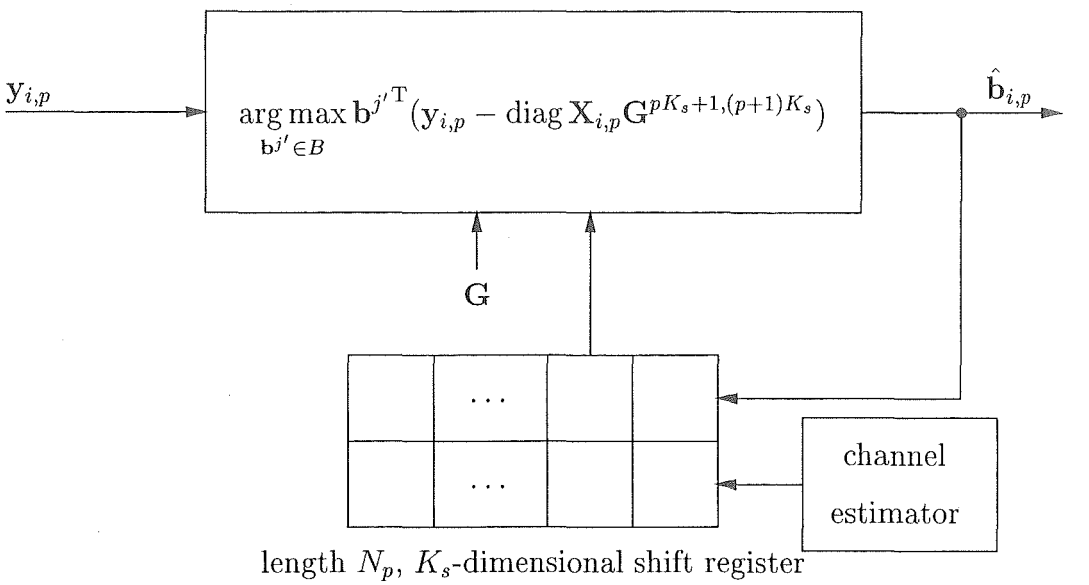

Figure 5.4: A Decision Feedback RSSE Reduced Complexity Receiver.

output of the bank of correlators and maximal-ratio combiners at symbol time $i = i_0$ is represented by the vector,

$$\mathbf{y}_{i_0} = [\, y_0(i_0)\, y_1(i_0)\, y_2(i_0)\, y_3(i_0)\,]^{\mathrm{T}},$$

where each of the four elements of the vector are the channel-estimate-weighted sums from the L correlators of each user given by (5.10).

At each state in the reduced trellis four paths from previous states compete to be the surviving path. The path metrics entering each state at $i = i_0$, $p = 0$ are calculated using (5.23) and the first set of outputs from the correlator bank and maximal-ratio combiners, $\mathbf{y}_{i_0,0} = [\, y_0(i_0)\, y_1(i_0)\,]^{\mathrm{T}}$. Consider the case where the competing paths enter the $\mathbf{b}^0$-state at $i = i_0$, $p = 0$, in this case $\mathbf{b}_{i_0,0} = [\,-1\ -1\,]^{\mathrm{T}}$. The receiver discards three of the four paths by choosing the most likely (surviving) path from the four contenders. The correlation matrix $\mathbf{G}_0$ is a constant during the calculations at any sub-interval and is a subset of the matrix of all user correlations $\mathbf{G}$ from (5.13). The matrix of hypothesised bits and channel estimates $\mathbf{X}_{i_0,0}$ is formed row-wise by tracing back from each state at $i = i_0$, $p = 0$ by $N_p = 2$ branches in the trellis filling

rows of $\mathbf{X}_{i_0,0}$ with the surviving bits along the path represented by the state labels $\mathbf{b}^{s'}$. Note that each branch metric calculation requires a different $\mathbf{X}_{i_0,0}$ since the $K-1$ hypothesised bits in each path are different. To illustrate, suppose a competing path arriving at the $\mathbf{b}^0$-state at $i=i_0$, $p=0$, had at $i=i_0-1$, $p=1$ passed through the $\mathbf{b}^2$-state, and had at $i=i_0-1$, $p=0$ passed through the $\mathbf{b}^1$-state, then,

$$\mathbf{X}_{i_0,0}^{\mathbf{b}^2,\mathbf{b}^0} = \begin{bmatrix} -\hat{\mathbf{h}}'_{i_0} & -\hat{\mathbf{h}}_{i_0-1} & \hat{\mathbf{h}}_{i_0-1} & \hat{\mathbf{h}}_{i_0-1} \\ -\hat{\mathbf{h}}'_{i_0} & -\hat{\mathbf{h}}_{i_0} & -\hat{\mathbf{h}}_{i_0-1} & \hat{\mathbf{h}}_{i_0-1} \end{bmatrix},$$

where the matrices of channel estimates are written,

$$\hat{\mathbf{h}}_i = \begin{bmatrix} \hat{h}_0^*(i)\hat{h}_0(i) & \hat{h}_0^*(i)\hat{h}_1(i) & \hat{h}_0^*(i)\hat{h}_2(i) \\ \hat{h}_1^*(i)\hat{h}_0(i) & \hat{h}_1^*(i)\hat{h}_1(i) & \hat{h}_1^*(i)\hat{h}_2(i) \\ \hat{h}_2^*(i)\hat{h}_0(i) & \hat{h}_2^*(i)\hat{h}_1(i) & \hat{h}_2^*(i)\hat{h}_2(i) \end{bmatrix} \tag{5.27}$$

and

$$\hat{\mathbf{h}}'_i = \begin{bmatrix} \hat{h}_0^*(i)\hat{h}_1(i) & \hat{h}_0^*(i)\hat{h}_2(i) \\ \hat{h}_1^*(i)\hat{h}_0(i) & \hat{h}_1^*(i)\hat{h}_2(i) \\ \hat{h}_2^*(i)\hat{h}_0(i) & \hat{h}_2^*(i)\hat{h}_1(i) \end{bmatrix}.$$

The branch metric $\bar{\Omega}^{\mathbf{b}^2}(\mathbf{b}_{i_0,0}^0)$ corresponding to the first path entering the $\mathbf{b}^0$-th state is,

$$\bar{\Omega}^{\mathbf{b}^2}(\mathbf{b}_{i_0,0}^0) = \mathbf{b}^{0\mathrm{T}} \operatorname{Re}\left(\mathbf{y}_{i_0,0} - \operatorname{diag} \mathbf{X}_{i_0,0}^{\mathbf{b}^2,\mathbf{b}^0} \mathbf{G}_0\right).$$

The other path entering the $\mathbf{b}^0$-state is calculated with another $\mathbf{X}_{i_0,0}$ matrix representing the previous bits from the other path in the trellis entering the $\mathbf{b}^0$-state. The surviving path entering the $\mathbf{b}^0$-state is calculated from (5.23). The same process is applied to determine the surviving path entering the other contending state $\mathbf{b}^3$ in the first super-state. The greater of the two metrics gives the surviving path entering the first super-state by (5.22) and the value assumed by the super-state at $i=i_0$, $p=0$ is given directly by (5.24). Similar calculations are made to determine survivors entering the candidate states $\mathbf{b}^1$

and $\mathbf{b}^2$ in the second super-state, the surviving path entering the super-state and its assumed value.

The Viterbi Algorithm searches through the two super-states for the largest path metric and follows the path corresponding to the greatest metric through the decision depth of the VA. The assumed value of the originating state of this path gives the most likely transmitted bits (from d signalling intervals earlier) for the first two users, $\hat{\mathbf{b}}_{i_0-d,0} = [\,\hat{b}_0(i_0-d)\,\hat{b}_1(i_0-d)\,]^{\mathrm{T}}$ under the constraint of the reduced trellis structure.

The second sub-interval is decoded considering the second set of outputs from the correlator bank and maximal-ratio combiners, $\mathbf{y}_{i_0,0} = [\,y_2(i_0)\,y_3(i_0)\,]^{\mathrm{T}}$. The matrix of hypothesised bits and channel estimates $\mathbf{X}_{i_0,1}$ includes bits in the paths at $i = 0$, $p = 0$; as an example suppose a competing path arriving at the $\mathbf{b}^3$-state at $i = i_0$, $p = 1$, had at $i = i_0$, $p = 0$ passed through the $\mathbf{b}^0$-state, and had at $i = i_0 - 1$, $p = 1$ passed through the $\mathbf{b}^3$-state, then

$$\mathbf{X}_{i_0,1}^{\mathbf{b}^0,\mathbf{b}^3} = \begin{bmatrix} \hat{\mathbf{h}}'_{i_0} & -\hat{\mathbf{h}}_{i_0} & -\hat{\mathbf{h}}_{i_0} & \hat{\mathbf{h}}_{i_0-1} \\ -\hat{\mathbf{h}}'_{i_0} & \hat{\mathbf{h}}_{i_0} & -\hat{\mathbf{h}}_{i_0} & -\hat{\mathbf{h}}_{i_0} \end{bmatrix}.$$

The correlation matrix for the second sub-interval is the sub-matrix of $\mathbf{G}$ with columns corresponding to the third and fourth users, namely $\mathbf{G}_1$. The same add, compare, select process is applied to the branch metrics and the estimated bits $\hat{\mathbf{b}}_{i_0-d,1} = [\,\hat{b}_2(i_0-d)\,\hat{b}_3(i_0-d)\,]^{\mathrm{T}}$ are returned by the VA by examining the originating state of the path with the greatest path metric. Note that in this example with $N_p = 2$ subsets, two iterations of the Viterbi Algorithm are required to estimate all the users and this requires two sets of add, compare, and select operations. The vector $\hat{\mathbf{b}}_{i_0-d}$ representing all the decoded users is a concatenation of the vectors obtained by the reduced VA during processing of each subset, and may be written as

$$\begin{aligned} \hat{\mathbf{b}}_{i_0-d} &= [\,\hat{\mathbf{b}}_{i_0-d,0}^{\mathrm{T}}\,\hat{\mathbf{b}}_{i_0-d,1}^{\mathrm{T}}\,]^{\mathrm{T}} \\ &= [\,\hat{b}_0(i_0-d)\,\hat{b}_1(i_0-d)\,\hat{b}_2(i_0-d)\,\hat{b}_3(i_0-d)\,]^{\mathrm{T}}. \end{aligned}$$

The decision feedback reduced complexity receiver for the same $K = 4$

users, $K_s = 2$ users per state system selects the state to be assumed by the super-state through (5.26). In this case, the estimate of the transmitted vector of user bits for the i_0-th symbol interval is

$$\hat{\mathbf{b}}_{i_0} = [\,\hat{\mathbf{b}}^{0\mathrm{T}}_{i_0,0}\,\hat{\mathbf{b}}^{0\mathrm{T}}_{i_0,1}\,]^{\mathrm{T}},$$

where $\hat{\mathbf{b}}^0_{i_0,0}$ and $\hat{\mathbf{b}}^0_{i_0,1}$ are the values assumed by the super-state during the two sub-intervals of the i_0-th symbol interval given directly by (5.26):

$$\hat{\mathbf{b}}^0_{i_0,0} = \arg\max_{\mathbf{b}^{s'}\in B} \mathbf{b}^{s'\mathrm{T}}_{i_0,0}\,\mathrm{Re}\left(\mathbf{y}_{i_0,0} - \mathrm{diag}\,\mathbf{X}_{i_0,0}\mathbf{G}_0\right),$$
$$\hat{\mathbf{b}}^0_{i_0,1} = \arg\max_{\mathbf{b}^{s'}\in B} \mathbf{b}^{s'\mathrm{T}}_{i_0,1}\,\mathrm{Re}\left(\mathbf{y}_{i_0,1} - \mathrm{diag}\,\mathbf{X}_{i_0,1}\mathbf{G}_1\right).$$

5.3 Performance Analysis

In this section performance measures for the RSSE reduced complexity receiver family in a multi-path fading channel with very slow fading are developed. The technique employed is the same used in the previous two chapters. Throughout the derivation it is assumed that the transmitted bits of different users are independent and that the effects of error propagation are small. The error propagation assumption allows the received errored path to be considered as a one sub-interval deviation from the transmitted path, which is assumed without loss of generality to be the all-zeros path through the trellis. The probability that the most likely of the estimated paths diverges from the transmitted path at one sub-interval and re-merges one sub-interval later, P_e, will be used to estimate the probability of bit error P_b.

Considering the metric in (5.23), the error event probability may be written as,

$$P_e = \frac{1}{K_s}\sum_{j'=0}^{2^{K_s}-1} \Pr\left(\Omega^{\mathbf{b}^0} < \Omega^{\mathbf{b}^{j'}}\right), \tag{5.28}$$

where the probability that the receiver chooses the wrong candidate state to

be assumed by the super-state is

$$\begin{aligned}\Pr\left(\Omega^{\mathbf{b}^0} < \Omega^{\mathbf{b}^{j'}}\right) &= \Pr\left(\Omega^{\mathbf{b}^0} - \Omega^{\mathbf{b}^{j'}} < 0\right) \\ &= \Pr\Big(\mathbf{b}_{i,p}^{0\ \mathrm{T}} \operatorname{Re}(\mathbf{y}_{i,p} - \operatorname{diag}\mathbf{X}_{i,p}\mathbf{G}_p) - \\ &\qquad \mathbf{b}_{i,p}^{j'\ \mathrm{T}} \operatorname{Re}(\mathbf{y}_{i,p} - \operatorname{diag}\mathbf{X}_{i,p}\mathbf{G}_p) < 0\Big). \qquad (5.29)\end{aligned}$$

Expanding the vector notation, (5.29) becomes

$$\begin{aligned}&\Pr\left(\Omega^{\mathbf{b}^0} < \Omega^{\mathbf{b}^{j'}}\right) = \\ &\quad \Pr\Bigg(\sum_{k=0}^{K_s-1}\Bigg\{\sum_{r=0}^{L-1} g_{\kappa(a),\kappa(a)}(\eta(a), r\,;\eta(a), r) h_r(\eta(a))\hat{h}_r^*(\eta(a)) \\ &\qquad + \sum_{l=1}^{K-1}\sum_{r=0}^{L-1}\sum_{r'=0}^{L-1} g_{\kappa(a),\kappa(a+l)}(\eta(a), r\,;\eta(a+l), r') \operatorname{Re}(h_{r'}(\eta(a+l))\hat{h}_r^*(\eta(a))) \\ &\qquad - \sum_{r=0}^{L-1} n_{\kappa(a)}(\eta(a)) \operatorname{Re}(\hat{h}_r^*(\eta(a)))\Bigg\} < 0\Bigg), \qquad (5.30)\end{aligned}$$

where the straight-forward substitution $a = iK + pK_s + k$ is made. Defining the sets of indices,

$$\begin{aligned}K_1 &= \left\{k : b_{\kappa(a+l)}^{j'}(\eta(a+l)) = b_{\kappa(a+l)}^{0}(\eta(a+l))\right\}, \\ K_2 &= \left\{k : b_{\kappa(a+l)}^{j'}(\eta(a+l)) \neq b_{\kappa(a+l)}^{0}(\eta(a+l))\right\},\end{aligned}$$

and

$$L = \left\{l : b_{\kappa(a+l)}^{j'}(\eta(a+l)) \neq b_{\kappa(a+l)}^{0}(\eta(a+l))\right\}.$$

(5.30) may be written as,

$$\Pr\left(\Omega^{\mathbf{b}^0} < \Omega^{\mathbf{b}^{j'}}\right) =$$
$$\Pr\Big(\sum_{k\in K_1}\sum_{l\in L}\sum_{r=0}^{L-1}\sum_{r'=0}^{L-1} g_{\kappa(a),\kappa(a+l)}(\eta(a), r\,; \eta(a+l), r')\,\mathrm{Re}(h_{r'}(\eta(a+l))\hat{h}_r^*(\eta(a)))$$
$$+ \sum_{k\in K_2}\sum_{r=0}^{L-1}\Big\{ g_{\kappa(a),\kappa(a)}(\eta(a), r\,; \eta(a), r)\,\mathrm{Re}(h_r(\eta(a))\hat{h}_r^*(\eta(a)))$$
$$- n_{\kappa(a)}(\eta(a))\,\mathrm{Re}(\hat{h}_r^*(\eta(a)))$$
$$- \sum_{r'=0}^{L-1}\sum_{l=1}^{K-1} g_{\kappa(a),\kappa(a+l)}(\eta(a), r\,; \eta(a+l), r')\,\mathrm{Re}(h_{r'}(\eta(a+l))\hat{h}_r^*(\eta(a)))\Big\} < 0\Big), \tag{5.31}$$

Combining the noise and interference terms and recognising that, if $w_{j'}$ is the Hamming weight of the $\mathbf{b}^{j'}$-state, there are $K - w_{j'}$ equal bits (and $w_{j'}$ unequal) in the correct path and the error path, the error event probability is written as,

$$\Pr\left(\Omega^{\mathbf{b}^0} < \Omega^{\mathbf{b}^{j'}}\right) =$$
$$\Pr\Big(\sum_{k\in K_2}\sum_{r=0}^{L-1}\Big\{ g_{\kappa(a),\kappa(a)}(\eta(a), r\,; \eta(a) r)\,\mathrm{Re}(h_r(\eta(a))\hat{h}_r^*(\eta(a)))$$
$$- n_{\kappa(a)}(\eta(a))\,\mathrm{Re}(\hat{h}_r^*(\eta(a)))$$
$$- \sum_{l=1}^{K-1}\sum_{r'=0}^{L-1} g_{\kappa(a),\kappa(a+l)}(\eta(a), r\,; \eta(a+l), r)\,\mathrm{Re}(h_{r'}(\eta(a+l))\hat{h}_r^*(\eta(a)))$$
$$+ \frac{1}{w_{j'}}\sum_{k\in K_1}\sum_{l\in L}\sum_{r'=0}^{L-1} g_{\kappa(a),\kappa(a+l)}(\eta(a), r\,; \eta(a+l), r')\,\mathrm{Re}(h_{r'}(\eta(a+l))\hat{h}_r^*(\eta(a)))\Big\} < 0\Big)$$
$$= \Pr\Big(\sum_{k\in K_2}\sum_{r'=0}^{L-1} g_{\kappa(a),\kappa(a)}(\eta(a), r\,; \eta(a), r)\,\mathrm{Re}(h_r(\eta(a))\hat{h}_r^*(\eta(a))) - \gamma < 0\Big). \tag{5.32}$$

We assume that the fading process is very slow so that $h_r = h_r(\eta(a))$. Under this assumption the h_r's are drawn from independent complex Gaussian distributions with variance $\sigma_r^2/2$. Then the combined noise and interference term

γ in (5.32) is zero mean and has variance given by,

$$\begin{aligned}
\mathrm{V}[\gamma] = \sum_{r=0}^{L-1} \Bigg\{ & \frac{E_b \tilde{h}_r N_o}{2} \\
& + \tilde{h}_r^2 \Bigg\{ \sum_{l=1}^{K-1} \int_0^T g^2_{\kappa(a),\kappa(a+l)}(\eta(a), r\,; \eta(a+l), r')\, d\tau_{\kappa(a)} \\
& - \frac{1}{w_j} \sum_{k \in K_1} \sum_{l \in L} \int_0^T g^2_{\kappa(a),\kappa(a+l)}(\eta(a), \eta(a+l))\, d\tau_{\kappa(a)} \Bigg\} \Bigg\} \\
= \sum_{r=0}^{L-1} \Bigg\{ & \frac{E_b \tilde{h}_r N_o}{2} \\
& + \tilde{h}_r^2 \Bigg\{ \sum_{l=1}^{K-1} \sum_{m=0}^{N_s-1} \int_{mT/N_s}^{(m+1)T/N_s} g^2_{\kappa(a),\kappa(a+l)}(\eta(a), \eta(a+l))\, d\tau_{\kappa(a)} \\
& - \frac{1}{w_j} \sum_{k \in K_1} \sum_{l \in L} \sum_{m=0}^{N_s-1} \int_{mT/N_s}^{(m+1)T/N_s} g^2_{\kappa(a),\kappa(a+l)}(\eta(a), \eta(a+l))\, d\tau_{\kappa(a)} \Bigg\} \Bigg\} \\
= \sum_{r=0}^{L-1} \Bigg\{ & \frac{E_b \tilde{h}_r N_o}{2} + \frac{E_b^2 \tilde{h}_r^2}{3} \Bigg\{ \sum_{l=1}^{K-1} g_v(l) - \frac{E_b^2}{3 w_j} \sum_{k \in K_1} \sum_{l \in L} g_v(l) \Bigg\} \Bigg\}, \qquad (5.33)
\end{aligned}$$

where $\tilde{h}_r = h_r^* h_r$ and where we have assumed ideal channel estimates. In (5.33) the interference term $g_v(l)$ is given in (4.16) in terms of the discrete aperiodic cross-correlation function of (2.8).

Calculations for $g_v(l)$ can be made for any set of spreading sequences using (4.16). As previously we calculate $g_v(l)$ for random spreading sequences from the set of m-sequences given in Table 2.1 giving the parameter g_v which is independent of l and dependant only on sequence length. In this case the noise and interference variance becomes

$$\mathrm{V}[\gamma] = \sum_{r=0}^{L-1} \left\{ \frac{E_b \tilde{h}_r N_o}{2} + \frac{E_b^2 \tilde{h}_r^2 g_v(K - K_s + w_{j'} - 1)}{3} \right\}. \qquad (5.34)$$

Modelling the noise and interference as a Gaussian process with the mean and variance as written above, a simple expression for the error event probability can be written as,

$$P_e = \frac{1}{2K_s} \sum_{j'=0}^{2^{K_s}-1} \mathrm{erfc} \left(\sqrt{\frac{w_{j'} E_b \sum_{r=0}^{L-1} \tilde{h}_r}{N_o + 2 g_v E_b \sum_{r=0}^{L-1} \tilde{h}_r (K - K_s + w_{j'} - 1)/3}} \right). \qquad (5.35)$$

The probability of bit error at medium to high E_b/N_o for the decision feedback reduced complexity receiver is well approximated by $P_b = P_e$ since for moderate to high E_b/N_o the effects of error propagation are small and there is only one path in the trellis. For the general RSSE receivers (5.35) can be used to calculate the approximate probability of any error path through the trellis and thus to determine an approximation to the bit error probability by union bound techniques. However, for medium to high E_b/N_o the error events are dominated by minimum distance error events and an approximation to the bit error probability is also $P_b \approx P_e$.

Since the super-state in the decision feedback RSSE reduced complexity receiver contains all possible 2^{K_s} binary vectors the bit error probability can be written using the binomial coefficient as

$$P_b = \frac{1}{2K_s} \sum_{j=1}^{K_s} \binom{K_s}{j} \operatorname{erfc}\left(\sqrt{\frac{jE_b \sum_{r=0}^{L-1} \tilde{h}_r}{N_o + 2g_v E_b \sum_{r=0}^{L-1} \tilde{h}_r (K - K_s + j - 1)/3}} \right). \tag{5.36}$$

The average error event probability (or the approximate bit error probability for the decision feedback reduced complexity receiver) for very slow fading can be found by averaging (5.35) over the distributions of the $\tilde{h}_r$'s. In (5.35) the $\tilde{h}_r$'s are each distributed χ^2 with two degrees of freedom and variance σ_r^4. In the special case where the delay power spectrum is uniform then $\sum_{r=0}^{L-1} \tilde{h}_r$ is distributed χ^2 with $2L$ degrees of freedom and variance $L\sigma_r^4$ since $\tilde{h}_r$ are independently and identically distributed. In general the average error event probability can be calculated numerically for any delay power spectrum by

$$P_e(\sigma_0^2, \sigma_1^2, \cdots, \sigma_{L-1}^2) = \iint \cdots \int P_e \, p_{\chi_2}(\tilde{h}_0) p_{\chi_2}(\tilde{h}_1) \cdots p_{\chi_2}(\tilde{h}_{L-1}) \, d\tilde{h}_0 \, d\tilde{h}_1 \cdots d\tilde{h}_{L-1}, \tag{5.37}$$

since the fading processes in each of the paths are considered independent. Note that the lower bound and single user bit error probability for a uniform delay power spectrum of an L-ray multi-path fading channel is the well known [59] error probability for binary signalling in an L-order diversity Rayleigh

fading channel given by,

$$P_b = \left(\frac{1-\mu}{2}\right)^L \sum_{r=0}^{L-1} \binom{L-1+r}{r} \left(\frac{1+\mu}{2}\right)^r, \text{where } \mu = \sqrt{\frac{E_b}{LN_o + E_b}}. \quad (5.38)$$

5.4 *Performance Results*

We have performed Monte Carlo simulations for the new receivers employing K equiprobable asynchronous binary sources with equal powers, uniformally distributed relative delays τ_k, rectangular m-sequence spreading signals in multi-path fading channels of different normalised Doppler shifts. In the simulations channel state information is obtained by transmitting a known sequence for one of the users. For the case of non-equal transmission powers among the users, an 'equivalent number of users' can be determined as discussed in earlier chapters and the error performance estimated using (5.36) and (5.37).

We justify our assumption of very slow fading by considering the receiver transmitting 32 kb/s with a carrier frequency of 1 GHz. In this case the receiver travelling directly toward (or away) from the base station at 200 km/h experiences a maximum normalised Doppler shift of approximately $f_D T \approx 0.005$—for lower carrier frequencies, higher data rates, slower moving mobiles and other arrival angles the Doppler shift is reduced.

In Fig. 5.5 we compare the theoretical results of (5.37) for the decision feedback receiver and (5.38) with simulation results for a flat Rayleigh faded channel with $K = 30$ users and $K_s = 1$ user per state. The results show that for very slow fading the receiver performs comparably to the theoretical bit error rate performance. Increasing the normalised Doppler worsens the receiver's performance as expected.

Figs. 5.6 and 5.7 show the performance for the same receiver in two and three ray multi-path channels. Here, we have assumed a discrete delay power spectrum function with resolvable paths separated by one chip interval T/N_s—the receiver is applicable to more general delay power spectra and for inter-path

delays less than a chip period, the paths appear as a single path. The delay power spectrum for the two ray channel in Fig. 5.6 has the first ray with power 0.75 and the second with 0.25; the three ray channel has ray powers 0.50, 0.33, and 0.17. In both cases the general improvement in performance is clear and is a result of the diversity effect in the extra paths.

In the region of interest for voice communications (BER = 10^{-4}) the receiver in the three path channel has an approximately 0.8 dB degradation with respect to the single user receiver at the same bit error rate for a normalised Doppler frequency of $f_D T = 0.005$. For a normalised Doppler of $f_D T = 0.05$, the degradation with respect to the single user receiver is approximately 2.8 dB.

In Figs. 5.8, 5.9 and 5.10 we present the same results for a RSSE reduced complexity receiver with $K_s = 2$ users per state and $S_s = 1$ state per super state. For BER = 10^{-4} the $K = 30$ user receiver in a three ray channel with normalised Doppler frequency of $f_D T = 0.005$ the degradation with respect to the single user receiver is now approximately 0.5 dB. When $f_D T = 0.05$ the degradation increases to 1 dB. Greater numbers of states reduce the degradation further. These results show that for modest increases in complexity, the performance of the receiver in faster fading channels can approach the very slow fading situation used in the receiver derivation. This situation of a mismatched channel, where the channel fade rate is higher than the very slow designed fade rate is similar to the case were the receiver has only poor estimates of the channel. In this case a receiver employing a trellis structure with a small number of states can approach the lower bounding performance of the receiver with perfect estimates of a very slow fading channel.

Comparing the performance of the reduced complexity receivers with the performance curves for the PIC detector in Fig. 2.6 shows that the reduced complexity receivers perform approximately 0.5 dB better at a bit error rate of BER=10^{-3}. However, the PIC detectors have a much better error floor performance than the reduced complexity receviers which would be significant for applications requiring a higher bit error rate.

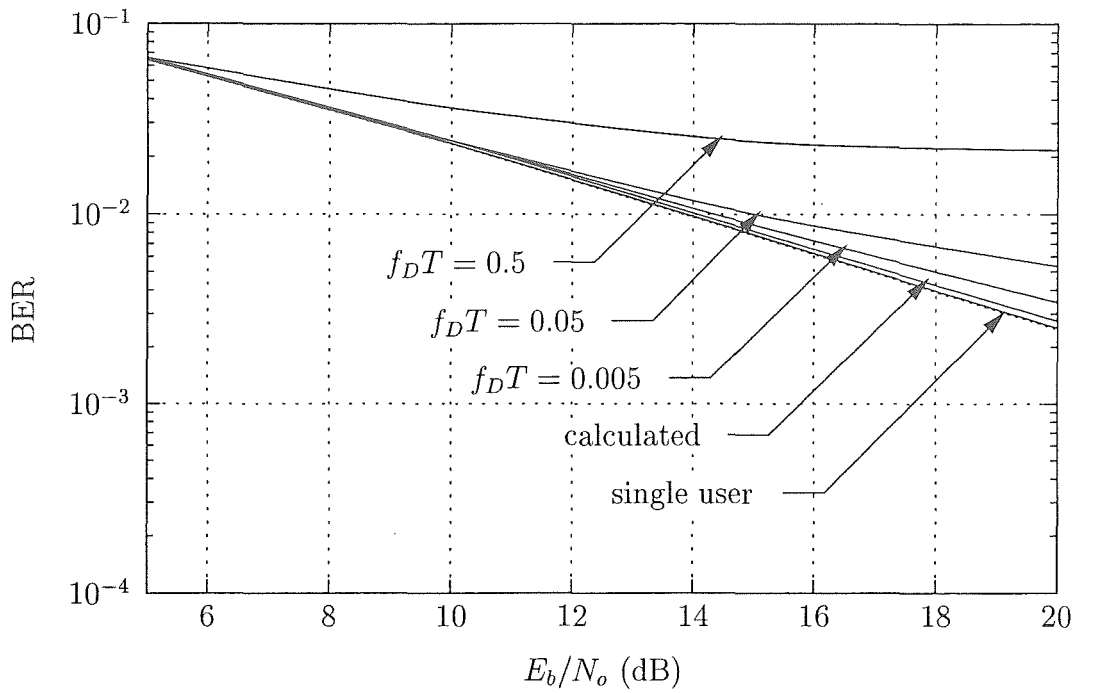

Figure 5.5: Decision feedback receiver performance in Rayleigh flat fading for $K = 30$ users, $N_s = 127$ and $K_s = 1$ user per state. Dotted line is the well-known diversity performance in Rayleigh fading result of (5.38).

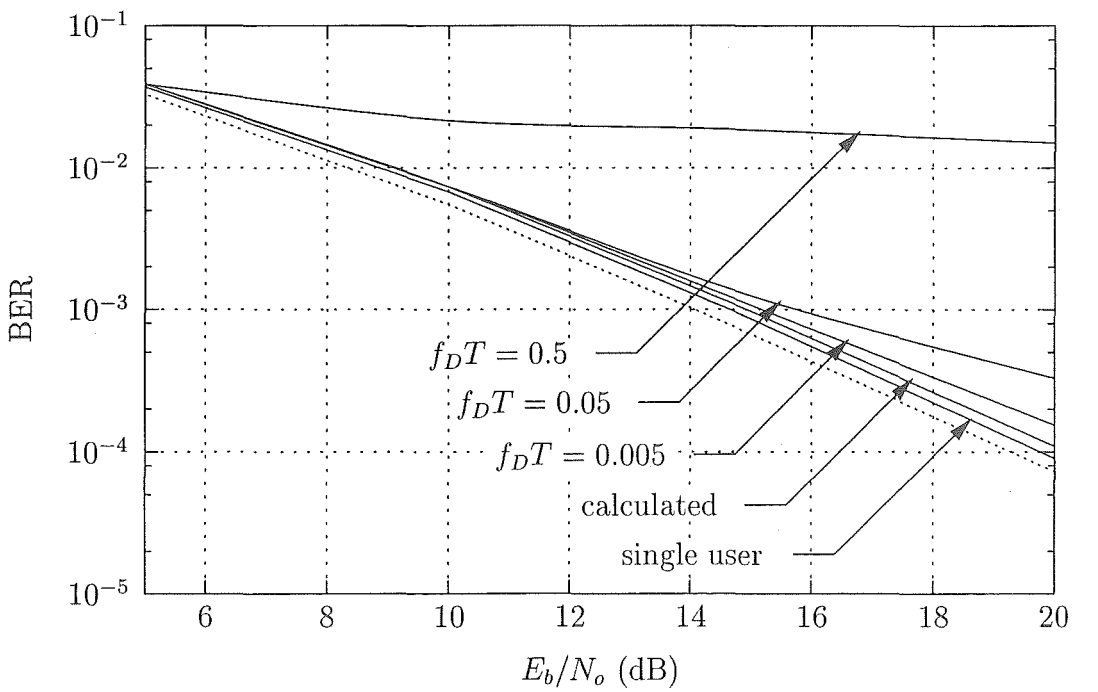

Figure 5.6: Decision feedback receiver performance in a two-ray Rayleigh faded multi-path channel with delay power spectra of 0.75 and 0.25 for $K = 30$ users, $N_s = 127$ and $K_s = 1$ user per state. Dotted line is the well-known diversity performance in Rayleigh fading result of (5.38).

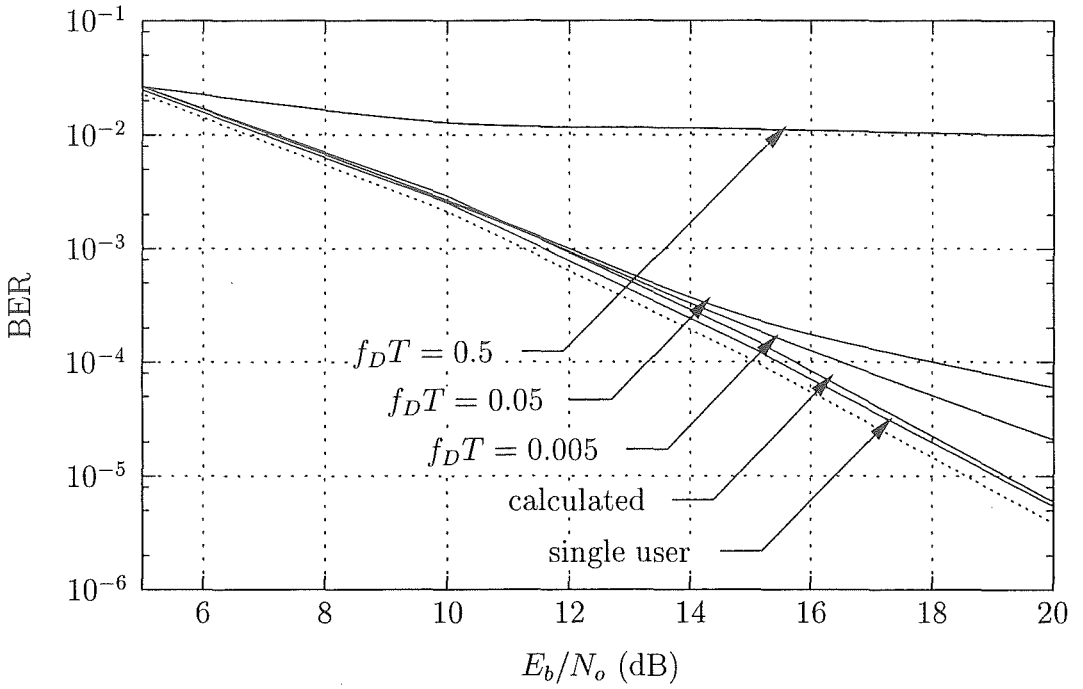

Figure 5.7: Decision feedback receiver performance in a three-ray Rayleigh faded multipath channel with delay power spectra of 0.50,0.33 and 0.17 for $K = 30$ users, $N_s = 127$ and $K_s = 1$ user per state. Dotted line is the well-known diversity performance in Rayleigh fading result of (5.38).

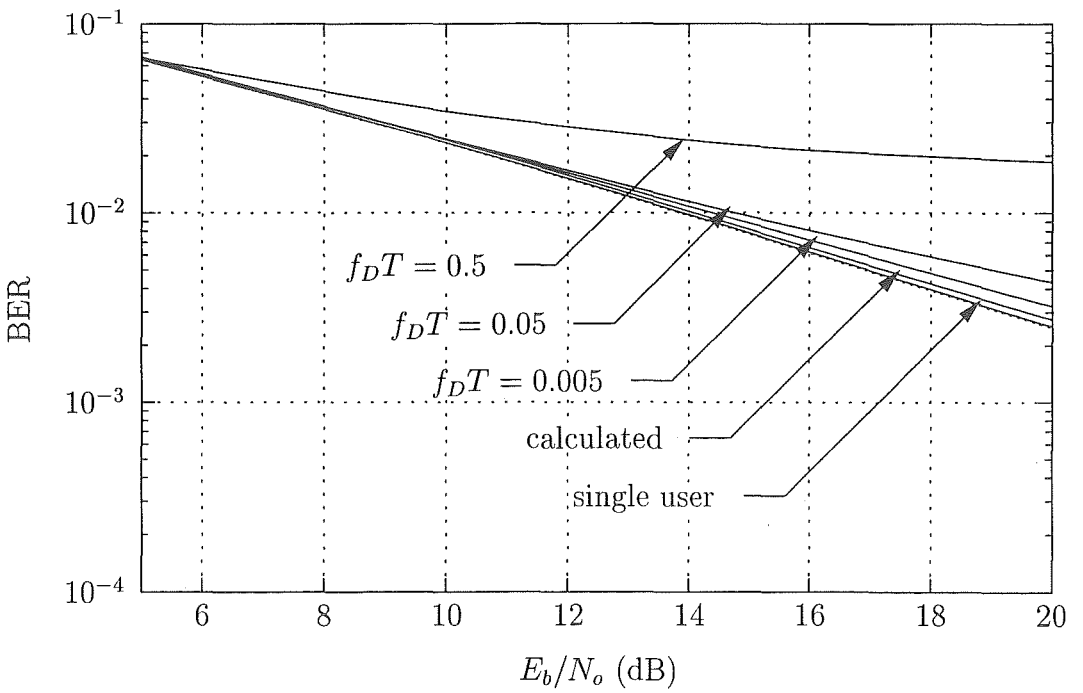

Figure 5.8: RSSE reduced complexity receiver performance in Rayleigh flat fading for $K = 30$ users, $N_s = 127$ and $K_s = 2$ users per state. Dotted line is the well-known diversity performance in Rayleigh fading result of (5.38).

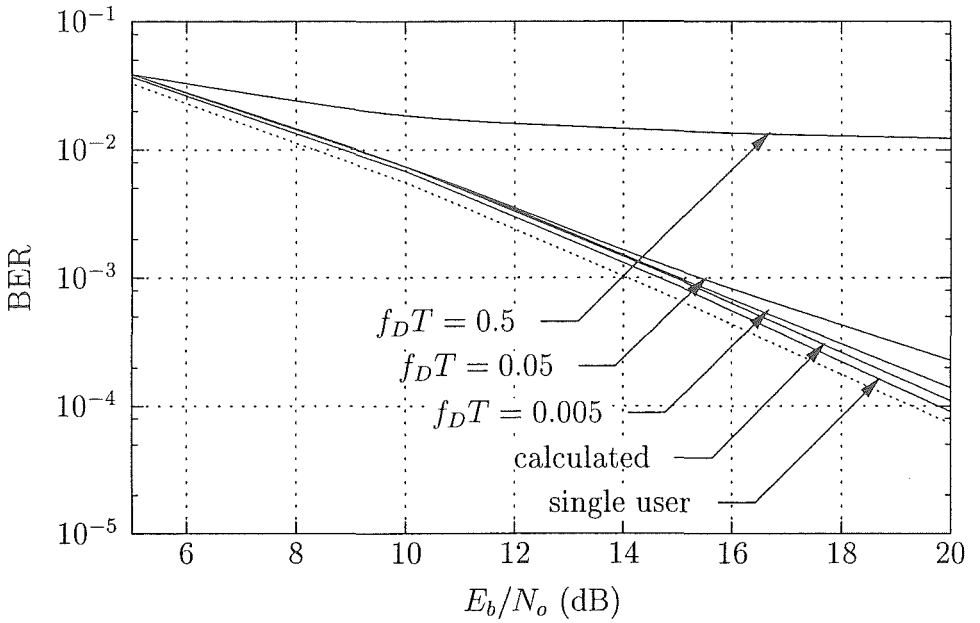

Figure 5.9: RSSE reduced complexity receiver performance in a two-ray Rayleigh faded multi-path channel with delay power spectra of 0.75 and 0.25 for $K = 30$ users, $N_s = 127$ and $K_s = 2$ users per state. Dotted line is the well-known diversity performance in Rayleigh fading result of (5.38).

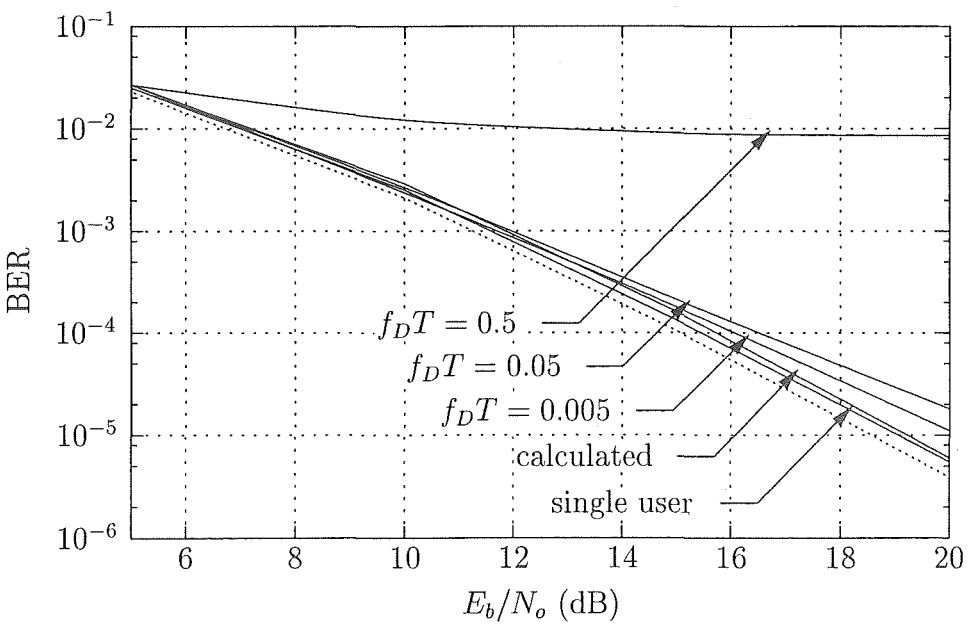

Figure 5.10: RSSE reduced complexity receiver performance in a three-ray Rayleigh faded multi-path channel with delay power spectra of 0.50,0.33 and 0.17 for $K = 30$ users, $N_s = 127$ and $K_s = 2$ users per state. Dotted line is the well-known diversity performance in Rayleigh fading result of (5.38).

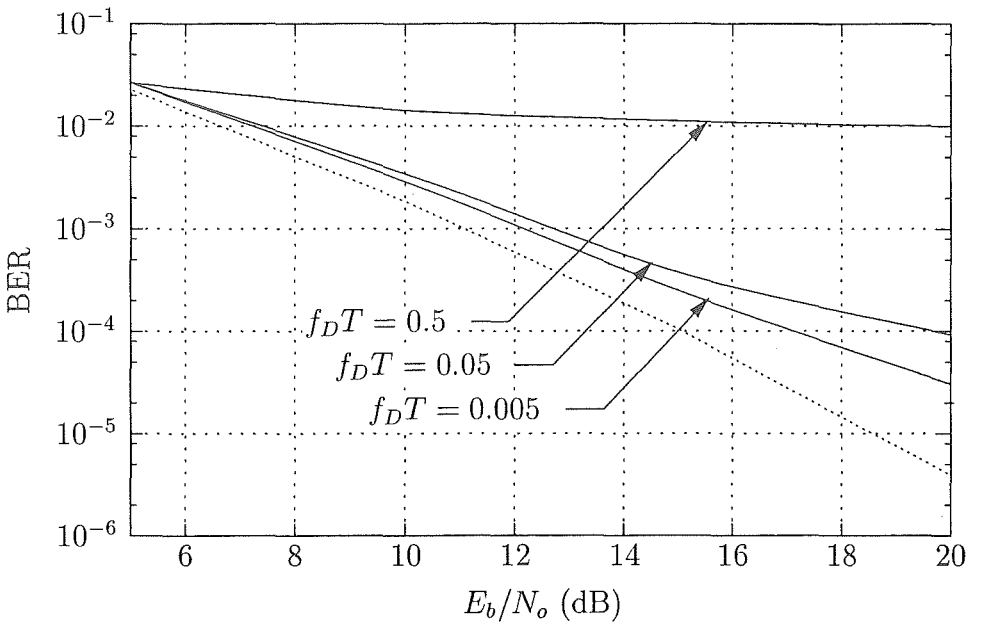

Figure 5.11: Decision feedback reduced complexity receiver performance in a communications environment where each user transmits over an independant three-ray Rayleigh faded channel with delay power spectra of 0.50,0.33 and 0.17 The system has $K = 30$ users and a $N_s = 127$ processing gain. Dotted line is the well-known diversity performance in Rayleigh fading result of (5.38).

In Figs. 5.11 and 5.12 we present simulation results for a system where each user transmits over a three-ray Rayleigh channel which is independant of the channel used by the other users. In this case the receiver calcualtes channel estimates for each of the K users. For slow to moderate fading, $f_DT = 0.005$ to $f_DT = 0.05$, the degration is less than 0.5 dB, and is smaller for systems with a higher number of states.

5.5 Conclusions

We have presented a family of reduced complexity multi-user detectors for asynchronous spread spectrum multiple access in multi-path fading channels of very slow-to-slow fading and have shown that, as expected, performance is dominated by the order of diversity of the channel. The receiver structure was formed by applying maximum-ratio combination techniques to the families of receiver structures presented in chapters 3 and 4 for the AWGN channel . The

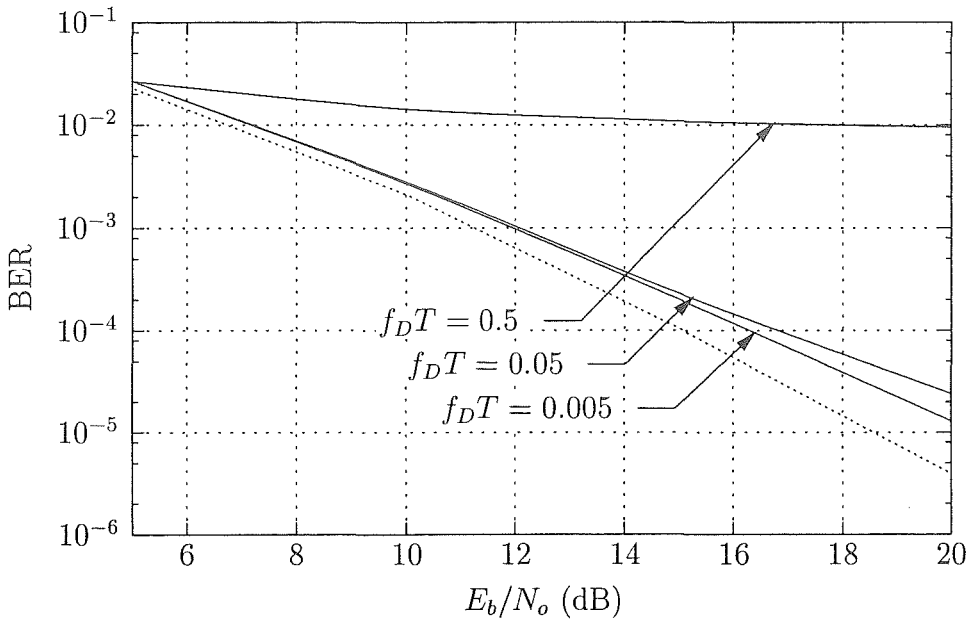

Figure 5.12: RSSE reduced complexity receiver performance in a communications environment where each user transmits over an independant three-ray Rayleigh faded channel with delay power spectra of 0.50,0.33 and 0.17 The system has $K = 30$ users, $K_s = 2$ users per state and a $N_s = 127$ processing gain. Dotted line is the well-known diversity performance in Rayleigh fading result of (5.38).

receiver structure allows the system designer to make performance/complexity tradeoffs with two degrees of freedom; one of which was shown to have a near negligible effect on error performance and results in a simple decision feedback structure. It is anticipated that the receiver may be easily modified to obtain further diversity gain from other sources such as spatial diversity.

The performance of the receivers was analysed and a lower bound on performance was presented for the case of an extremely slow fading channel. For a more realistic normalised Doppler frequency of $f_DT = 0.005$ corresponding to a 1 GHz carrier frequency, a bit rate of 32 kb/s and a maximum velocity of 200 km/h, it was shown that an RSSE reduced complexity receiver with $K_s = 2$ users per state and a processing gain of $N_s = 127$ performed only 0.5 dB worse than the single user receiver for a BER $= 10^{-4}$.

Chapter 6

CONCLUSIONS AND OPEN PROBLEMS

6.1 Summary

The main objective of this thesis was to investigate and develop reduced complexity multi-user receivers for spread spectrum multiple access (SSMA) communication systems suitable for mobile radio. The motivation for the thesis results from the poor performance of the conventional multi-user detector and the high complexity of the maximum likelihood multi-user detector. As a result of the complexity issues multi-user detectors employing joint detection have not attracted much attention for implementation in practical systems.

The goal was to develop families of receivers which would reduce the computational complexity to a point where implementation is possible in cellular and micro-cellular environments using contemporary technology. The system should be flexible such that as technology improves any loss in performance due to the reduced complexity nature of the receiver families can be reduced. Furthermore, the detection schemes should not be applicable only the the additive white Gaussian noise (AWGN) channel, but also to the multi-path slow fading channels encountered in the cellular mobile environment.

The receiver development started in chapter 3 where we took the maximum likelihood multi-user receiver and reduced the number of states required to be processed by the Viterbi algorithm per bit by performing a serial expansion of the maximum likelihood trellis. While the expansion increased the number of stages in the trellis to be processed per signalling interval, it resulted in a geometric increase in states from the expansion process while an exponential decrease occurred due to a fewer number of users per state. The degree of serial

expansion of the trellis was controlled by a system parameter determining the number of users to be processed by each trellis state. It was shown that when the number of users per state equalled the number of users in the system, the receiver reverted to the maximum likelihood receiver. As expected the biggest reduction in complexity was achieved with a single user per state. We analysed the system and showed that the serial expansion resulted in a sub-optimal receiver whose performance was a function of the processing gain, number of users and number of users per state of the system. We showed that a system with twenty users and a processing gain of 27 dB suffers at most a 0.5 dB loss with respect to the maximum likelihood receiver at a bit error rate of 10^{-4}. Lower processing gains resulted in worse performance but for a processing gain of 21 dB the performance degradation was only 2 dB.

In chapter 4 we applied reduced state sequence estimation methods to the simple reduced complexity receiver in order to reduce the number of computations further. The result was a new family of receivers with two system parameters, the number of users per state K_s and the number of states per super-state S_s. These parameters allowed for a trade in system performance for complexity. It was shown that system performance was dominated by the number of users per state and that the second parameter, the number of super-states, had little effect on performance at moderate to high signal to noise ratio but resulted in a significant reduction in complexity. With only one super-state the trellis collapsed to a one state, one path, memory-less receiver structure with decision feedback. It was shown that for a system with thirty users, and eight users per state the decision feedback receiver performed only 0.5 dB worse than the maximum likelihood receiver with a processing gain of 27 dB; for 21 dB processing gain the degradation increased to 2 dB. In both cases the computational complexity of the thirty user system was approximately equivalent to the maximum likelihood receiver with only six users.

The last chapter developed the receivers for the multi-path fading channel. As the mobile channel is slowly fading we assumed very slow fading in the

development. The result was a receiver whose performance is dominated by the diversity of the channel. A slight reduction in performance was shown for a normalised Doppler frequency of $f_D T = 0.005$. While the performance worsened still for $f_D T = 0.05$ the degradation could be reduced by increasing the number of users per state. Receiver performance was shown to be catastrophic for the extremely fast fading ($f_D T = 0.5$) channel.

6.2 Future Work

There are many areas in which further work is required. Some of the areas envisaged are—

- *forward-backward processing*: we suggest that performance improvements could be obtained by employing a forward-backward Viterbi process over small block lengths. The complexity reductions obtained in this thesis could easily offset the forward-backward approach.

  The forward-backward approach was originally used by Schneider [69]. His receiver was more complex than the maximum likelihood receiver which employs only a forward processor. In the case of the receivers presented in this thesis we suggest that forward-backward processing could help improve near-far performance for only a moderate increase in system complexity. Performance improvement would occur by a (partial) removal of the leakage term of the receiver performance equations. If the block-lengths over which the forward-backward processing occurs were small enough then the delay incurred by the extra processing could be kept small. A trade-off between processing delay and system complexity, and system performance would probably exist and be a function of block length.

- *near-far problem*: we indicated that the near-far problem and hence the requirement for strict power control could be less stringent than the conventional receiver. This needs to be quantified.

- *other diversity sources*: the fading channel analysis showed (as expected) that system performance is dominated by the order of channel diversity. Other sources of diversity such as spatial diversity should be investigated.

- *joint channel estimation*: joint channel estimation and detection seems possible, but effects of the system parameters, of the number of users per state and the number of super-states are unknown.

  Simple trellis-based channel estimation techniques such as linear prediction could be employed since the channel is slowly time varying.

- *imperfect channel estimation*: performance loss due to imperfect channel estimation needs investigation and quantification.

- *forward error correction coding*: could offset any performance degradation from imperfect channel estimation and needs to be studied in the context of the reduced complexity receivers of this thesis.

Appendix A

COMPUTER SIMULATION OF FADING PROCESSES

Highly correlated fading processes, corresponding to very slow fading, are generated by passing samples of a normally distributed complex Gaussian random process through a Doppler filter with a very small cutoff frequency. The resulting filter structure is complicated since infinite impulse response (IIR) filters may become unstable and finite impulse response filters (FIR) require long, computationally intensive convolutions.

The filter impulse response is found to be

$$\begin{aligned} h(t) &= \int_{-f_D}^{f_D} \cos(2\pi f t)\sqrt{W(f)}\, dt \\ &= \frac{a}{\sqrt[4]{t}} J_{\frac{1}{4}}(2\pi f_D t), \end{aligned} \tag{A.1}$$

and

$$\lim_{t\to 0} \frac{1}{\sqrt[4]{t}} J_{\frac{1}{4}}(2\pi f_D t) = \frac{\sqrt[4]{\pi f_D}}{\Gamma(\frac{5}{4})}. \tag{A.2}$$

Use of multi-rate filtering techniques can mitigate some of the computation burden. An M-tap filter is arranged by up-sampling the sampled Gaussian processes by U and calculating a K-tap convolution for each iteration. The order of the filter is reduced by a function of the up-sampling factor, $U = M/K$.

Define the matrix of filter taps as

$$\mathbf{H} : H_{u,k} = \begin{cases} 1.4688\sqrt[4]{f_D} & t = 0 \\ \frac{1}{\sqrt[4]{|t|}} J_{\frac{1}{4}}(2\pi f_D |t|) & |t| > 0 \end{cases} \tag{A.3}$$

where the time index t is given by

$$t = kU + u - \frac{UK - 1}{2}. \tag{A.4}$$

The filtering algorithm is:

INPUTS:	$\mathbf{x}$, L_x-length filter input vector
	$\mathbf{H}$, $U \times K$ matrix of filter taps
OUTPUT:	$\mathbf{y}$, UL_x-length filter output vector
LOCAL VARIABLES:	$\mathbf{s}$, K-length filter state vector
	i, loop index
	u, up-sampling index
PROCEEDURE:	

for $i = 0$ **to** $L_x - 1$
  if $(u = U)$
    $\mathbf{s} := [\mathbf{x}_i \, \mathbf{s}_0 \, \mathbf{s}_1 \cdots \mathbf{s}_{K-2}]$
    $u := 1$
  end if

  $\mathbf{y}_i := \mathbf{H}_u \mathbf{s}^{\mathrm{T}}$
  $u := u + 1$
end for

Fig. A.1 shows the autocorrelation of the fading process plotted against the theoretical for and normalised Doppler frequency of $f_D = 0.05$ and parameters $K = 100$, $U = 10$.

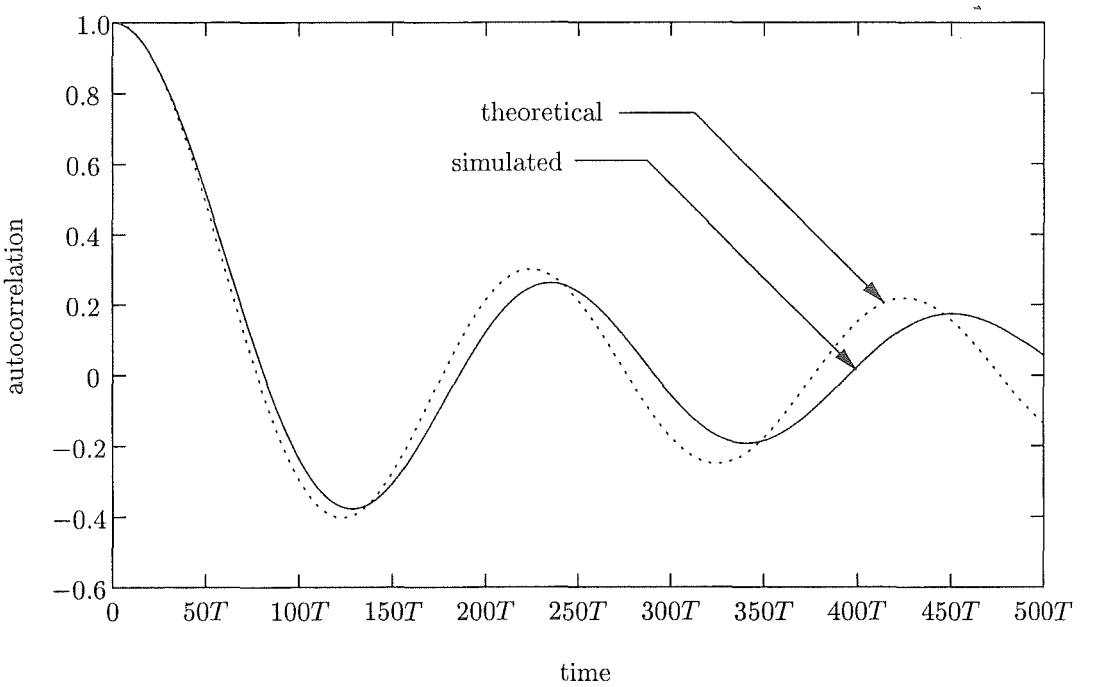

Figure A.1: Autocorrelation of simulated fading signal plotted against the theortetical autocorrelation for Doppler frequency of $f_D = 0.05$ and parameters $K = 100$, $U = 10$.

GLOSSARY

A

a general index variable

A_{bm} number of arithmetic operations per branch metric

A_b number of arithmetic operations per bit

B

b data bit

$\mathbf{b}$ vector of data bits, also used to label the states in trellis

B the set of all possible bit vectors

BER bit error rate

C

c chip index

c coded bits

$\mathbf{c}$ vector of coded bits

$c(\cdot)$ input delay spread function

$C_{k,k'}(\cdot)$ aperiodic correlation function between the k=th and k'=th users' signals

$\hat{C}_{k,k'}(\cdot)$ periodic correlation function between the k=th and k'=th users' signals

C_{bm} number of branch metric calculations per signalling interval

D

d decoding delay

d code distance

d_f code free distance

E

E_c chip energy

E_b bit energy

F

f frequency

f_d Doppler frequency

f_D maximum Doppler frequency

F linear feedback shift register state transition matrix

${}_2\mathrm{F}_1(\cdot)$ confluent hyper-geometric function

G

g linear feedback shift register generator polynomial

$g(\cdot)$ spreading sequence correlation function

g_v interference term

$\mathbf{G}$ matrix of spreading sequence correlations

γ noise and interference term

$\boldsymbol{\gamma}$ vector of noise and interference terms

H—J

$h(\cdot)$ channel fading process

i bit index (within signalling interval)

j bit index (within transmission interval)

K

k user index

K number of users

K_s number of user per state

κ convolutional code constraint length

$\kappa(\cdot)$ user identification function

L

l previous bit index

L number of multi-paths

M

m general index

m matrix column index

N

n general index

n matrix row index

n noise

N transmitted sequence length

N_s processing gain, number of chips per bit

N_o additive white Gaussian noise power spectral density

N_p number of sub-intervals per signalling interval

$\eta(\cdot)$ signalling interval identification function

O

$\Omega(\cdot)$ path metric

$\bar{\Omega}(\cdot)$ branch metric

P

p probability density function (pdf)

$p_r(\cdot)$ rectangular pulse signal

$P(\cdot)$ delay power spectrum

P_b probability of bit error

P_e probability of error

$\rho(\cdot)$ sub-interval identification function

R

r multi-path index

$r(\cdot)$ received signal

r_c auto-correlation function

$R_c(\cdot)$ input delay spread auto-correlation function

S

s trellis state index

$s(\cdot)$ spreading signal

S scattering function

S number of super-states

S_s number of states per super-state

σ^2 multi-path power

T

t time

T bit period

τ user delay

ξ path delay

V—Y

ν shift register length

w hamming weight

$x(\cdot)$ transmitted signal

X matrix of previous bits

$y(\cdot)$ correlator output

y vector of correlator outputs

LIST OF FIGURES

BIBLIOGRAPHY

[1] BAINES, S. J., BURR, A. G., AND TOZER, T. C. "Double Window Wireless Multi-user Detection for Asynchronous DS-CDMA". *Electron. Lett.* vol. 32, no. 24, pp. 2199–2201, Nov. 1996.

[2] BELLO, P. A. "Characterization of Randomly Time-Variant Linear Channels". IEEE Trans. Commun. Sys. *vol. CS-11*, pp. 4–37, Dec. 1963.

[3] BELLO, P. A. "Aeronautical Channel Characterization". *IEEE Trans. Commun.* vol. COM-21, no. 5, pp. 548–563, May 1973.

[4] BRUEHRER, R. M., KAUL, A., STRIGLIS, S., AND WOERNER, B. D. "Analysis of DS-CDMA Parallel Interference Cancellation with Phase and Timing Errors". *IEEE J. Select. Areas Commun.* vol. 44, no. 10, pp. 1308–1321, Oct. 1996.

[5] BUEHRER, N. S. C. R. M., AND WOERNER, B. D. "A Comparison of Multiuser Receivers for Cellular CDMA". In *Proc. IEEE Globecom '96* (1996), pp. 1571–1577.

[6] CACOPARDI, S., FRESCURA, F., GAMBI, M., AND REALI, G. "New Concatenated Sequences for Wireless Indoor Asynchronous DS-CDMA Communications". In *IEEE International Conference on Communications* (1996), vol. 1, pp. 63–67.

[7] CHAN, C.-K., AND LAM, W.-H. "Efficient Use of Pseudo-noise Sequences in Synchronous Direct-Sequence Spread-Spectrum Multiple-Access Communications Systems". In *1994 IEEE 44th Vechicular Technology Conference* (1994), vol. 1, pp. 540–544.

[8] CLARKE, R. H. "A Statistical Theory of Mobile-Radio Reception". Bell Syst. Tech. J. *vol. 47*, pp. 957–1000, 1968.

[9] DINGMAN, R. C. "A New Upper Bound on Trellis Code Error Performance on Rayleigh Flat-Fading Channels". Master's thesis, McMaster University, Ontario, Canada, 1992.

[10] DIVSALAR, D., AND SIMON, M. K. "The Design of Trellis Coded MPSK for Fading Channels: Performance Criteria". *IEEE Trans. Commun.* vol. 36, no. 9, pp. 1004–1012, Sept. 1988.

[11] DIXON, R. *Spread Spectrum Systems.* Willey Interscience, New York, 1984.

[12] DOU, R. H., AND MILSTEIN, L. B. "Error Probability Bounds and Approximations for DS Spread-Spectrum Communications Systems with Multiple Tone or Multiple-Access Interference". IEEE Trans. Commun. *vol. COM-32*, pp. 493–502, May 1984.

[13] DUEL-HALLEN, A. "Decorrelating Decision-Feedback Multiuser Detector for Synchronous Code-Division Multiple Access Channels". *IEEE Trans. Commun.* vol. 41, no. 2/3/4, pp. 285–290, Feb/Mar/Apl 1993.

[14] DUEL-HALLEN, A. "A Family of Multi-User Decision-Feedback Detectors for Asynchronous Code-Division Multiple Access Channels". *IEEE Trans. Commun.* vol. 43, no. 2/3/4, pp. 421–4334, Feb/Mar/Apl 1995.

[15] DUEL-HALLEN, A., AND HEEGARD. "Delayed Decision-Feedback Sequence Estimation". IEEE Trans. Commun. *vol. 37*, pp. 428–436, May 1989.

[16] ELDERS-BOLL, H., BUSBOOM, A., AND SCHOTTEN, H. P. "Spreading Sequences for Zero-Forcing DS-CDMA Mulituser Detectors". In

IEEE 8th International Symposium on Personal, Indoor and Mobile Radio Communications (1997), vol. 1, pp. 53–57.

[17] ESTEVES, E. "Per-survivor Interference Cancellation Structures for Low-complexity ML Detection of DS/CDMA Signals". In *Proceedings of IEEE Globecom* (Dec. 1999), vol. 1a, pp. 482–486.

[18] ESTEVES, E., AND SCHOLTZ, R. A. "Reduced Complexity ML Multiuser Sequence Detection with Per-survivor Interference Cancellation". In *Proceedings of Asilomar Conference* (Oct. 1997), vol. 2, pp. 1415–1419.

[19] EYUBOĞLU, V. M., AND QURESHI, S. U. "Reduced-state Sequence Estimation with Set Partitioning and Decision Feedback". IEEE Trans. Commun. *vol. 36*, pp. 13–20, Jan. 1988.

[20] GERANIOTIS, E. A., AND PURSLEY, M. "Error Probability for Direct-Sequence Spread-Spectrum Multiple-Access Communications–Part II: Approximations". IEEE Trans. Commun. *vol. COM-30*, pp. 985–995, May 1982.

[21] GILHOUSEN, K. S., JACOBS, I. M., PADOVANI, R., VITERBI, A. J., JR, L. A. W., AND III, C. E. W. "On the Capacity of a Cellular CDMA System". *IEEE Trans. Vechic. Technol.* vol. 40, no. 2, pp. 303–312, May 1991.

[22] GOLOMB, S. W. *Shift Register Sequences.* Aegean Park Press, Laguna Hills, California, 1982.

[23] GRIECO, D. M., AND SCHILLING, D. L. "The Capacity of Broadband CDMA Overlaying a GSM Cellular System". In *1994 IEEE 44th Vechicular Technology Conference* (1994), vol. 1, pp. 31–35.

[24] HAFEEZ, A., AND STARK, W. E. "Delayed Feedback Sequence Estimation for Unwhitened ISI Channels with Applications to Multiuser Detection". IEEE J. Select. Areas Commun. *vol. 16*, pp. 1785–1795, Sept. 1998.

[25] HARTMAN, H. P. "Analysis of a Dithering Loop fir PN Code Tracking". IEEE Trans. Aerosp. Electron. Syst. *vol. AES-10*, pp. 2–9, Jan. 1974.

[26] HAYKIN, S. *Communication Systems*, third ed. John Wiley & Sons, Inc, 1994.

[27] HO, P., AND FUNG, D. "Error Performance of Multiple-Symbol Differential Detection of PSK Signals Transmitted Over Correlated Rayleigh Fading Channels". *IEEE Trans. Commun.* vol. 40, no. 10, pp. 1566–1569, Oct. 1992.

[28] HO, P., AND FUNG, D. K. P. "Error Performance of Interleaved Trellis-Coded PSK Modulations in Correlated Rayleigh Fading Channels". *IEEE Trans. Commun.* vol. 40, no. 12, pp. 1800–1809, Dec. 1992.

[29] HOEHER, P. "A Statistical Discrete-Time Model for the WSSUS Multipath Channel". *IEEE Trans. Commun.* vol. 41, no. 4, pp. 461–468, Nov. 1992.

[30] HOLTZMAN, J. M. "A Simple, Accurate Method to Calculate Spread Spectrum Multiple-Access Error Probabilities". *IEEE Trans. Commun.* vol. 40, no. 3, pp. 461–464, Mar. 1992.

[31] HUI, L. C., AND LETAIEF, K. B. "Successive Interference Cancellation for Multiuser Asynchronous DS/CDMA Detectors in Multipath Fading Links". *IEEE Trans. Commun.* vol. 46, no. 3, pp. 384–391, Mar. 1998.

[32] JUNTTI, M. J., AAZHANG, B., AND LILLEBERG, J. O. "Iterative Implementation of Linear Multiuser Detection for Dynamic Asynchronous CDMA Systems". IEEE Trans. Commun. *vol. 46*, pp. 503–508, Apr. 1998.

[33] JUNTTI, M. J., LATVA-AHO, M., AND HEIKKILA, M. "Performance Comparison of PIC and Decorrelating Multiuser Receivers in Fading Channels". In *Proc. IEEE Globecom '97* (1997), pp. 609–613.

[34] KALOFONOS, D. N., STOJCNOVIC, M., AND PROAKIS, J. G. "On the Performance of Adaptive MMSE Detection for a MC-CDMA System in Flat Fading Rayleigh Channels". In *IEEE 9th International Symposium on Personal, Indoor and Mobile Radio Communications* (1998), vol. 3, pp. 1309–1313.

[35] KAMMERLANDER, K. "Benefits of Combined TDMA/CDMA Operation for Third Generation Mobile Radio Systems". In *IEEE 4th International Symposium on Spread Spectrum Technology and Applications* (1996), vol. 2, pp. 507–512.

[36] KARKKAINNE, K. H. A. "Correlation, Spread Spectrum Multiple Access and Linear Complexity Properties of Non-linear Feedforward Logic (NLFFL) Pseudonoise Sequences". In *IEEE Military Communications Conference* (1993), vol. 2, pp. 568–574.

[37] KIM, S. R., LEE, J. G., AND LEE, H. "Interference Cancellation Scheme with Simple Structure and Better Performance". *Electron. Lett.* vol. 32, no. 23, pp. 2115–2117, Nov. 1996.

[38] KOHNO, R., HATORI, M., AND IMAI, H. "Cancellation Techniques of Co-Channel Interference in Asynchronous Spread Spectrum Multiple Access Systems". *Elec. and Commun. in Japan* vol. 66-A, no. 5, pp. 20–29, 1983.

[39] KOHNO, R., IMAI, H., HATORI, M., AND PASUPATHY, S. "An Adaptive Canceller of Cochannel Interference for Spread-Spectrum Multiple-Access Communication Networks in a Power Line". *IEEE J. Select. Areas Commun.* vol. 8, no. 4, pp. 691–699, May 1990.

[40] KOHNO, R., IMAI, H., HATORI, M., AND PASUPATHY, S. "Combination of an Adaptive Array Antenna and a Canceller of Interference for Direct Sequence Spread-Spectrum Multiple Access System". *IEEE J. Select. Areas Commun.* vol. 8, no. 4, pp. 675–681, May 1990.

[41] KREYZIG, E. *Advanced Engineering Mathematics*, 6 ed. Wiley, New York, 1988.

[42] LEE, Y.-H., AND TANTARATANA, S. "Sequential Acquisition of PN Sequences for DS/SS Communications: Design and Performance". *IEEE J. Select. Areas Commun.* vol. 10, no. 4, pp. 750–759, May 1992.

[43] LINDHOLM, J. H. "An Analysis of the Pseudo-Randomness Properties of Subsequences of Long m-Sequences". *IEEE Trans. Inform. Theory* vol. IT-14, no. 4, pp. 569–576, July 1968.

[44] LUPAS, R., AND VERDU, S. "Near-Far Resistance of Multi-User Detectors in Asynchronous Channels". *IEEE Trans. Commun.* vol. 38, no. 4, pp. 496–508, Apr. 1990.

[45] MACWILLIAMS, F. J., AND SLOANE, N. J. A. "Pseudo-random Sequences and Arrays". Proc. IEEE *vol. 64*, pp. 1715–1729, Dec. 1976.

[46] MATTHEWS, J. W. "Eigenvalues and Troposcatter Multipath Analysis". *IEEE J. Select. Areas Commun.* vol. 10, no. 3, pp. 497–505, Apr. 1992.

[47] MITRA, U., AND POOR, H. V. "Adaptive Decorrelating Detectors for CDMA Communications". In *Proceedings of the IEEE International Conference on Communication* (June 1995), pp. 1075–1079.

[48] MIYAGAKI, Y. A., MORINAGA, N., AND NAMEKAWA, T. "Error Probability Characteristics for CPSK Signal Through m-Distributed Fading Channel". IEEE Trans. Commun. *vol. 26*, pp. 88–100, Jan. 1978.

[49] MORROW, R. K., AND LEHNERT, J. S. "Bit-to-bit Error Dependence in Slotted DS/SSMA Packet Systems with Random Signiture Sequences". IEEE Trans. Commun. *vol. 37*, pp. 1052–1061, Oct. 1989.

[50] MOSHAVI, S. "Multi-User Detection for DS-CDMA Communications". IEEE Commun. Mag., pp. 124–136, Oct. 1996.

[51] NAIN, P., GEROGANAS, N. D., AND STEWART, W. J. "Analysis of a Hybrid Multiple Access Protocol with Free Access of New Arrivals During Conflict Resolution". *IEEE Trans. Commun.* vol. 36, no. 7, pp. 806–815, July 1988.

[52] OPPENHEIM, A. V., AND SCHAFER, R. W. *Discrete-Time Signal Processing.* Prentice Hall, Inc, 1989.

[53] PATEL, P., AND HOLTZMAN, J. "Performance Comparison of a DS/CDMA Szstem Using a Successive Interference Cancellation (IC) Scheme Under Fading". In *IEEE Proc. IEEE ICC'94* (1997), pp. 510–514.

[54] PETERSON, R. L., ZIEMER, R. E., AND BARTH, D. E. *Introduction to Spread Spectrum Communications.* Prentice-Hall Inc, 1995, ch. 3, pp. 89–148.

[55] PICKHOLTZ, R. L., SCHILLING, D. L., AND MILSTEIN, L. B. "Theory of Spread-Spectrum Communication - A Tutorial". *IEEE Trans. Commun.* vol. COM-30, no. 5, pp. 855–889, May 1982.

[56] POLYDOROS, A., AND WEBER, C. "A Unified Approach to Serial Search Spread-Spectrum Code Acquisition: Part I. General Theory". IEEE Trans. Commun. *vol. COM-32*, pp. 542–549, May 1984.

[57] POLYDOROS, A., AND WEBER, C. "A Unified Approach to Serial Search Spread-Spectrum Code Acquisition: Part II. A Matched Filter Receiver". IEEE Trans. Commun. *vol. COM-32*, pp. 550–560, May 1984.

[58] PRASAD, R., NIJHOF, J. A. M., AND CAKIL, H. I. "Hybrid TDMA/CDMA Multiple Access Protocol for Multimedia Communications". In *IEEE International Conference on Personal Wireless Communications* (1996), pp. 123–128.

[59] PROAKIS, J. G. *Digital Communications*, third ed. McGraw-Hill, Inc, 1995.

[60] PURSLEY, M. "Performance Evaluation for Phase Coded Spread Spectrum Multiple-Access Communication. Part I: System Analysis". IEEE Trans. Commun. *vol. COM-25*, pp. 795–799, Aug. 1977.

[61] RAPPAPORT, T. S. *Wireless Communications: Principles and Practice.* Prentice Hall, 1996.

[62] RASMUSSEN, L. K., LIM, T. J., AND AULIN, T. M. "Breadth-First Maximum Likelihood Detection in Multiuser CDMA". *IEEE Trans. Commun.* vol. 45, no. 10, pp. 1176–1178, Oct. 1997.

[63] SADOWSKY, J. S., AND KATEDZISKI, V. "On the Correlation and Scattering Functions of the WSSUS Channel for Mobile Communications". *IEEE Trans. Vechic. Technol.* vol. 47, no. 1, pp. 270–282, Feb. 1998.

[64] SARWATE, D. V., AND PURSLEY, M. "Crosscorrelation Properties of Pseudorandom and Related Sequences". *Proc. IEEE* vol. 68, no. 5, pp. 593–619, May 1980.

[65] SAWATE, D. V., AND PURSLEY, M. B. "Crosscorrelation Properties of Pseudorandom and Related Sequences". *Proc. IEEE* vol. 68, no. 5, pp. 593–619, May 1980.

[66] SCHILLING, D. L., MILSTEIN, L. B., PICKHOLTZ, R. L., BRUNO, F., KANTERAKIS, E., KULLBACK, M., ERCEG, V., BIEDERMAN, W., FISHMAN, D., AND SALERNO, D. "Broadband CDMA for Personal Communications Systems". IEEE Commun. Mag., pp. 86–93, Nov. 1991.

[67] SCHILLING, D. L., MILSTEIN, L. B., PICKHOLTZ, R. L., KULLBACK, M., AND MILLER, F. "Spread Spectrum for Commercial Communications". IEEE Commun. Mag., pp. 66–79, Apr. 1991.

[68] SCHLEGEL, C., ROY, S., ALEXANDER, P. D., AND XIANG, Z. J. "Multiuser Projection Receivers". *IEEE J. Select. Areas Commun.* vol. 14, no. 8, pp. 1610–1618, Oct. 1996.

[69] SCHNEIDER, K. S. "Optimum Detection of Code Division Multiplexed Signals". *IEEE Trans. Aero. Elec. Sys.* vol. AES-15, no. 1, pp. 181–185, Jan. 1979.

[70] SCHOLTZ, R. A. "The Spread Spectrum Concept". IEEE Trans. Commun. *vol. COM-25*, pp. 748–755, Aug. 1977.

[71] SCHOTTEN, H. D., AND ANTWEILER, M. "Iterative Construction of Sequences with Low Crosscorrelation Values". In *IEEE International Conference on Communications* (1993), vol. 1, pp. 156–160.

[72] SHANNON, C. "A Mathematical Theory of Communication". Bell System Technical Journal *vol. 27*, pp. 379–423, 623–656, 1948.

[73] SIM, M. L., GUNAWAN, E., AND SOH, C. B. "Charateristics of Closed Loop Power Control Algorithms for a Cellular DS/CDMA System". *IEE Proc. Comms.* vol. 145, no. 5, pp. 355–362, Oct. 1998.

[74] SIMON, M. K. "Noncoherent Pseudonoise Code Traking Performance of Spread Spectrum Receviers". IEEE Trans. Commun. *vol. COM-25*, pp. 327–345, Mar. 1977.

[75] SIMON, M. K., OMURA, J. K., SCHOLTZ, R. A., AND LEVITT, B. K. *Spread Spectrum Communications*, vol. III. Computer Science Press, Rockville, Md., 1985.

[76] SIMON, M. K., OMURA, J. K., SCHOLTZ, R. A., AND LEVITT, B. K. *Spread Spectrum Communications*, vol. I. Computer Science Press, Rockville, Md., 1985.

[77] SIMON, M. K., OMURA, J. K., SCHOLTZ, R. A., AND LEVITT, B. K. *Spread Spectrum Communications*, vol. II. Computer Science Press, Rockville, Md., 1985.

[78] SIMON, M. K., OMURA, J. K., SCHOLTZ, R. A., AND LEVITT, B. K. *Spread Spectrum Communications Handbook.* McGraw Hill, New York, 1994.

[79] SKELTON, B. C., AND TAYLOR, D. P. "A Family of Reduced Complexity Multi-User Detectors for Asynchronous Spread Spectrum Multiple Access". submitted to IEEE Trans. Commun.

[80] SKELTON, B. C., AND TAYLOR, D. P. "Multi-User Detectors with Decision Feedback for Asynchronous Spread Spectrum Multiple Access in Multi-path Fading Channels". submitted to IEEE Trans. Commun.

[81] SKELTON, B. C., AND TAYLOR, D. P. "Reduced State Sequence Estimation Based Multi-User Detectors for Asynchronous Spread Spectrum Multiple Access". submitted to IEEE Trans. Commun.

[82] SPILKER, J. J., AND MAGILL, D. T. "The Delay-Lock Discriminator: An Optimum Tracking Device". Proc. IRE *vol. 49*, pp. 1403–1416, Sept. 1961.

[83] STEELE, R. *Mobile Radio Communications.* Pentech, London, 1992.

[84] TAM, W. M., AND LAN, F. C. M. "Analysis of Imperfect Power Control in CDMA Systems". In *IEEE 8th International Symposium on Personal, Indoor and Mobile Radio Communications* (1997), vol. 3, pp. 892–897.

[85] TINGWU, W., AND HAIGER, X. "System Capacity and Power Control of Satellite Mobile Communication". In *IEEE International Conference on Communications Technology* (1996), vol. 1, pp. 305–310.

[86] TORRIERI, D. J. "Performance of Direct-Sequence Systems with Long Pseudonoise Sequences". *IEEE J. Select. Areas Commun.* vol. 10, no. 4, pp. 770–781, May 1992.

[87] TSAI, Y.-R., AND CHANG, J.-F. "Feasibility of Adding a Personal Communications Network to an Existing Fixed-Service Microwave System". *IEEE Trans. Commun.* vol. 44, no. 1, pp. 76–83, Jan. 1996.

[88] VAN ETTEN, W. "Maximum Likelihood Receiver for Multiple Channel Transmissions Systems". *IEEE Trans. Commun.* vol. 24, no. 2, pp. 76–83, Feb. 1976.

[89] VAN NOBELEN, R. *Coding for the Rayleigh Fading Channel.* PhD thesis, Dept of Electrical and Electronic Engineering, University of Canterbury, Christchurch, New Zealand, 1996.

[90] VARANASI, M. K., AND AAZHANG, B. "Multistage detection in Asynchronous Code-Division Multiple Access Communications". *IEEE Trans. Commun.* vol. 38, no. 4, pp. 509–519, Apr. 1990.

[91] VERDÚ, S. "Minimum Probability of Error for Asynchronous Gaussian Multiple-Access Channels". *IEEE Trans. Inform. Theory* vol. IT-32, no. 1, pp. 85–96, Jan. 1986.

[92] VERDÚ, S. *Recent Progress in Multiuser Detection.* IEEE Press, New York, 1993.

[93] VITERBI, A. J. *Principles of Digital Communication and Coding.* McGraw-Hill, New York, 1979.

[94] VITERBI, A. J. "Very Low Rate Convolutional Codes for maximum Theoretical Performance of Spread Spectrum Multiple Access Channels". *IEEE J. Select. Areas Commun.* vol. 8, no. 4, pp. 641–649, May 1990.

[95] VITERBI, A. J. "The Orthogonal-Random Waveform Dichotomy for Digital Mobile Personal Communication". IEEE Personal Commun., pp. 18–24, First Quarter 1994.

[96] VITERBI, A. J. *CDMA : Principles of Spread Spectrum Communication.* Addison-Wesley Publishing Company, Massachusetts, 1995, ch. 6, pp. 179–233.

[97] WARD, R. B. "Acquistion of Pseudo-Noise Signals by Sequential Estimation". IEEE Trans. Commun. Tech. *vol. COM-13*, pp. 474–483, Dec. 1965.

[98] WARD, R. B. "Digital Communications on a Pseudonoise Tracking Link Using Sequence Inversion Modulation". IEEE Trans. Commun. Tech. *vol. CT-15*, pp. 69–78, Feb. 1967.

[99] XIE, Z., RUSHFORTH, C. K., AND SHORT, R. T. "Multiuser Signal Detection Using Sequential Decoding". *IEEE Trans. Commun.* vol. 38, no. 5, pp. 578–583, May 1990.

[100] XIE, Z., RUSHFORTH, C. K., SHORT, R. T., AND MOON, T. K. "Joint Signal Detection and Parameter Estimation in Multiuser Communications". *IEEE Trans. Commun.* vol. 41, no. 7, pp. 1208–1215, Aug. 1993.

[101] XIE, Z., SHORT, R. T., AND RUSHFORTH, C. K. "A Family of suboptimum detectors for coherent multi-user communications". IEEE J. Select. Areas Commun. *vol. 8*, pp. 683–690, May 1990.

[102] YIP, K.-W., AND NG, T.-S. "Efficient Simulation of Digital Transmission over WSSUS Channels". *IEEE Trans. Commun.* vol. 43, no. 12, pp. 2907–2913, Dec. 1995.

[103] YIP, K. W., AND NG, T. S. "Discrete-time Model for Digital Communications Over a Frequency-Selective Rician Fading WSSUS Channel". *IEE Proc. Commun.* vol. 143, no. 1, pp. 37–42, Feb. 1996.

[104] ZHU, B., ANSARI, N., AND SIVESKI, Z. "Convergence and Stability Analysis of a Synchronous Adaptive CDMA Receiver". *IEEE Trans. Commun.* vol. 43, no. 12, pp. 3073–3078, Dec. 1995.

[105] ZVONAR, Z. "Multiuser Detection in Asynchronous CDMA Frequency-Selective Fading Channels". *Wireless Personal Communications* vol. 3, no. 3–4, pp. 373–392, 1996.

[106] ZVONAR, Z., AND BRADY, D. "Linear Multipath-Decorrelating Receivers for CDMA Frequency-Selective Fading Channels". *IEEE Trans. Commun.* vol. 44, no. 6, pp. 650–653, June 1996.